Dosimetric evaluation of four techniques used in stereotactic radiosurgery

Pierre E. Charpentier

Department of Medical Physics

McGill University, Montreal

December 2007

A thesis submitted to the Faculty of Graduate Studies and Research in partial fulfillment of the requirements of the degree of Master of Science in Medical Radiation Physics.

Your file Votre référence
ISBN: 978-0-494-51076-6
Our file Notre référence
ISBN: 978-0-494-51076-6

ABSTRACT

The thesis presents a comparison of four techniques used for stereotactic radiosurgery, consisting of the static conformal beam, static cone-based, proton therapy, and the Gamma Knife techniques. The comparisons involved six test cases in which phantom target lesions were created in the center of the modified anthropomorphic Rando® head. The phantom lesions presented in the study were extreme irregular cases that ranged in shape and volume and were near a critical structure to receive minimal dose during treatment planning. The best treatment plans from each technique for all studies were selected and the extracted data was analyzed using physical and biological parameters. Correlations between integral biological effective dose (normal brain) and normal tissue complication probability were analyzed as a function of dose conformity (PITV), and correlations between tumor control probability and integral biological effective dose (tumor) as a function of dose homogeneity (MDPD) were analyzed, as well. These parameter pairings showed strong links. The static conformal beam and the proton SOBP techniques consistently provided low PITV and MDPD values for all cases, including the most irregular and complicated cases. Higher PITV and MDPD values, typically associated with static cone-based and the Gamma Knife techniques, were due to normal tissue and tumor tissue, respectively, being irradiated at higher dose levels than the prescribed dose. For these cases, as the PITV increased, the NTCP increased, as well, due to high doses created within the normal tissue found within the prescription isodose surface.

Résumé

Une comparaison de quatre techniques utilisées en radiochirurgie stéréotaxique, soit le faisceau statique conforme, les collimateurs circulaires statiques, le faisceau de protons ainsi que le Gamma Knife® est présentée. L'étude a impliqué six cibles qui ont été créées dans le centre de la tête du fantôme anthropomorphique Rando®. Ces cibles étaient toutes des formes extrêmement irrégulières de différents volumes et étaient situées près de structures critiques ne pouvant recevoir qu'une dose minimale. Les meilleurs plans de traitement de chaque technique pour chaque cible ont été sélectionné et les plans de traitement ont été analysés en utilisant des paramètres physiques et biologiques. Les corrélations entre la dose biologique effective totale et la probabilité de complications fûrent analysées en fonction de l'indice de conformité de la dose (PITV). Les corrélations entre la probabilité de contrôle tumoral et la dose biologique effective intégrale (tumeur) en fonction de l'indice d'homogénéité de la dose (MDPD) ont aussi été analysées. Le faisceau statique conforme et les protons SOBP ont constamment montré des valeurs faibles de PITV et de MDPD pour tous les cas, incluant les cas les plus irréguliers et complexes. Les valeurs plus élevées de PITV et MDPD, associées aux collimateurs circulaires statiques et au Gamma Knife, étaient dues au tissues normaux et tumoraux, respectivement irradiés à des niveaux de dose plus élevés que la dose prescrite. Pour ces cas, lorsque le PITV augmentait, le NTCP augmentait aussi, dû aux grandes doses créées à l'intérieur des tissues normaux situés dans la surface d'isodose de prescription.

ACKNOWLEDGEMENTS

I would like to greatly express my gratitude to my two supervisors, Dr. Ervin Podgorsak and Horacio Patrocinio, for their continued guidance, support and encouragement throughout this project. Also, I would like to greatly thank Dr. Matthew Podgorsak, Roswell Park Cancer Institute, and Marc Bussiere, Massachusetts General Hospital, for allowing me to use their facilities and equipment and especially their time in explaining and teaching the fundamentals of the Gamma Knife and proton therapy, respectively.

I would also like to thank the staff and colleagues of the Medical Physics Department for their friendship, discussions and help throughout the last two years and with the thesis project. In particular I would like to thank the following staff and colleagues: Dr. Wamied Abdel-Rahman, Dr. Francois Deblois, Dr. Slobodan Devic, Michael Evans, Margery Knewstubb, Pierre Leger, William Parker, Dr. Bridgette Reniers, Russell Ruo, Dr. Jan Seuntjens, Dr. Frank Verhaegen, Robin Van Gils, Ismail Al-Dahlawi, Magdalena Bazalova, Erika Chin, Jason Hancock, Derek Liu, Monica Margeanu, Emily Poon, Eric Reynard, Arman Sarfehnia, Edwin Sham, Laurent Tantot, and Katie Woch.

Lastly, and most importantly, I would like to thank my wife, Ellen, and my children, Andre and Jean-Pierre, for their absolute patience, support, and strength, especially in the last two years during the McGill Medical Physics program. They have brought happiness and laughter in my life. I would like to thank my father and mother-

in-law, Dr. Paul and Barbara Schraeder, for constant support and advice; my parents for teaching me to push myself and follow my dreams; my sister, Jackie and my nephew, Michael for their love and support as well. For goals are accomplished with the support and assistance of great people.

Table of Contents

Abstract.....i

Resume.....ii

Acknowledgements.....iii

Table of Contents.....v

List of Figures.....vii

List of Tables.....ix

Chapter 1: Introduction to Stereotactic Radiosurgery Procedure.....1

1.1 Overview.....1
1.2 Historical Development of Stereotactic Radiosurgery.....1
1.3 Diseases treated with Stereotactic Radiosurgery.....5
1.4 Stereotactic Radiosurgery Components.....5
1.4.1 Stereotactic Frames.....5
1.4.2 Imaging modalities for stereotactic radiosurgery.....6
1.4.3 Treatment Planning Systems.....8
1.5 Stereotactic Radiosurgery Techniques.....10
1.5.1 Introduction.....10
1.5.2 Linear Accelerator.....10
1.5.2.1 Static Conformal Beam Technique.....10
1.5.2.2 Static Cone-Based Technique.....12
1.5.3 Proton Therapy (Spread-Out Bragg Peak Technique).....13
1.5.4 Leksell Gamma Knife.....14
1.6 Radiosurgery Plan Evaluation Tools.....16
1.7 Purpose of Thesis.....16
1.8 References.....19

Chapter 2: Treatment Planning and Plan Evaluation.....24

2.1 Introduction.....24
2.2 Treatment Planning Systems.....24
2.2.1 Static Conformal Beam Technique (LINAC).....24
2.2.2 Static Cone Based Beam Technique (LINAC).....27
2.2.3 Proton Therapy (Spread-Out Bragg Peak Technique).....29
2.2.4 Leksell Gamma Knife.....34
2.3 Plan Evaluation Tools.....37
2.3.1 Qualitative Tools.....37
2.3.2 Quantitative Tools.....39
2.3.2.1 Dose-volume Histograms (DVHs).....39
2.3.2.2 Tumor dose conformity and homogeneity.....40
2.3.2.3 Biological Indices.....42
2.3.2.3.1 Integral Biological Effective Dose (IBED).....42
2.3.2.3.2 Tumor Control Probability (TCP).....45

2.3.2.3.3 Normal Tissue Complication Probability (NTCP).....48
2.4 References.....52

Chapter 3: Methods and Materials.....56

3.1 Phantom Targets.....56
3.1.1 Phantom targets and setup.....56
3.1.2 Collection of Images for the Different Treatment Planning Systems.....58
3.2 Generating optimum treatment plans.....59
3.2.1 Static Conformal Beam Technique (Linac).....59
3.2.2 Static Cone Based Beam Technique (Linac).....60
3.2.3 Proton Therapy (Spread-Out Bragg Peak Technique).....62
3.2.4 Leksell Gamma Knife.....63
3.3 Plan Evaluation.....64
3.3.1 Conformity (PITV) and Homogeneity (MDPD) Indices.....65
3.3.2 Integral Biological Effective Dose (IBED).....66
3.3.3 Tumor Control Probabiltiy (TCP).....67
3.3.4 Normal Tissue Complication Probability (NTCP).....67
3.4 References.....69

Chapter 4: Results and Discussions.....70

4.1 Phantom Targets to be evaluated by four Radiosurgical techniques.....70
4.2 Results from comparative study—Physical and biological parameters.....71
4.3 Correlation between physical and biological parameters.....76
4.4 Analysis.....90

Chapter 5: Conclusion and Future Work.....94

5.1 Summary of the Thesis.....94
5.2 Future Work.....96

Appendix A.....98

Bibliography.....101

LIST OF FIGURES

Figure 1.1: (left to right)DSA image of AVM; CT axial image of brain; and MR axial image of brain. **7**

Figure 1.2: Above is the Varian Clinac-2300 with the BrainLab m3 micro-multileaf collimator attached performing the static conformal beam technique. **11**

Figure 1.3: Circular collimators are attached to the linac in a similar fashion as shown above for the static cone-based technique. **12**

Figure 1.4: Stereotactic radiosurgery with protons at the Massachusetts General Hospital is performed using the 110-ton gantry or the Stereotactic Alignment for Radiosurgery (STAR) apparatus (Courtesy of Massachusetts General Hospital). **14**

Figure 1.5: The Leksell Gamma Knife® 4C is shown above (Courtesy of Elekta). **15**

Figure 2.1: Example of BrainSCAN treatment plan displaying the BEV with the micro-multileaf collimator from a particular field and isodose lines on the axial, sagittal and coronal views. **25**

Figure 2.2: Example of SimuPlan treatment plan displaying isodose lines on the axial, sagittal and coronal views. **28**

Figure 2.3: Comparison of different proton beam energies and 6 MV photon beam depositing dose in water phantom (Courtesy of Massachusetts General Hospital)....**30**

Figure 2.4: Example of the CMS XiO treatment plan displaying isodose lines on the axial, sagittal and coronal views, along with the DVH display for the contoured structures....**33**

Figure 2.5: Example of the "bubble" skull attachment for taking measurements of the patient's skull prior to planning on the GammaPlan® 4C. A phantom is measured in preparation for treatment planning....**34**

Figure 2.6: Example of Gamma Plan ® treatment planning, displaying isodose lines on the axial, sagittal and coronal views....**35**

Figure 2.7: Dose calculation methodology for the algorithm used by the Gamma Plan ® 4C. (Courtesy of A. Wu, G. Lindner, A. H. Maitz, A. M. Kalend, L. D. Lunsford, J. C. Flickinger, W. D. Bloomer, "Physics of gamma knife approach on convergent beams in stereotactic radiosurgery," Int. J. Radiat. Oncol., Biol., Phys. **18**, 941-949 (1990)....**36**

Figure 2.8: Example of how the PITV is determined for a stereotactic case. The prescription isodose (red) volume is 6 cm^3 and this is divided by the tumor volume (orange) (3 cm^3) giving a PITV of 2.0....**40**

Figure 2.9: Example of how the MDPD is determined for a stereotactic case. The maximum dose in this example is 100 and this is divided by the prescription dose of 50 giving the MDPD to be 2.0....**41**

Figure 2.10: This graph shows a typical cell survival curve, illustrating both the linear and quadratic components. The graph is plotted in a logarithmic scale (Number of cells surviving vs dose).(Courtesy of E.J. Hall and A.J. Giaccia, Radiobiology for the Radiologist (Lippincott Williams & Wilkins Publishers, Philadelphia, PA, 2006)....**43**

Figure 2.11: This graph shows the characteristic sigmoidal curves for normal tissue complication probability (NTCP) and tumor control probability (TCP)....**46**

Figure 3.1 The phantom test cases block insert for Cases 1 through 6 in order from left to right(top row). The frame attached to the modified slab insert for the Rando head phantom. The square opening can be seen as the 4 pins fixed to the slab were never unattached during the scanning (bottom left). Alderson Rando® Phantom (bottom middle) The Rando® phantom completely assembled with insert case pair blocks and CT attachment on the stereotactic radiosurgery frame prior to acquiring images(bottom right).**58**

Figure 3.2: The Picker PQ-5000 CT scanner was used for the collection of diagnostic images for the six test case studies.....**59**

Figures 4.1 (a) and (f): Graphs present the $NTCP_{brain}$ and PITV relation for all techniques for test case 1 through test case 6.....**77**

Figures 4.2 (a) and (g): Graphs present the TCP and MDPD relation for all techniques for test case 1 through test case 6.....**82**

Figures 4.3 (a) and (f): Graphs present the $IBED_{brain}$ and PITV relation for all techniques for test case 1 through test case 6.....**85**

Figures 4.4 (a) and (g): Graphs present the $IBED_{tumor}$ and MDPD relation for all techniques for test case 1 through test case 6.....**86**

Figures 4.5 (a) and (b): Graphs present the $NTCP_{brain\ stem}$ /$IBED_{brain\ stem}$ and PITV, respectively for all techniques for test case 6.....**89**

LIST OF TABLES

Table 3.1: General description of the tumors and critical organs examined in the treatment planning comparison using various radiosurgical techniques and machines.....**56**

Table 3.2: Above are the fit parameters used for the calculations as discussed in Section 2.3. (Courtesy of C. Burman, G. J. Kutcher, B. Emami, and M. Goitein, "Fitting of normal tissue tolerance data to an analytical function," Int. J. Radiat. Oncol., Biol., Phys. **21**, 123-135 (1991).....**68**

Table 4.1: Physical parameters (PITV and MDPD), biological parameters (TCP, NTCP, IBED for the tumor and brain) and the number of beams/isocenters for each optimum treatment plan acquired using the static cone-based, Gamma Knife, static conformal beam and proton SOBP techniques for test case 1 are presented.....**72**

Table 4.2: Physical parameters (PITV and MDPD), biological parameters (TCP, NTCP, IBED for the tumor and brain) and the number of beams/isocenters for each optimum treatment plan acquired using the static cone-based, Gamma Knife, static conformal beam and proton SOBP techniques for test case 2 are presented.....**72**

Table 4.3: Physical parameters (PITV and MDPD), biological parameters (TCP, NTCP, IBED for the tumor and brain) and the number of beams/isocenters for each optimum treatment plan acquired using the static cone-based, Gamma Knife, static conformal beam and proton SOBP techniques for test case 3 are presented.....**72**

Table 4.4: Physical parameters (PITV and MDPD), biological parameters (TCP, NTCP, IBED for the tumor and brain) and the number of beams/isocenters for each optimum treatment plan acquired using the static cone-based, Gamma Knife, static conformal beam and proton SOBP techniques for test case 4 are presented.....**73**

Table 4.5: Physical parameters (PITV and MDPD), biological parameters (TCP, NTCP, IBED for the tumor and brain) and the number of beams/isocenters for each optimum treatment plan acquired using the static cone-based, Gamma Knife, static conformal beam and proton SOBP techniques for test case 5 are presented.....**73**

Table 4.6: Physical parameters (PITV and MDPD), biological parameters (TCPs, NTCPs, IBED for the tumors, brain stem and brain) and the number of beams/isocenters for each optimum treatment plan acquired using the static cone-based, Gamma Knife, static conformal beam and proton SOBP techniques for test case 6 are presented.....**74**

Table 4.7: For each optimum treatment plan for test case 1 through test case 3 acquired using the static cone-based, Gamma Knife, static conformal beam and proton SOBP techniques, the volumes of normal tissue with respect to dose are displayed to show dose homogeneity within the normal brain tissue.....**79**

Table 4.8: For each optimum treatment plan for test case 4 through test case 6 acquired using the static cone-based, Gamma Knife, static conformal beam and proton SOBP techniques, the volumes of normal tissue with respect to dose are displayed to show dose homogeneity within the normal brain tissue.....**79**

Table 4.9: The table presents how the TCP decreases and the tumor receives a more homogeneous dose distribution. High TCP values are obtained with increasingly high doses with larger tumor volumes receiving the high doses.....**83**

Table 4.10: For each optimum treatment plan for test case 1 through test case 3 acquired using the static cone-based, Gamma Knife, static conformal beam and proton SOBP techniques, the volumes of tumor with respect to dose are displayed to show dose homogeneity within the tumor tissue.....**87**

Table 4.11: For each optimum treatment plan for test case 4 through test case 6 acquired using the static cone-based, Gamma Knife, static conformal beam and proton SOBP techniques, the volumes of tumor with respect to dose are displayed to show dose homogeneity within the tumor tissue.....**88**

Table 4.12: For each optimum treatment plan for test case 6 acquired using the static cone-based, Gamma Knife, static conformal beam and proton SOBP techniques, the volumes of brain stem with respect to dose are displayed to show dose homogeneity within the brain stem tissue.....**89**

CHAPTER 1

INTRODUCTION TO STEREOTACTIC RADIOSURGERY PROCEDURE

1.1 OVERVIEW

Stereotactic radiosugery is characterized by its precise and accurate, high dose delivery of radiation to a small lesion, rapid dose falloff outside the tumor volume, and the tumor being well localized and immobilized by using immobilization and an external three-dimensional coordinate system.[1, 2] High dose with rapid dose falloffs outside the lesion is achieved by having numerous non-coplanar beam orientations incident on the hemisphere above the transverse plane of the lesion. Typical tumor volumes irradiated are between 1 and 35 cm^3 and usual total prescribed doses administered to lesions are between 10 to 50 Gy. External beam stereotactic irradiation is divided into two categories: stereotactic radiosurgery (total dose delivered in single session) and stereotactic radiotherapy (total dose delivered in multiple fractionations). Radiosurgery is commonly used to describe both categories because there is essentially no technical difference between the two; therefore, in this document, the term radiosugery will refer to both categories unless specified.

1.2 HISTORICAL DEVELOPMENT OF STEREOTACTIC RADIOSURGERY

The Swedish neurosurgeon Lars Leksell from Karolinska Institute in Stockholm first introduced the novel procedure in 1951 to treat neurological disorders[3]. He coined the term radiosurgery and his treatment with radiation became known as stereotactic radiosurgery. During his initial use, Leksell used 200 kVp X-rays to deliver, in a single session, a high radiation dose of approximately 100 Gy to the lesion inside the skull. He

delivered the dose from several directions in order to focus the dose on the tumor within the brain while sparing vital structures. Because the photon beam used was in the orthovoltage energy range, it became evident that, since the energy was not penetrating enough, an undesirable high entrance dose was being delivered to the skin. Leksell then abandoned the use of orthovoltage energies by the mid 1950s and began working with the radiobiologist Borge Larsson from Gustaf Werner Institute at the University of Uppsala in Sweden who had developed research using proton radiation. The two began working with proton beams due to advantageous characteristics of protons interacting with tissue. With the Bragg peak characteristics, protons were able to deliver a high dose deep below the surface at a specific distance with no exit dose and a minimal surface dose.

At the time Larsson began experimenting with protons, there was a growing interest in research using protons in radiotherapy based upon the concept of clinical applications introduced in 1946 by Wilson[4]. In the early 1950s, studies performed at the Lawrence Berkeley Laboratory in California by Lawrence and Tobias[5] using a 340 MeV proton beam on a 184-inch synchrocyclotron on research animals, showed positive results and led to studies on actual patients for treating pituitary tumors. By 1958, Larsson and Leksell[6] experimented with proton radiation on patients using a 185 MeV synchrocyclotron. Use of Leksell's stereotactic radiosurgery concept was modified to use proton radiation, since the adverse effects of orthovoltage beams were unacceptable.

By the mid-1960s, Leksell began developing a dedicated radiosurgery device using ^{60}Co gamma ray beams. He wanted a radiosurgery device that could be easily installed and practical for a hospital setting. By 1968, a prototype of this device, now known as the Gamma Knife, was used clinically. The first Gamma unit had 179 ^{60}Co

closely collimated sources producing circular beams aimed to a focal point within the unit. The initial activity of each source was 1.1 TBq and the beams had nominal diameters of 4, 8 or 14 mm.[2] The initial prototype was followed with a commercial version that increased the number of ^{60}Co sources to 201. The sources were focused to a point inside the unit at 40 cm from the sources and used the same nominal beam diameters as the prototype unit, with the addition of an 18 mm collimator helmet.

In 1974, Larsson[7] initially proposed the concept of using an isocentric linear accelerator (linac) as a viable radiation source for stereotactic radiosurgery, and during the next ten years, physicists were developing this concept. In 1984, Betti and Derechinsky[8] from Buenos Aires, Argentina developed the multiple non-coplanar converging arcs radiosurgery technique using a 10 MV linac. A year later, Colombo[9, 10] from Vicenza, Italy developed another technique using a 4 MV linac. In 1986, the first two institutions in North America to use linac-based stereotactic radiosurgery were Harvard University in Boston and McGill University in Montreal. Harvard University[11,12] developed a technique using 4 multiple non-coplanar converging arcs with a 6 MV linac. McGill University[13] developed its own radiosurgical technique, known as the dynamic stereotactic radiosurgery, in which the couch and the gantry move simultaneously during treatment with a 10 MV linac.

Originally, linacs used for stereotactic radiosurgery used multiple converging non-coplanar arcs, and circular collimators with various sizes. Therefore, if an irregularly shaped tumor were present, various circular collimators and multiple isocenters were superimposed to minimize the dose given to normal healthy tissue surrounding the tumor. Delivery of radiation using multiple non-coplanar converging

arcs has been very efficient and successful in treating intracranial lesions, and is still used today by many centers around the world.

Additional linear accelerator techniques have been developed with the widely accepted use of a micro-multileaf collimator. Micro-multileaf collimators are specialized multileaf collimators (MLCs) that provide smaller irregularly shaped dose fields of several centimeters, and each leaf is of the order of one millimeter at the isocenter. Therefore, the micro-multileaf collimator systems have allowed use of new techniques that may provide better conformity of beams to irregularly shaped tumors, while minimizing the dose to surrounding normal structures. With irregularly shaped tumors, the micro-multileaf collimator typically uses a single isocenter, allowing for a faster treatment than does the use of multiple isocenters with circular collimators, while achieving a more homogenous dose distribution in the tumor volume.

With the use of micro-multileaf collimator systems, dynamic fields are achievable. Hence intensity-modulated stereotactic radiosurgery (IMRS) has been accepted as an effective clinical modality for treatment of intracranial lesions that also minimizes the dose to normal healthy tissue surrounding the tumor. Also, the "CyberKnife" (Accuray Incorporated, Santa Clara, CA, USA) has gained acceptance as another stereotactic radiosurgery modality.[14] The "CyberKnife" consists of a miniature 6 MV linear accelerator attached to an industrial robotic arm. An interesting feature of the "CyberKnife" system is the use of the non-invasive image guided target localization. This system's image-guided dose delivery method aims the radiation beam into the on-line determined tumor position and achieves a dose delivery accuracy of the order of 1 mm.

1.3 DISEASES TREATED WITH STEREOTACTIC RADIOSURGERY

Initially when Leksell introduced the concept of stereotactic radiosurgery, he intended its use for non-neoplastic neurological diseases, such as intractable pain, Parkinson's disease and epilepsy. Subsequently, primary benign and malignant tumors, vascular lesions and metastatic tumors were also treated. Currently, stereotactic radiosurgery is used to treat vascular malformations, benign tumors, malignant and metastatic tumors, and functional neurological diseases.

1.4 STEREOTACTIC RADIOSURGERY COMPONENTS

1.4.1 Stereotactic Frames

In order to deliver a highly focused dose of radiation during stereotactic radiosurgery, a rigid stereotactic frame is fixed to the patient's skull during Computed Tomography (CT), Magnetic Resonance Imaging (MRI), and/or Digital Subtraction Angiography (DSA) imaging, and during treatment the frame is used to immobilize the patient during the imaging and treatment procedures, but also provides the three-dimensional coordinate system on the patient by providing a geometrical relationship between the frame and anatomical structures, including the tumor and other structures of concern. It also serves as the base for the stereotactic localizer(s) and stereotactic positioner.[15] The localizer box (CT and MRI) provides a way of determining the position on the three-dimensional images required for the treatment planning system and also defines the origin of the coordinate system. During the entire procedure, from initial imaging to treatment, the stereotactic frame must not be removed from the patient.

After the stereotactic radiosurgery frame is fixed to the patient's skull using pins or screws, the localizer box is placed on the frame before the patient is imaged. The localizer box contains fiducial markers that are specific for each imaging modality, since the localization rods are composed of different materials. The fiducial markers will appear on every image slice of interest for planning. These markers define the link between the stereotactic coordinates and the imaging coordinates, so that for any point in the image(s) the three-dimensional stereotactic coordinates can be determined. Immediately prior to treatment, the stereotactic positioner is attached to the frame, allowing therapists to position the patient so that the isocenter(s) are accurately positioned for treatment setup.

Many different stereotactic frame systems are described in detail in the literature: the Brown-Roberts-Wells (BRW) system,[16] the Cosman-Roberts-Wells (CRW) system;[17] the Leksell system[18, 19] and the BrainLAB frame. Every system varies as to material makeup for the frame, frame design and attachments (imager and positioner), and the origin of the coordinate system. Also, they will vary to a certain degree on how the frame is attached to the patient. For proton stereotactic radiosurgery, a non-invasive frame is used, but fiducial markers are implanted in the patient's skull. In our study, the stereotactic frame is based on the Leksell frame, as modified by the Medical Physics department of the Montreal General Hospital.

1.4.2 Imaging modalities for stereotactic radiosurgery

The diagnostic imaging used in stereotactic radiosugery allows for localization and positioning, for defining the target volume and organs at risk, and for calculation and

three-dimensional representation of the isodose distribution. Several imaging modalities may be used for stereotactic radiosurgery such Digital Subtraction Angiography (DSA), Computed Tomography (CT), and Magnetic Resonance Imaging (MRI), depending on the lesion (see Figure 1.1).

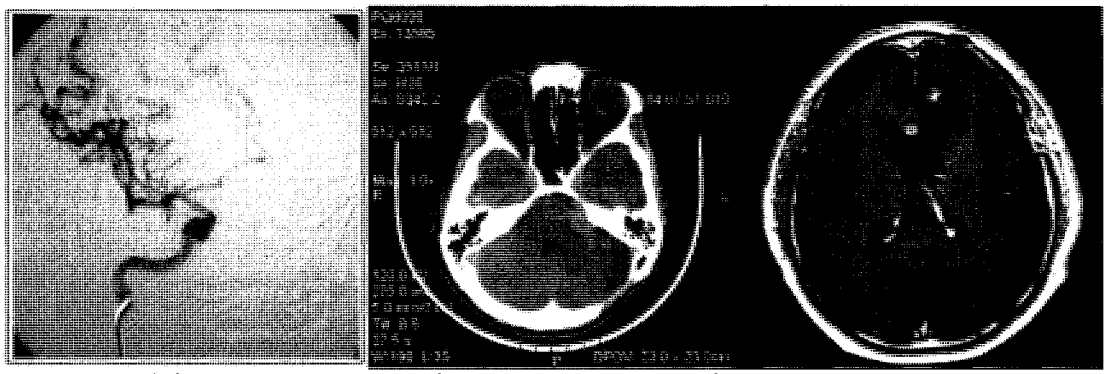

Figure 1.1: (left to right) DSA image of AVM; CT axial image of brain; and MR axial image of brain.

DSA images vascular lesions, such as arteriovenous malformations (AVMs) for stereotactic radiosurgery treatment. A special localizer box is attached to the frame prior to imaging. The box has four fiducial markers that are metallic beads placed in each of the four panes surrounding the patient's head. The AVM and the fiducial markers are localized by using two orthogonal image pairs with an accuracy of ±1 mm. The coordinates of the lesion are determined from the relative positions of the eight fiducial markers visible on the image. Following the DSA acquired angiogram, the patients receive a CT scan with attached stereotactic frame and the CT localizer box because DSA will not provide an accurate image of the head which is required for treatment planning. The two image sets will then be fused together prior to treatment planning.

CT is the most common imaging system used for target localization in stereotactic radiosurgery. During the CT imaging, the localizer box with CT-compatible fiducial markers is attached to the frame fastened to the patient's skull. CT scans for stereotactic radiosurgery are able to provide high resolution with minimal distortion and provide an

accurate representation of the patient's anatomy with an accuracy of ±1 mm. The CT images represent variations in photon attenuation coefficient between the tumor and normal brain tissue. While CT scans provide excellent images of the skull and of tumors containing calcium, there often is little contrast between the brain matter and non-calcium containing tumor, since CT image acquisition cannot differentiate between these two tissues due to the diagnostic energy range and the structures' attenuation coefficients.

MRI provides better contrast between brain tissue and tumor when compared with CT. Use of MRI for localization and positioning requires high homogeneity of the magnetic field to avoid spatial distortions artifacts, which could disturb the geometrical correlation between the stereotactic coordinate system and imaging coordinate system.[20, 21] Geometric artifacts are mainly produced by eddy currents which may be produced within the stereotactic radiosurgery frame. Most distortions seen on the MRI images are visible near the frame base and become less visible as the image slice is further away from the frame. CT image sets are required to be fused with the MRI image sets just like when DSA images are used. Once fused, treatment planning can be performed.

1.4.3 Treatment Planning Systems

The main objective in obtaining an optimum treatment plan for stereotactic radiosurgery is to cover precisely and accurately the entire tumor volume with the prescribed dose and a homogenous dose distribution. Also, the treatment plan should have sharp dose fall offs on the margin of the tumor volume and the surrounding tissues should get minimal dose or at least a dose not exceeding a tolerable dose range.[2]

Initially, stereotactic radiosurgery treatment planning was relatively simple in concept, consisting of locating the lesion and irradiating it. Little thought was given to producing a homogenous dose distribution, conformity or even radiobiological effects during treatment planning. Many institutions developed their own treatment planning systems for stereotactic radiosurgery that involved three-dimensional planning for dose distributions within the skull using available imaging modalities, such as CT, MRI and DSA.[22,23]

Today, many commercial products are available that are stand-alone systems dedicated to radiosurgery. Treatment planning workstations have three-dimensional dose calculation algorithms, numerous displays and other user-friendly planning tools (see Section 2.2). Linac treatment planning systems have numerous options for radiation delivery depending upon the system available to the center. For instance, linac stereotactic radiosurgery may deliver the dose by aiming at the lesion with a certain number of non-coplanar radiation beams or by using multiple non-coplanar arcs with circular field collimators. The Gamma Knife treatment planning system has been upgraded since its initial use and currently employs an automatic planner for developing a treatment plan. Proton therapy is still site specific with the proton center working with a commercial vendor to create a user friendly treatment planning workstation that has typical standardized planning tools that are incorporated with the center's individual needs.

A detailed description of the four stereotactic radiosurgery techniques evaluated in this study and the characteristics of their own treatment planning systems is presented in Section 1.5 and Section 2.2, respectively.

1.5 STEREOTACTIC RADIOSURGEY TECHNIQUES

1.5.1 INTRODUCTION

The ability to deliver precisely focused high dose of radiation to a small lesion with a steep dose gradient outside the tumor margin in a single session is what makes stereotactic radiosurgery unique to radiation oncology. In general, radiosurgery is accomplished by having the beam(s) enter in the upper hemisphere of the patient's skull, allowing the dose to be distributed throughout and avoiding any dose buildup in normal tissue. For proton therapy, beams may be parallel-opposed, unlike in photon beam treatment, since in proton therapy there is no significant exit dose. The following section describes linac techniques that are currently used at the Montreal General Hospital.

1.5.2 LINEAR ACCELERATOR

1.5.2.1 STATIC CONFORMAL BEAM TECHNIQUE

The most sophisticated linac-based radiosurgical technique practiced at the Montreal General Hospital is the static conformal beam technique which uses a micro-multileaf collimator attached to the linac head and non-coplanar, static fields. The static conformal beam technique is able to deliver focused radiation by converging 6-12 beams on the lesion. For each static beam, the micro-multileaf collimator conforms to the beam's eye projection of the target. Typically one isocenter is used per a given lesion.

The micro-multileaf collimator used in this study is the BrainLAB m3 (BrainLAB, AG, Heimstetten, Germany) which is attached to the head of our linac prior to use. The BrainLAB m3 is able to shape each static field by moving its 26 leaf pairs

and has a maximum field area at the isocenter of approximately 100 cm^2 (9.8cm x 9.8 cm).

The static conformal beam technique uses a 6 MV beam from the Varian, Clinac-2300 linac (Varian Medical Systems, Palo Alto, CA, USA) (See Figure 1.2). The technique can use two types of commercially available stereotactic frames that are couch-mounted: 1) the OBT frame (Tipal Instruments, Montreal) and 2) the Leksell frame

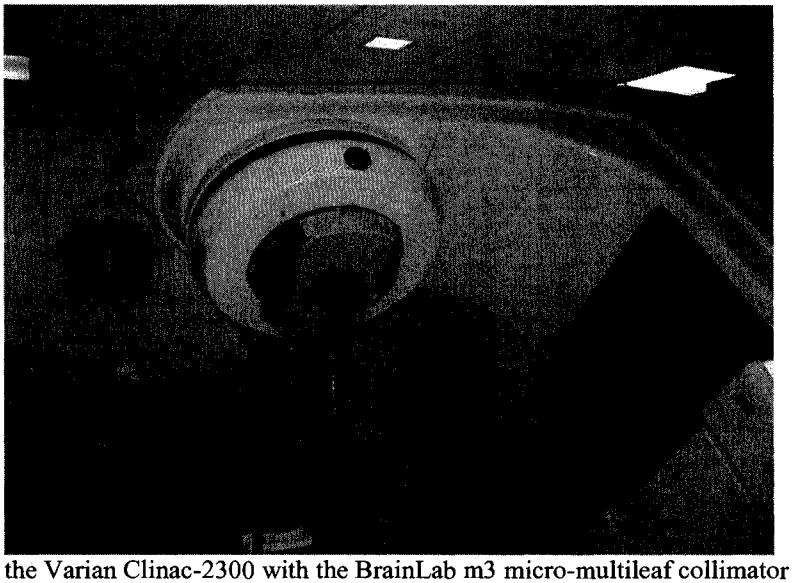

Figure 1.2: Above is the Varian Clinac-2300 with the BrainLab m3 micro-multileaf collimator attached performing the static conformal beam technique.

(Elekta Instruments, Stockholm, Sweden). The patient is treated in the supine position with the couch-mounted stereotactic frame attached to the patient's skull during all phases, including localizing, immobilization and treatment. The treatment planning is conducted using the stand alone system for stereotactic radiosurgery called BrainSCAN[24] (BrainLAB, AG, Heimstetten, Germany).

1.5.2.2 STATIC CONE-BASED TECHNIQUE

A simpler linac-based technique in use at the Montreal General Hospital is the static cone-based technique. This technique also uses a 6 MV beam, but in this case, is done with a Varian, Clinac-21EX linac (Varian Medical Systems, Palo Alto, CA, USA), (See Figure 1.3). Similar to the static conformal beam technique, the static cone-based technique can use the stereotactic radiosurgery frame, as mentioned in Section 1.5.2.1, and the patient is treated in the supine position.

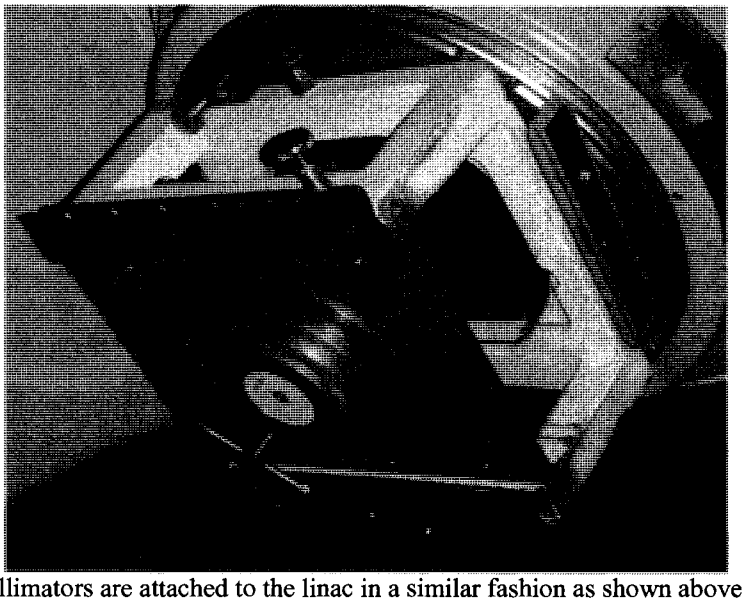

Figure 1.3: Circular collimators are attached to the linac in a similar fashion as shown above for the static cone-based technique.

The technique uses circular collimators with diameters ranging from 0.5 cm to 4.0 cm, and the dose distribution at the isocenter is generally spherical in geometry for high level isodose surfaces. Each isocenter used for treatment will have ten non-coplanar, converging beams with pre-selected gantry and couch combinations. The beam entry points may be varied, but the pre-selected combination sufficiently disperses the dose to avoid dose buildup in normal tissue. A single isocenter is typically used for a lesion that is spherical in shape, but multiple isocenters may be used for irregularly shaped lesions.

The treatment planning system used for the static cone-based technique is the SimuPlan[25] (see Section 2.2.2) originally developed at McGill University for another linac-based technique, the dynamic rotation technique.[13]

1.5.3 PROTON THERAPY (SPREAD-OUT BRAGG PEAK TECHNIQUE)

The proton spread-out Bragg peak (SOBP) technique used at the Massachusetts General Hospital (MGH), in Boston, MA, for stereotactic radiosurgery proton therapy uses a 235 MeV cyclotron built by Ion Beam Applications (IBA), Incorporated (Louvain-la-Neuve, Belgium). Stereotactic radiosurgery may be performed using a 110-ton gantry treatment room or the dedicated stereotactic radiosurgery treatment room using a fixed beam that has a specially designed apparatus, called the Stereotactic Alignment for Radiosurgery (STAR)[26] (see Figure 1.4), which is used for patient positioning, and provides five independent axes of movement. In proton therapy, 1-mm diameter stainless steel micro-spheres are implanted in the outer table of the patient's skull for imaging; therefore, not requiring the typical CT/MRI stereotactic frame attachment. A modified non-invasive stereotactic frame, the Gill-Thomas-Cosman (GTC) frame from Radionics, Inc.(Burlington, MA, USA),[27] is used for patient immobilization during imaging and treatment.

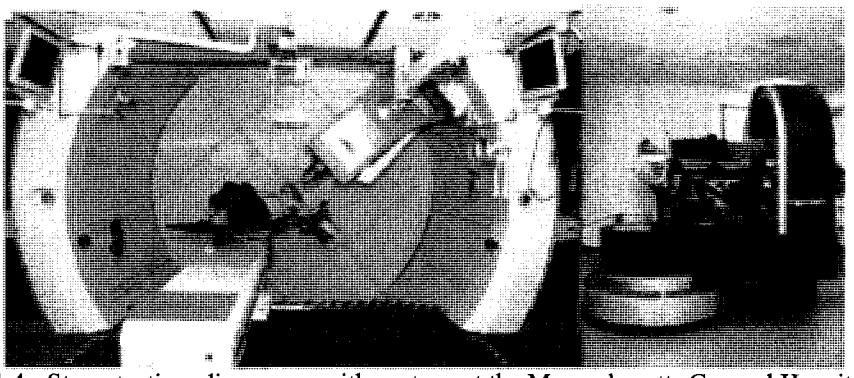

Figure 1.4: Stereotactic radiosurgery with protons at the Massachusetts General Hospital is performed using the 110-ton gantry or the Stereotactic Alignment for Radiosurgery (STAR) apparatus (Courtesy of Massachusetts General Hospital).

Treatment fields are shaped to the lesion's contour using custom milled brass apertures. The aperture edge is typically defined as the lesion's projection to the level of the isocenter and the beam penumbra of 50% of the prescribed dose. The depth of the protons for each portal, or field, is controlled by using custom milled compensators, typically fabricated of Lucite, that reduce the range of the protons. The maximum required range within a portal, defined as the distal 90% dose of the proton beam in tissue, is the thinnest point on the compensator.[27]

Typically one isocenter is used for treatment planning with 1-6 portals, but more commonly 3-5 portals are used. The treatment planning system was built in collaboration between the Massachusetts General Hospital and the CMS XiO planning system (St. Louis, MO, USA) (see Section 2.2.3).

1.5.4 LEKSELL GAMMA KNIFE

The Leksell Gamma Knife model 4C[28] used in our study is located at the Roswell Park Cancer Institute in Buffalo, NY. It houses 201 ^{60}Co sources, (total activity of approximately 2.22 x 10^{14} Bq in initial loading) located within the central body of the unit

(see Figure 1.5). Because the sources are heavily shielded, the shielding makes up the majority of the equipment. The sources converge to a single focal point at a source-focus distance of approximately 40 cm. The dose distribution at the focal point is defined by using one of four helmets delivering circular fields with diameters of 4, 8, 14 and 18 mm at the machine focal point.

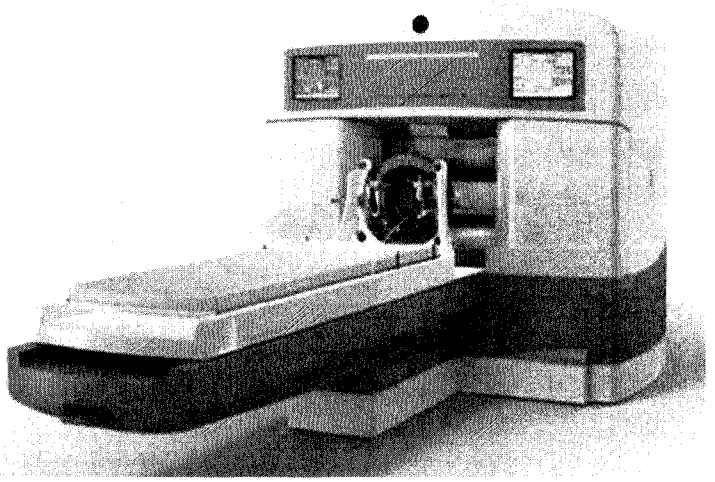

Figure 1.5: The Leksell Gamma Knife® 4C is shown above (Courtesy of Elekta).

The patient is treated in the supine position using the Leksell stereotactic radiosurgery frame that is attached to the patient's skull. The patient is positioned on the sliding couch, while the frame is locked into place in the Automatic Positioning System (APS).[28] The APS is a newly added feature that automatically moves the patient to each new isocenter position during treatment for each set of collimator helmets used.

The treatment planning system used for the Leksell Gamma Knife® 4C is the Leksell Gamma Plan ® 4C[28] (see Section 2.2.4). The number of "shots" used for treatment of irregularly shaped lesions may be between 1and 18, but typically, the number of "shots" does not exceed ten due to the required extended patient irradiation treatment time.

1.6 RADIOSURGERY PLAN EVALUATION TOOLS

Evaluation of a three-dimensional treatment plan for stereotactic radiosurgery is not a simple task because of the large quantity of information presented in a typical treatment plan. Several tools are available for the planner to draw on when developing and evaluating treatment plans, such as qualitative and quantitative tools.

The stereotactic radiosurgery planner may review the plan(s) qualitatively by visually inspecting the isodose lines and using the Beam's Eye View (BEVs) (see Section 2.3.1) for assistance in determining full coverage, with a specific prescribed isodose to the lesion or minimizing dose to critical structures.

The main quantitative planning tool is the dose volume histogram (DVH)[29] (see Section 2.3.2.1). The DVH is a histogram which may plot the accumulated volume of a tissue receiving dose in a specified dose interval against a set of equispaced dose intervals. From the DVH data, other quantitative tools have been developed to assist the planner in developing and evaluating the plan(s), such as, for example, the planning isodose volume to the prescription dose ratio (PITV), the maximum dose to the prescription dose ratio (MDPD), the integral biologically effective dose (IBED), the tumor control probability (TCP), and the normal tissue complication probability (NTCP).

In Chapter 2, Section 2.3, physical and biological indices implemented to compare and evaluate the stereotactic radiosurgery modalities are described in detail.

1.7 PURPOSE OF THE THESIS

Many studies performed over the years in stereotactic radiosurgery compared different techniques and modalities, including the Leksell Gamma Knife, linac-based

techniques and protons[30-56]. Physical (conformity and homogeneity indices) and biological (tumor control probability (TCP), normal tissue complication probability (NTCP) and integral biological effective dose (IBED) parameters have been used as a basis for discussion of techniques and their ability to cover certain volumes or shapes of lesions.

In this study, the data presented compares four different techniques (Leksell Gamma Knife, two linac-based techniques and proton therapy) used for stereotactic radiosurgery for different targets of differing shapes and volumes. The lesions examined are complex and limiting cases. Also, this study is an extension of a previous work performed by Oliveira[54] in 2003. Oliveira compared three simple target shapes for three linac techniques. In this study, the same static conformal beam technique is used as in her study, along with a different linac technique (static coned-based technique). In addition, two techniques, proton SOBP and the Gamma Knife techniques are incorporated in this study. Similar to Oliveira's study, endpoints used for comparison amongst techniques are: (1) physical parameters such as PITV and MDPD; (2) dose volumes within defined structures; and (3) biological parameters, such as TCP, NTCP and IBED.

To conduct the stereotactic radiosurgical treatment plan comparisons, a phantom head was modified in order to allow different phantom tumor cases to be evaluated by four techniques. Contours drawn on images were not directly transferable across the different planning systems; therefore, each case was redrawn in each planning system, as described in Chapter 3.

Chapter 3 will describe the methods and materials used for this comparison and Chapter 4 will present the results and discussion obtained from the study. The study will complete with Chapter 5 where conclusions and suggestions for future work are presented.

1.8 REFERENCES

1 J. Van Dyk (editor), The Modern Technology of Radiation Oncology (Medical Physics Publishing, Madison, WI, 1999).

2 T. R. Mackie and J. R. Palta, Teletherapy: Present and Future (Advanced Medical Publishings, Madison, WI, 1996).

3 L. Leksell, "The stereotaxis method and radiosurgery of the brain," Acta Chir. Scand. **102**, 316-319 (1951).

4 R. R. Wilson, "Radiological Use of Fast Protons," Radiology **47**, 487-491 (1946).

5 C. A. Tobias, J. H. Lawrence, J. L. Born, R. K. McCombs, J. E. Roberts, H. O. Anger, B. V. A. Low-Beer, and C. B. Huggins, "Pituitary Irradiation with High-Energy Proton Beams A Preliminary Report," Cancer Research **18**, 121-134 (1958).

6 B. Larsson, L. Leksell, B. Rexed, P. Sourander, W. Mair, B. Andersson, "The high-energy proton beam as a neurosurgical tool," Nature **182**, 1222-1223 (1958).

7 B. Larsson, K. Liden, and B. Sorby, "Irradiation of small structures through intact skull," Acta Radiol. Ther. Phys. Biol. **13**, 513-534 (1974).

8 O. O. Betti and V. E. Derechinsky, "Hyperselective Encephalic Irradiation with Linear Accelerator," Acta Neurochir. Suppl. (Wien) **33**, 385-390 (1984).

9 F. Colombo, A. Benedetti, F. Pozza, A. Zanardo, R. C. Avanzo, G. Chierego, and C. Machetti, "Stereotactic radiosurgery utilizing a linear accelerator," Appl. Neurophysiol. **48**, 133-145 (1985).

10 F. Colombo, A. Benedetti, F. Pozza, R. C. Avanzo, C. Machetti, G. Chierego, and A. Zanardo, "External Stereotactic Irradiation by Linear accelerator," Neurosur. **16**, 154-159 (1985).

11 W. Lutz, K. R. Winston, and N. Maleki, "A system for stereotactic radiosurgery with a linear accelerator," Int. J. Radiat. Oncol., Biol., Phys. **14**, 373-381 (1988).

12 K. R. Winston and W. Lutz, "Linear Accelerator as a Neurosurgical Tool for Stereotactic Radiosurgery," Neurosur. **22**, 454-463 (1988).

13 E. B. Podgorsak, A. Olivier, M. Pla, P. Y. Lefebvre, and J. Hazle, "Dynamic stereotactic radiosurgery," Int. J. Radiat. Oncol., Biol., Phys. **14**, 115-125 (1988).

[14] International Atomic Energy Agency (IAEA), Radiation Oncology Physics: A Handbook for Teachers and Students. E. B. Podgorsak, (International Atomic Energy Agency, Vienna, Austria, 2005).

[15] W. Schlegel, T. Bortfeld, and A. L. Grosu, New Technologies in Radiation Oncology (Springer, Berlin, Heidelberg, NewYork, 2006).

[16] R. A. Brown, "Stereotactic headframe for use with the CT body scanners," Invest Radiol. **14**, 300-304 (1979).

[17] W. T. Couldwell and M. Apuzzo, "Initial experience related to the use of the Cosman-Roberts-Wells stereotactic instrument," J. Neurosurg. **72**, 145-148 (1990).

[18] L. Leksell and B. Jernberg, "Stereotaxis and tomography. A technical note," Acta Neurochir. **52**, 1-7 (1980).

[19] L. Leksell, D. Leksell and Y. Schwebel, "Stereotaxis and nuclear magnetic resonance," J. Neurol. Neurosurg Psychiatry **48**, 14-18 (1985).

[20] T. M. Peters, J. A. Clark, A. Olivier, E. P. Marchand, G. Mawko, M. Diemeregard, L. W. Muresan, and R. Ethier, "Integrated stereotaxic imaging with CT, MRI, and DSA," Radiol. **161**, 821-826 (1986).

[21] A. Olivier, T. M. Peters, and G. Bertrand, "Stereotaxic systems and apparatus for use with MRI, CT and DSA," Appl. Neurophysiol. **48**, 94-96 (1986).

[22] B. G. Pike, E. B. Podgorsak, T. M. Peters, and C. Pla, "Dose distributions in dynamic stereotactic radiosurgery," Med. Phys. **14**, 780-789 (1987).

[23] H. M. Kooy, L. A. Medzi, J. S. Loeffler, E. Alexander, C. W. Cheng, E. G. Mannarino, E. J. Holupka, and R. L. Siddon, "Treatment planning for stereotactic radiosurgery of intracranial lesions," Int. J. Radiat. Oncol., Biol., Phys. **21**, 44-45 (1991).

[24] BrainSCAN Software Guide Revision 1.0 - Version 5.2x" (BrainLAB, AG, Heimstetten, Germany, 2002).

[25] "SimuPlan treatment planning system manual-version for Apple Macintosh power PC computers" (SimuPlan Sociedad Limitada, Valencia, Spain, 2000).

[26] G. Harsh, J. S. Loeffler, A. Thornton, A. Smith, M. Bussiere, and P. H.Chapman, "Stereotactic Proton Radiosurgery," Neurosurg. Clinics of North America **10**, 243-256, (1999).

[27] M. R. Bussiere and J. A. Adams, "Treatment Planning for Conformal Proton Radiation Therapy," Tech. Canc. Res. Treat., **2**, 389-399, (2003).

[28] "Leksell Gamma Knife ® 4C System Description Guide," (Elekta, Stockholm, Sweden, 2004).

[29] R. E. Drzymala, R. Mohan, L. Brewster, J. Chu, M. Goitein, W. Harms, and M. Urie, "Dose-volume histograms," Int. J. Radiat. Oncol., Biol., Phys. **21**, 71-78 (1991).

[30] V. Smith, L. Verhey, and C. F. Serago, "Comparison of radiosurgery treatment modalities based on complication and control probabilities," Int. J. Radiat. Oncol., Biol., Phys. **40**, 507-513 (1998).

[31] S. Webb and A. E. Nahum, "A model for calculating tumour control probability in radiotherapy including the effects of inhomogeneous distributions of dose and clonogenic cell density," Phys. Med. Biol. **38**, 653-666 (1993).

[32] J. E. Mignano, M. J. Engler, J. S. Tsai, and D. E. Wazer, "Comparison of radiobiologic modeling for one- and two- isocenter dose distributions applied to ellipsoidal radiosurgery targets," Int. J. Radiat. Oncol., Biol., Phys. **49**, 833-837 (2001).

[33] J. T. Lyman, "Complication probability as assessed from dose-volume histograms," Radiat. Res. **104**, S13-S19 (1985).

[34] J. T. Lyman and A. B. Wolbarst, "Optimization of radiation therapy, III: A method of assessing complication probabilities from dose-volume histograms," Int. J. Radiat. Oncol., Biol., Phys. **13**, 103-109 (1987).

[35] C. Burman, G. J. Kutcher, B. Emami, and M. Goitein, "Fitting of normal tissue tolerance data to an analytical function," Int. J. Radiat. Oncol., Biol., Phys. **21**, 123-135 (1991).

[36] B. Emami, J. Lyman, A. Brown, L. Coia, M. Goitein, J. E. Munzenrider, B. Shank, L. J. Solin, and M. Wesson, "Tolerance of normal tissue to therapeutic irradiation," Int. J. Radiat. Oncol., Biol., Phys. **21**, 109-122 (1991).

[37] G. J. Kutcher, C. Burman, L. Brewster, M. Goitein, and R. Mohan, "Histogram reduction method for calculating complication probabilities for three-dimensional treatment planning evaluations," Int. J. Radiat. Oncol., Biol., Phys. **21**, 137-146 (1991).

[38] L. J. Verhey, V. Smith, and C. F. Serago, "Comparison of radiosurgery treatment modalities based on physical dose distributions," Int. J. Radiat. Oncol., Biol., Phys. **40**, 497-505 (1998).

[39] R. J. Hamilton, F. T. Kuchnir, P. Sweeney, S. J. Rubin, M. Dujovny, C. A. Pelizzari, and G. T. Y. Chen, " Comparison of static conformal field with multiple noncoplanar arc techniques for stereotactic radiosurgery or stereotactic radiotherapy," Int. J. Radiat. Oncol., Biol., Phys. **33**, 1221-1228 (1995).

[40] S. Y. Woo, W. H. Grant, D. Bellezza, R. Grossman, P. Gildenberg, L. S. Carpenter, M. Carol, and E. B. Butler, "A comparison of intensity modulated conformal therapy with a conventional external beam stereotactic radiosurgery system for the treatment of single and multiple intracranial lesions," Int. J. Radiat. Oncol., Biol., Phys. **35**, 593-597 (1996).

[41] A. S. Shiu, H. M. Kooy, J. R. Ewton, S. S. Tung, J. Wong, K. Antes, and M. H. Maor, "Comparison of miniature multileaf collimation (mmlc) with circular collimation for stereotactic treatment," Int. J. Radiat. Oncol., Biol., Phys. **37**, 679-688 (1998).

[42] R. M. Cardinale, S. H. Benedict, Q. Wu, R. D. Zwicker, H. E. Gaballa, and R. Mohan, "Comparison of three stereotactic radiotherapy techniques; arcs vs. noncoplanar fixed fields vs. intensity modulation," Int. J. Radiat. Oncol., Biol., Phys. **42**, 431-436 (1998).

[43] V. S. Khoo, M. Oldham, E. J. Adams, J. L. Bedford, S. Webb, and M. Brada, "Comparison of intensity-modulated tomotherapy with stereotactically guided conformal radiotherapy for brain tumors," Int. J. Radiat. Oncol., Biol., Phys. **45**, 415-425 (1999).

[44] C. Yu, G. Luxton, G. Jozsef, M. L. J. Apuzzo, and Z. Petrovich, "Dosimetric comparison of three photon radiosurgery techniques for an elongated ellipsoid target," Int. J. Radiat. Oncol., Biol., Phys. **45**, 817-826 (1999).

[45] L. Ma, P. Xia, L. J. Verhey, and A. L. Boyer, "A dosimetric comparison of fan-beam intensity modulated radiotherapy with Gamma Knife stereotactic radiosurgery for treating intermediate intracranial lesions," Int. J. Radiat. Oncol., Biol., Phys. **45**, 1325-1330 (1999).

[46] T. D. Soldberg, K. L. Boedeker, R. Fogg, M. T. Selch, and A. A. F. DeSalles , "Dynamic arc radiosurgery field shaping: A comparison with static field conformal and noncoplanar circular arcs," Int. J. Radiat. Oncol., Biol., Phys. **49**, 1481-1491 (2001).

[47] B. G. Clark, J. L. Robar, and A. M. Nichol, "Analysis of treatment parameters for conformal shaped field stereotactic irradiation: Comparison with non-coplanar arcs," Phys. Med. Biol. 3089-3103 (2001).

[48] B. G. Baumert, I. A. Norton, and J. B. Davis, "Intensity-modulated stereotactic radiotherapy vs. stereotactic conformal radiotherapy for the treatment of

meningioma located predominantly in the skull base," Int. J. Radiat. Oncol., Biol., Phys. **57**, 580-592 (2003).

[49] J.Y. Jin, F. F. Yin, S. Ryu, M. Ajlouni and J. H. Kim, "Dosimetric study using different leaf-width MLCs for treatment planning of dynamic conformal arcs and intensity-modulated radiosurgery," Med. Phys. **32**, 405-411 (2004).

[50] A. Grzadziel, A. L. Grosu, and P. Kneschaurek, "Three-dimensional conformal versus intensity-modulated radiotherapy dose planning in stereotactic radiotherapy: Application of standard quality parameters for plan evaluation," Int. J. Radiat. Oncol., Biol., Phys. **66**, S87-S94 (2006).

[51] C. F. Serago, A. F. Thornton, M. M. Urie, P. Chapman, L. Verhey, S. J. Rosenthal, K. P. Gall, and A. Niemierko, "Comparison of proton and x-ray conformal dose distributions for radiosurgery applications," Med. Phys. **22**, 2111-2116 (1995).

[52] R. Lin, E. B. Hug, R. A. Schaefer, D. W. Miller, J. M. Slater, and J. D. Slater, "Conformal proton radiation therapy of the posterior fossa: A study comparing protons with three-dimensional planned photons in limiting dose to auditory structures," Int. J. Radiat. Oncol., Biol., Phys. **48**, 1219-1226 (2000).

[53] B. G. Baumert, A. J. Lomax, V. Miltchev, and J. B. Davis, "A comparison of dose distributions of proton and photon beams in stereotactic conformal radiotherapy of brain lesions," Int. J. Radiat. Oncol., Biol., Phys. **49**, 1439-1449 (2001).

[54] S. C. Oliveira, Comparison of three linac-based stereotactic radiosurgery techniques, M. Sc. Thesis, McGill University, Montreal, Quebec, (2003).

[55] B. G. Baumert, I. A. Norton, A. J. Lomax, and J. B. Davis, "Dose conformation of intensity-modulated stereotactic photon beams, proton beams, and intensity-modulated proton beams for intracranial lesions," Int. J. Radiat. Oncol., Biol., Phys. **60**, 1314-1324 (2004).

[56] D. C. Weber, J. Bogner, J. Verwey, D. Georg, K. Dieckmann, L. Escude, M. Caro, R. Potter, g. Goitein, A. J. Lomax and R. Miralbell, "Proton beam radiotherapy versus fractionated stereotactic radiotherapy for uveal melanomas: A comparative study," Int. J. Radiat. Oncol., Biol., Phys. **63**, 373-384 (2005).

CHAPTER 2

TREATMENT PLANNING AND PLAN EVALUATION

2.1 INTRODUCTION

The four stereotactic radiosurgery techniques described in this thesis have different methods of delivering the radiation dose to the lesion. Regardless if photons or protons are used to deliver dose for stereotactic radiosurgery, the planner must precisely and accurately place the radiation dose on the lesion, minimizing dose to nearby critical structures and observing steep gradient isodose lines on the margin of the tumor. Each technique will have similarities and differences in their respective treatment planning systems that will aid the planner to optimize the treatment plans. All treatment planning systems can calculate the dose-volume histograms and the data can be used to compute biological parameters for the specific treatment plan (see Section 2.3).

2.2 TREATMENT PLANNING SYSTEMS

2.2.1 STATIC CONFORMAL BEAM TECHNIQUE (LINAC)

The treatment planning system used for the static conformal beam technique was the BrainSCAN[1] (BrainLAB, AG, Heimstetten, Germany) treatment planning system, version 5.2x. Planning a stereotactic radiosurgery case with the BrainSCAN treatment planning system, requires the following steps: 1) acquisition of patient data (diagnostic images); 2) CT localization; 3) image fusion; 4) defining structures;
5) placement of isocenter(s) with respective beams; and 6) dose calculation.

After diagnostic images have been acquired and localization has been completed, the lesion as well as any pertinent structures nearby will need to be outlined by the

planner, for the dose-volume calculations. Next, an isocenter will be placed in the center-of-mass for the outlined lesion. After placement of the isocenter, the planner will begin placement of beams, ensuring the avoidance of critical structures, such as to spread the dose in the upper hemispherical section of the skull and avoiding parallel-opposed beams. To account for the beam penumbra, a margin may be used for each beam, typical values being 1-2 mm. Also, the use of collimator angle optimization allows the planner to select the optimum positioning angle of the collimator to spare normal tissue. The Beam's Eye View (BEV) (see Section 2.3.1) display and the three-dimensional visualization of structures aid the planner in beam placement. The individual leafs of the micro-multileaf collimator are able to be selected and moved in the BEV display; thus, shielding critical structures and/or opening the field in a specific area to account for the beam penumbra to fully cover the lesion. Figure 2.1 is an example of planning data provided by the BrainSCAN treatment planning system.

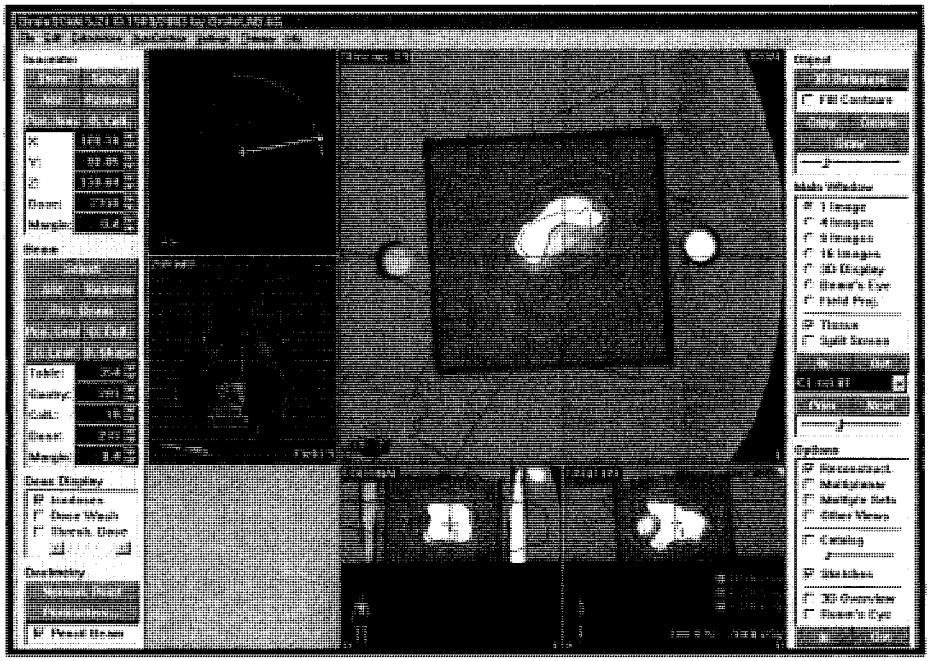

Figure 2.1: Example of BrainSCAN treatment plan displaying the BEV with the micro-multileaf collimator from a particular field and isodose lines on the axial, sagittal and coronal views.

Dose calculations performed by the BrainSCAN planning system are based on the pencil beam algorithm designed by Mohan,[2,3] in which the algorithm divides the incident beam into many small pencil beams and provides a more accurate dose calculation. The following is the dose calculation for the pencil beam algorithm in BrainSCAN:[1]

$$Dose(x,y,d) = MU \cdot M_{\mathrm{NLin}} \cdot S_t\left(c_{\mathrm{mlc}}, c_{\mathrm{jaw}}\right) \cdot TMR_{\mathrm{PB}}\left(\min\left(c_{\mathrm{mlc}}, c_{\mathrm{jaw}}\right), r_{\mathrm{rad}}\right) \cdot \left(\frac{SID}{SSD+d}\right)^2 \cdot IDD(x',y',r_{\mathrm{rad}}), \tag{2.1}$$

where

MU is the number of monitor units applied to the linac;

M_{NLin} is the nominal linac output (ratio of absolute dose, measured in a water phantom for a calibrated field size at a calibrated depth, divided by amount of monitor units;

r_{rad} is the radiological pathlength of the beam from the tissue surface to the observation point, corrected for tissue density inhomogeneities;

c_{mlc} and c_{jaw} are the size of the equivalent squared MLC and jaw field;

SSD is the source to surface distance;

SID is the source to isocenter distance;

d is the depth of observation;

d_{cal} is the depth of point where M_{NLin} and scatter factors were measured;

$S_t(c_{\mathrm{mlc}}, c_{\mathrm{jaw}})$ is the total scatter factor describing the relative output factor for a squared field;

$TMR_{\mathrm{PB}}(min(c_{\mathrm{mlc}}, c_{\mathrm{jaw}}), r_{\mathrm{rad}})$ is the tissue-maximum ratio for an equivalent squared field for the MLC/jaw field in depth r_{rad}, using a special renormalization to measured TMRs;

and $IDD(x',y',r_{\mathrm{rad}})$ is the idealized dose distribution (IDD).

The *IDD* for a collimator with a shape is the two-dimensional convolution of the polyenergetic pencil beam kernel with the photon fluence. The *IDD* describes the dose distribution in photon beams in a homogeneous water phantom in a "fan-line coordinate system" and is expressed by:

$$IDD(x,y,d) = \iint \phi(x',y',d) \cdot p(x'-x, y'-y, d) \cdot dx', dy'. \tag{2.2}$$

The photon fluence in an isocenter plane perpendicular to the central beam at a depth d is given by the following expression:

$$\phi(x,y,d) = \phi_0(x,y) \cdot RFS(r,d), \tag{2.3}$$

where the ϕ_0 (x,y) is the fluence at the isocenter plane and *RFS* is the radial factor giving the photon fluence at a distance from the central beam at a depth d in the phantom.

The dose-volume histograms are calculated using a three-dimensional matrix of points that are centered on the planned treatment volume. The resolution for the matrix is 2 mm, but the planner can adjust the resolution from 0.5 mm to 16 mm. The DVH can be selected to be displayed as a differential or cumulative plot.

2.2.2 STATIC CONE-BASED TECHNIQUE (LINAC)

The static cone-based technique uses the SimuPlan[4] version 8.1c treatment planning system. As with BrainSCAN, in order to properly plan a radiosurgery treatment with the SimuPlan planning system, the following steps are performed: 1) acquisition of patient data (diagnostic images); 2) CT localization and external skull contour; 3) defining structures; 4) placement of isocenter(s) with respective collimator size; 5) dose calculation; and 6) selection of isodose surface and prescription dose.

Localization is performed similarly to the BrainSCAN treatment planning system, but the patient skull surface must be outlined for the SimuPlan treatment planning system to create the three-dimensional surface. The planner must define the lesion and any critical structure(s) for dose-volume calculations. Treatment planning is then initiated with the placement of an isocenter with its respective collimator field size and may be placed in the center-of-mass for the outlined lesion. For irregularly shaped or larger sized lesions, additional isocenters will be used and the planner will have to place them strategically to ensure conformity and homogeneity requirements. To optimize the plans, the planner may use various display views, such as axial, coronal or sagittal, to inspect the isodose surfaces and ensure full tumor coverage as well as minimization of dose to nearby structures. Figure 2.2 is an example of the SimuPlan treatment planning screen, displaying a series of axial slices which are used for three-dimensional reconstruction of the relevant patient anatomy. The screen also shows idodose distributions for three orthogonal planes.

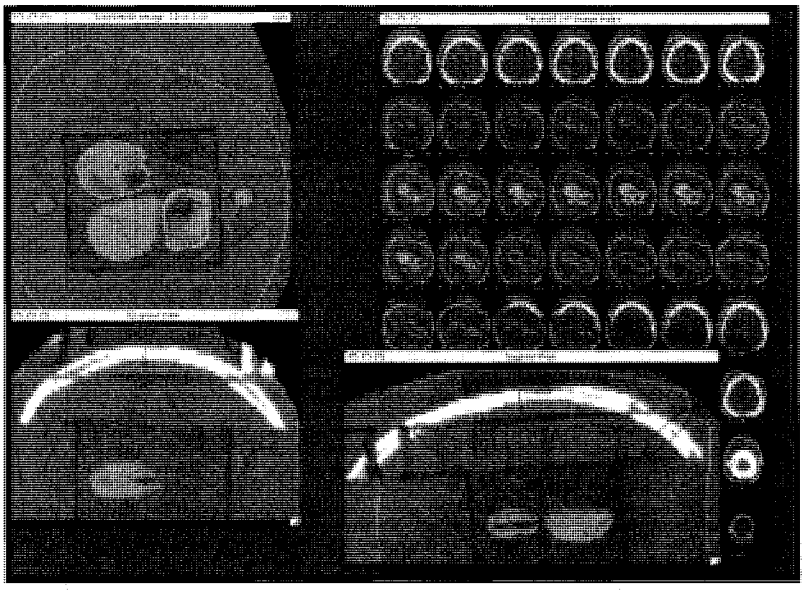

Figure 2.2: Example of SimuPlan treatment plan displaying isodose lines on the axial, sagittal and coronal views.

Dose calculations performed by the SimuPlan treatment planning system are based on the modified Milan and Bentley algorithm[5] using measured tissue-maximum ratios (TMR) (converted to percent-depth dose (PDD) values) and off-axis ratios (OAR) at various depths in water. To account for the dependence of the beam output on field size, measured relative dose factors (RDFs) are used in the dose calculation. The following expression is used to calculate the dose at a point of interest Q:[5]

$$D_{\mathrm{Q}}(z, A_{\mathrm{Q}}) = PDD\left(z, A_{\mathrm{i}} \frac{f_{\mathrm{i}} - z_{\mathrm{i}} + z}{f_{\mathrm{i}} + z}, f_{\mathrm{i}}\right) \left(\frac{f_{\mathrm{i}} + z}{f_{\mathrm{i}} + z_{\max}}\right)^2 \left(\frac{f_{\mathrm{i}}}{f_{\mathrm{i}} - z_{\mathrm{i}} + z}\right)^2 OAR(z, r_{\mathrm{Q}}) \qquad (2.4)$$

where z is the depth of the point of interest Q; $z_{\max}$ and z_{i} are depth of maximum dose and the isocenter depth, respectively; A_{Q} and A_{i} are field diameters at point Q and at the isocenter, respectively; f_{i} is the source-axis distance; and r_{Q} is the distance from the central axis to point Q at depth z.

The dose-volume histograms are displayed either in cumulative or differential format for the desired structure of interest. The system assumes all tissues, including skull, brain matter and tumor to be homogeneous with unit density.

2.2.3 PROTON THERAPY (SPREAD-OUT BRAGG PEAK TECHNIQUE)

The major difference between proton and photon (x-ray) therapy is in the dose deposition in tissue and the resulting dose distribution. Photons are indirect ionizing radiation, and the dose distribution is represented with most of the dose being deposited at a shallow depth of a few centimeters with a gradual exponential-like decrease in dose as depth increases into the patient. On the other hand, protons, which are directly ionizing radiation (heavy charged particles), deliver the majority of their dose in the Bragg peak at a specific depth related to the energy of the incoming beam, followed by a

sharp fall-off of dose to zero. Figure 2.3 shows typical depth profiles for photons and protons. Protons deposit their energy in tissue via Coulombic interactions with orbital electrons of tissue, and their path is considered to be straight, since they do not diverge from their path even when experiencing Coulombic interactions with orbital electrons.

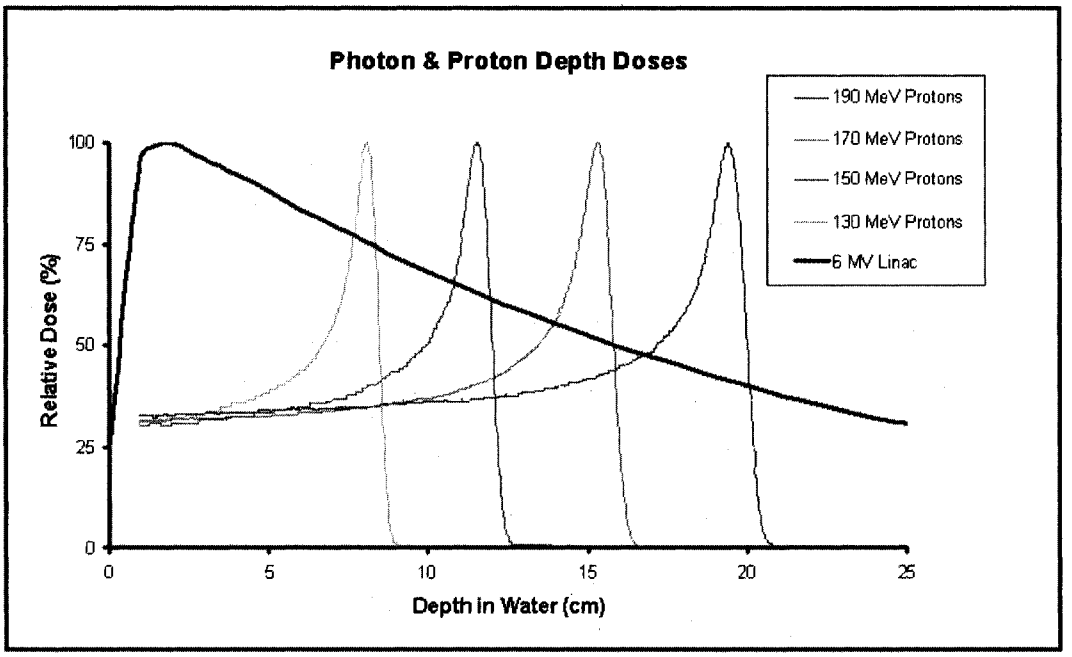

Figure 2.3: Comparison of different proton beam energies and 6 MV photon beam depositing dose in water phantom (Courtesy of Massachusetts General Hospital).

Doses for proton therapy are described in cobalt gray equivalent (CGE), but the units are the same as those for dose (Gy). The distinction is noted because protons produce different magnitudes of cell kill. The radiobiological effectiveness (RBE), the ratio of surviving cells irradiated by the same dose from protons compared to ^{60}Co is 1.1.[6,7]

The spread-out Bragg peak technique uses a modified version of the commercial CMS XiO treatment planning system. The dose calculation algorithm, developed at the Massachusetts General Hospital, is a variation of the pencil beam algorithm for protons explained in published literature by Hong *et al.*[8] The pencil beam algorithm, not only

separates the beam into multiple pencil beams, but takes into account the air gap between the equipment nozzle and the patient and accounts for multiple scattering effects near the lesion. The pencil beam algorithm is separated into two components: 1) the dose computation of a single beam and 2) the summation of the contributing pencil beams. The dose at a point $d(x', y', z')$ is separated into the central-axis term $C(z')$ and an off-axis term, $O(x', y', z')$:

$$D(x', y', z') = C(z')\, O(x', y', z'). \tag{2.5}$$

The $C(z')$ is taken from measured broad-beam central-axis depth dose from a water phantom and adjusted with the inverse square correction:

$$C(z') = DD(d_{eff})\left(\frac{ssd_0 + d_{eff}}{z'}\right)^2, \tag{2.6}$$

where $DD(d_{eff})$ is the central-axis depth-dose distribution of the open beam in a water phantom, ssd_0 is the source-to-surface distance. The effective depth, d_{eff}, is expressed by:

$$d_{eff} = R_0 - (R_r - rpl(z')), \tag{2.7}$$

where $rpl(z')$ is the radiographic path length along the central axis, R_0 is the initial range and R_r is the residual proton range once it enters the patient.

The $O(x', y', z')$ off-axis term is the lateral flux distribution. It is considered to be Gaussian:

$$O(x', y', z') = \frac{1}{2\pi[\sigma_{tot}(z')]^2}\exp\left(-\frac{x'^2 + y'^2}{2[\sigma_{tot}(z')]^2}\right), \tag{2.8}$$

where σ_{tot} is the radial emittance standard deviation.

Finally, the summation of all pencil beams is performed by the following expression:

$$D(x,y,z) = \iint dx'\,dy'\,\Psi_0(x',y')\frac{C(x',y',z)}{2\pi[\sigma_{tot}(x',y',z)]^2}\exp\left(-\frac{(x'-x)^2+(y'-y)^2}{2[\sigma_0(x',y',z)]^2}\right) \quad (2.9)$$

where Ψ_0 (x,y) is the intensity profile of the open beam and the integration is performed over the beam area.

When properly planning a stereotactic radiosurgery plan with the CMS XiO treatment planning system, the following steps are required: 1) acquisition of patient data (diagnostic images); 2) CT localization and external contour; 3) image fusion; 4) defining structures; 5) placement of isocenter with 1-6 portals with their respective modulation and compensator; 6) dose calculation; and 7) selection of isodose surface and prescription dose.

Localization is performed by selecting the microspheres that are implanted in the patient's skull and the patient's outer surface must be outlined. The lesion and any critical structures should be contoured to obtain data for dose-volume calculations. Treatment planning commences with the placement of an isocenter in the center-of-mass of the outlined lesion. The planner selects each field of entry or portal, avoiding critical structures, where each portal will have the field contouring the shape of the lesion and 50-90% isodose surface. Once the portal has been defined, the modulation will be entered to ensure the SOBP of the 90% isodose line encompasses the lesion from the respective entry point. The air-gap must be considered between the compensator and the patient, since it may degrade the penumbra if the air-gap is too large. Typical planned air gap measurement for stereotactic radiosurgery is 1 cm - 2 cm. Three to six fields are used per lesion and the fields may be abutted (at the 50% isodose) to avoid critical structures. Fields are noncoplanar and the lack of an exit dose makes proton therapy favorable in some situations. Depending on the size and shape of the tumor, the level of

dose to normal tissue may increase toward the entry level due to the SOBP characteristic.[6]

Similar to other radiosurgery planning systems the planner has similar options with the CMS XiO treatment planning system, such as BEVs, as well as coronal, sagittal, and axial views to see the isodose surface coverage. The portal(s) may be modified as the planner continues to evaluate a specific plan. Portal modification allows the planner to ensure tumor coverage and/or shielding and minimizing the dose to nearby structures. Figure 2.4 shows a typical screen for the CMS XiO treatment planning system.

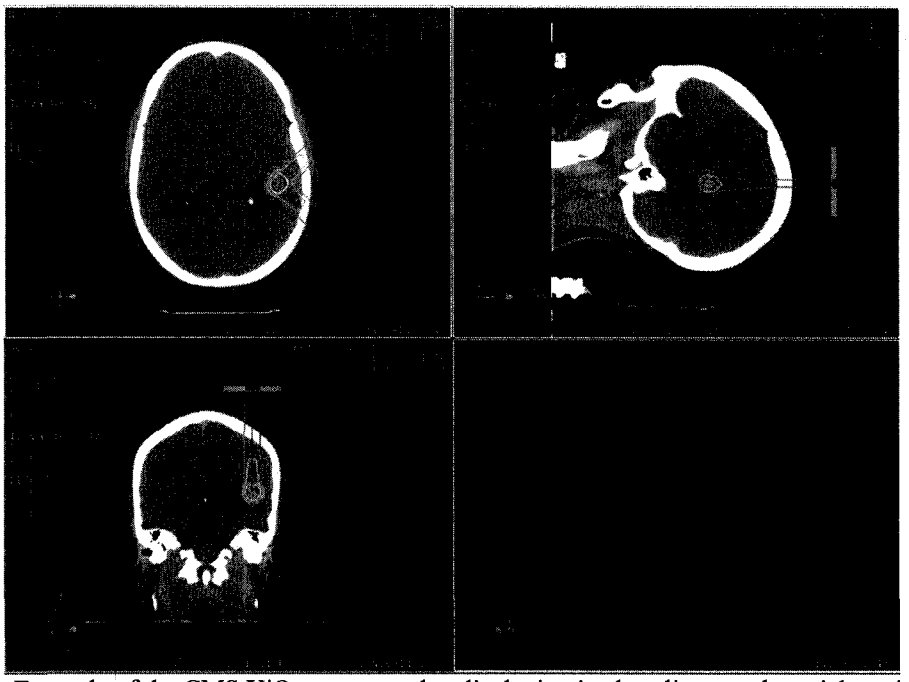

Figure 2.4: Example of the CMS XiO treatment plan displaying isodose lines on the axial, sagittal and coronal views, along with the DVH display for the contoured structures.

The dose-volume histograms are displayed either in cumulative or differential plots of the contoured structure. The treatment planning system does not assume the different tissues in the images to be homogeneous, and does have a manual input for the electron density of each tissue.

2.2.4 LEKSELL GAMMA KNIFE

The treatment planning system used by the Leksell Gamma Knife ® 4C[9] was the GammaPlan® 4C. Using the GammaPlan ® 4C to plan a stereotactic radiosurgery case, the following steps are necessary: 1) acquisition of patient data (diagnostic images); 2) bubble skull attachment measurement; 3) CT localization; 4) image fusion; 5) structure outlining; 6) selection size of dose matrix; 7) placement of isocenter(s) with respective collimator helmet size selection; 8) dose calculation; and 9) selection of isodose surface and prescription.

The GammaPlan ® 4C is similar to the other treatment planning systems. Prior to planning, the manual measurement using the "bubble" skull attachment has to be conducted on the patient to acquire the separations between the edge of the attachment and the skull of the patient. This data is manually entered into the planning system and used by the dose calculation algorithm. Figure 2.5 shows a "bubble" skull attachment used in conjunction with a Leksell-type stereotactic frame measuring a phantom case. There are 24 fixed points of measurement for the "bubble" attachment.

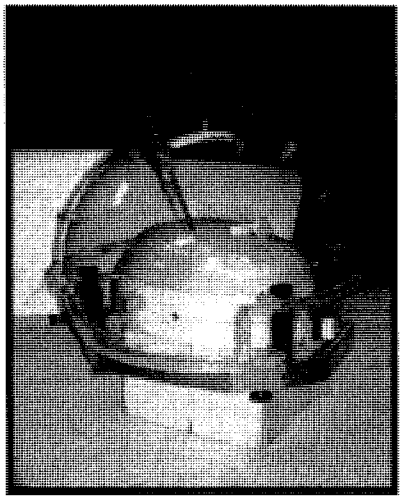

Figure 2.5: Example of the "bubble" skull attachment for taking measurements of the patient's skull prior to planning on the GammaPlan® 4C. A phantom is measured in preparation for treatment planning.

After the acquisition of images, localization and contouring of structure(s), the planner then selects a size for calculation dose matrix centered on the lesion. If there is a complex case with numerous lesions, multiple dose matrices of smaller size may be used for the planning. Placement of isocenter(s) may be adjusted quickly by the planner through a visual inspection of the isodose(s) lines selected for possible prescription. The planner has the usual display tools, such as axial, coronal, and sagittal views (see Figure 2.6) to assist in the treatment planning process.

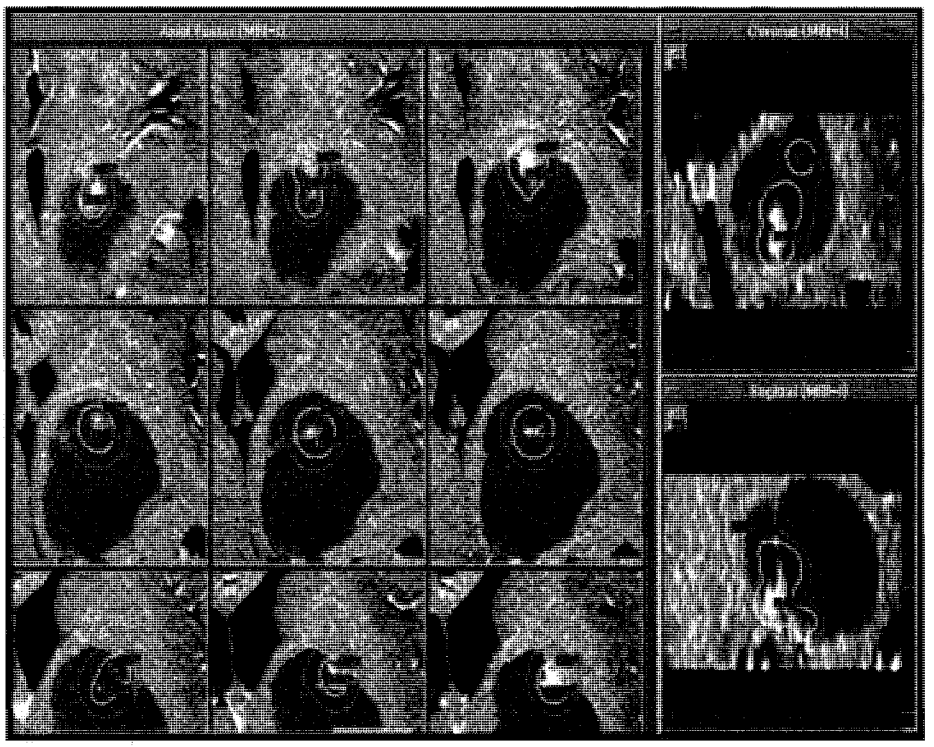

Figure 2.6: Example of Gamma Plan ® treatment planning, displaying isodose lines on the axial, sagittal and coronal views.

The GammaPlan ® 4C Wizard™ is an automatic planning tool that may be used by the planner on a complex case. The planner may select a specific helmet collimator size or any combination of the four collimator helmets. The automatic planning tools assists the planner by ensuring the isocenters selected in the planning are evenly

distributed throughout the lesion. Nonetheless, the planner will need to evaluate the proposed solution and may modify the plan to satisfy the dose conformity and homogeneity requirements.

The dose calculation algorithm[10,11] used by the GammaPlan ® 4C calculates the dose at the point of interest P from a single beam of a specific collimator. The dose calculation from a single beam incorporates the patient's skull configuration, the dose rate at a reference point, the linear attenuation coefficient of the ^{60}Co gamma ray beam, and the transverse radiation dose profile. Figure 2.7 shows the geometry for the simple algorithm calculation.

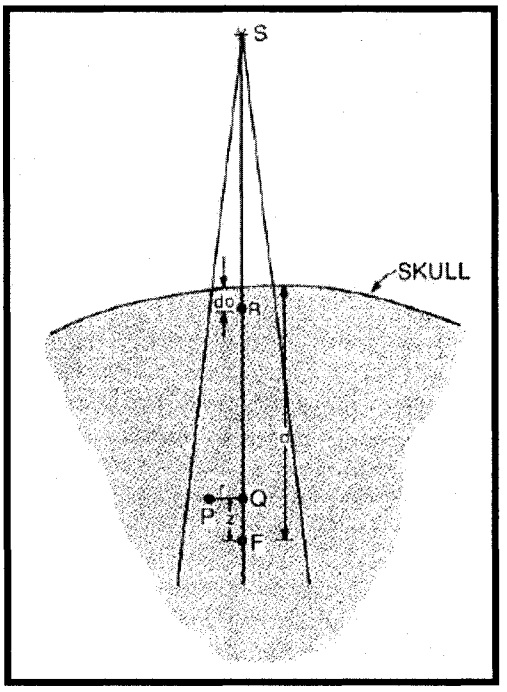

Figure 2.7: Dose calculation methodology for the algorithm used by the Gamma Plan ® 4C. (Courtesy of A. Wu, G. Lindner, A. H. Maitz, A. M. Kalend, L. D. Lunsford, J. C. Flickinger, W. D. Bloomer, "Physics of gamma knife approach on convergent beams in stereotactic radiosurgery," Int. J. Radiat. Oncol., Biol., Phys. **18**, 941-949 (1990).

By knowing the dose at point R, the reference point, the calculation at any arbitrary point P can be determined by first taking the inverse square law and the linear

attenuation exponential formula to point Q. Then using an off-axis ratio (OAR), the dose at point P can be determined from the known dose profiles. Point F is the machine isocenter which is approximately 40 cm from the source. The total dose to point P is the summation of all the dose contributions from the 201 sources. If multiple isocenters are used, then the same process is repeated for all isocenters and the summation of all points is performed by the algorithm inside the dose matrix.

GammaPlan ® 4C calculates the dose distribution in a matrix (Grid) volume covered by 31x31x31 points. The separation between the points may be adjusted by the planner for the dose calculation. The minimum grid is about 0.6 mm and the maximum grid is 3 mm (separation between points) producing approximately a 6.43 cm^3 and 804 cm^3, respectively, calculation dose matrix. The resolution for the DVHs is the same reflecting the three-dimensional matrix of points. The DVH is displayed as a cumulative or differential plot for the selected defined structure.

2.3 PLAN EVALUATION TOOLS

Since treatment planning systems for stereotactic radiosurgery use three-dimensional dose distributions, several qualitative and quantitative planning tools are essential for effective evaluation of treatment plans.

2.3.1 Qualitative Tools

Analyzing stereotactic radiosurgery treatment plans can be done with the following qualitative tools. Visual inspection of the isodose lines can be performed by viewing the axial, coronal or sagittal images. These images with the isodose lines

superimposed will be two-dimensional, but the planner may scan through each image and visually inspect each one to determine the appropriate prescribed isodose contour for the lesion. A visual inspection of the isodose contours will also allow the planner to determine the avoidance of the critical structures that may be in the vicinity of the tumor volume or help reduce the dose to the normal tissue structure. Also, since the dose gradient is visible, the planner can determine if more beams, isocenters or additional shielding are required to optimize the plan. However, the isodose contour inspection does not tell the planner anything about the exact volume being treated.

Another tool that may be helpful in treatment evaluation is the beam's eye view (BEV). The BEV places the observer's eye from the beam source as the reference and allows the planner to determine the extent of coverage of the tumor volume and surrounding normal tissue by a specific beam. The BEV display shows the tumor and any outlined structure. The planner can also determine, if a certain beam is too close to a critical structure, allowing for complete deletion or reposition of the beam or the addition of shielding. Because BEVs and inspecting isodose lines are simple and useful qualitative tools, they aid the planner when used in combination with other tools to determine whether or not a plan is optimal.

Since qualitative tools are not numerical, quantitative tools are then required to provide a numerical number from calculation to determine the effectiveness of the treatment plan. The following quantitative tools provide numerical figures that aid in treatment planning comparisons.

2.3.2 Quantitative Tools

Several quantitative tools are available to the planner for use in evaluating stereotactic radiosurgery treatment plans. They include dose-volume histograms[12] (DVHs), dose conformity and dose homogeneity indices, and integral biological effective dose (IBED)[13], tumor control probability (TCP) and normal tissue complication probability (NTCP).[14]

2.3.2.1 Dose-Volume Histograms (DVHs)

Dose-volume histograms[12] provide the distribution of dose values within a defined structure volume that may include the tumor volume or a critical organ that is located near the tumor volume. Two forms of displaying the DVH information are: 1) cumulative DVH and 2) differential DVH. With the cumulative DVH, the volume accumulates starting at the highest dose bin and proceeds to zero dose that eventually includes 100% of the total volume of the structure being treated. The differential DVH displays the results as the volume of the structure defined (in percentage or absolute volume) accumulated separately for each dose.

Planners using DVHs as a quantitative tool for stereotactic radiosurgery must realize that there is a loss of spatial distribution of dose resulting from the data being condensed when the DVHs are calculated. Nonetheless, obtaining the volume of under irradiated or over irradiated volume is extremely helpful for the planner and may adjust the treatment planning accordingly for further optimization. DVH data is also very useful for further digesting the treatment plans by reviewing biological effects.

2.3.2.2 Tumor dose conformity and homogeneity

When evaluating a radiosurgical treatment plan, tumor dose conformity and homogeneity are key parameters to consider during evaluation as quantitative tools. ICRU Report 62[15] defines a conformity index as a ratio of the treated volume and the planning target volume (PTV). Similarly, stereotactic radiosurgery has a conformity index that is referred to as PITV and defined as the ratio of the prescription isodose (PI) volume to the target volume (TV). Other conformity indices, but less commonly used in practice, have been described for brachytherapy, external beam irradiation and other expressions for radiosurgery.[16-19] Figure 2.8 illustrates how the PITV ratio is determined.

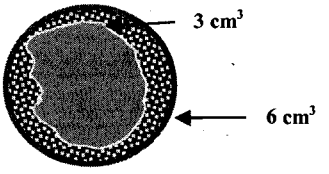

$$PITV = \frac{6\ cm^3}{3\ cm^3} = 2.0$$

Figure 2.8: Example of how the PITV is determined for a stereotactic case. The prescription isodose (red) volume is 6 cm^3 and this is divided by the tumor volume (orange) (3 cm^3) giving a PITV of 2.0.

The PITV index was one of several guidelines proposed by the Radiation Therapy Oncology Group (RTOG) protocol 90-05[20] in the process of evaluating stereotactic radiosurgery treatment plans. When evaluating the PITV parameter, the plan is considered to be per protocol when a value between 1.0 and 2.0 is achieved. Minor protocol deviations are considered when the PITV ratio is between 0.9 and 1.0 or between 2.0 and 2.5. Major protocol deviations are considered when the PITV ratio is less than 0.9 or greater than 2.5.

Dose homogeneity in standard radiotherapy, as described in the ICRU Report 50[21], recommends that the tumor dose homogeneity should be within +7% and –5% of the dose delivered to a well defined prescription point within the tumor. In stereotactic radiosurgery, the tumor dose homogeneity is usually relaxed in order to allow better tumor dose conformity to the target volume. The reason for dose homogeneity requirement relaxation is because a high dose delivered in healthy brain tissue surrounding the tumor significantly increases the risk of complications. The resulting prescription dose to the tumor is then the lowest isodose surface that covers the tumor volume.

The RTOG protocol 90-05,[20] also included the homogeneity index called the MDPD, defined as the ratio between the maximum dose inside the tumor (MD) to the prescription dose (PD). Figure 2.9 illustrates how the MDPD index is calculated.

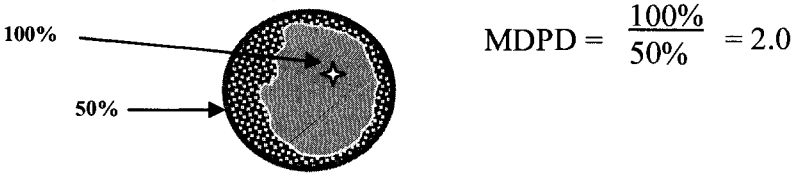

Figure 2.9: Example of how the MDPD is determined for a stereotactic case. The maximum dose in this example is 100 and this is divided by the prescription dose of 50 giving the MDPD to be 2.0.

When evaluating the MDPD parameter, the plan is considered to be per RTOG protocol when a value between 1.0 and 2.0 is achieved. Minor deviations are considered when the MDPD ratio is between 2.0 and 2.5, and major deviation is considered when the MDPD ratio is greater than 2.5.

2.3.2.3 Biological Indices

Biological parameters present the biological aspect of what may occur with a specific treatment plan to various tissues in question. The prescribed dose may be analyzed for its biological effectiveness, tumor control probability and normal tissue complication probability. The treatment plans are analyzed with the following biological indices.

2.3.2.3.1 Integral Biological Effective Dose (IBED)

The biological effective dose (BED) concept is based on the linear-quadratic (LQ) model that assumes there are two components that influence cell killing which results in lethal radiation doses to tissue cells by radiation.[22,23] The first component of the cell survival curve is linearly proportional to dose and the second component is proportional to the square of the dose (see Figure 2.10). The cell surviving curve is described by the following expression

$$S = e^{-\alpha D - \beta D^2} \tag{2.10}$$

where S is the fraction of cells surviving a dose D. α and β are constants characteristic for a particular tissue or tumor irradiated.[23]

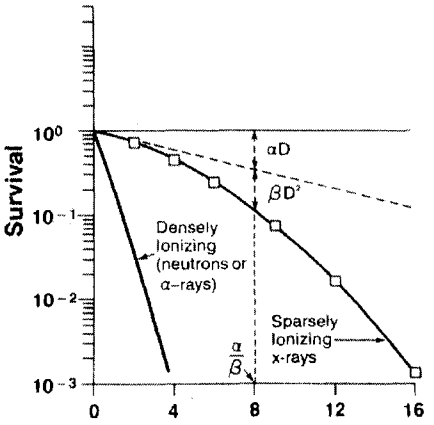

Figure 2.10: This graph shows a typical cell survival curve, illustrating both the linear and quadratic components. The graph is plotted in a logarithmic scale (Number of cells surviving vs dose).(Courtesy of E.J. Hall and A.J. Giaccia, Radiobiology for the Radiologist (Lippincott Williams & Wilkins Publishers, Philadelphia, PA, 2006).

When the two components of the cell survival curve are equal, then the following expression for dose D is

$$D = \frac{\alpha}{\beta}. \tag{2.11}$$

When a single fraction dose is delivered, the biologic effect E of the irradiation is determined by the following expression

$$E = \alpha D + \beta D^2. \tag{2.12}$$

This expression can be rewritten as

$$\frac{E}{\alpha} = D\left(1 + \frac{D}{\frac{\alpha}{\beta}}\right). \tag{2.13}$$

The biological effective dose (BED) can be used to determine the optimal fractionated scheme that will be used for the specific treatment.[23] When multiple fractions are used, the biological effective dose equation becomes

$$\frac{E}{\alpha} = nd\left(1+\frac{d}{\frac{\alpha}{\beta}}\right) \tag{2.14}$$

where n is the number of fractions used for treatment and d is the dose per fraction. This equation means that the biological effective dose is equal to the total dose multiplied with the relative effectiveness.

In determining the values for the α/β ratio for tissues, several values have been widely accepted. For early-responding tissues, a "general" tumor, the α/β is said to be 10 Gy, and for a "general" typical late-responding tissue the α/β is assumed to be 3 Gy.[22, 24] Specifically for our stereotactic radiosurgery study, the accepted α/β values for late responding tissues are actually 2.0 Gy for normal brain tissue and 2.5 Gy for the brain stem.[24]

When conducting stereotactic radiotherapy, the biological effective dose is determined by using the incremental biological effective dose (ΔBED) concept. Because the target is irradiated with a non-homogeneous dose, the differential DVH is used when each dose bin for a particular defined structure is considered to be constant. Therefore, the outlined structure is divided into I dose bins and extends to the maximum dose delivered, i_{th} dose bin. The volume for each dose bin Δv_i is divided by the total volume V of the defined structure that expresses the partial volume for each dose bin.

The IBED is calculated by summing the incremental BED (i.e., ΔBED) for each dose bin from a differential DVH. The ΔBED is expressed as follows

$$\Delta \mathrm{BED} = n \cdot d_i \left(1 + \frac{d_i}{\frac{\alpha}{\beta}} \right) \frac{\Delta v_i}{V}. \tag{2.15}$$

Once each incremental BED has been calculated, the sum of all bins will be the IBED for the specific tissue in question. The IBED[13, 25] is then given by the following expression:

$$\mathrm{IBED} = \sum_i n \cdot d_i \left(1 + \frac{d_i}{\frac{\alpha}{\beta}} \right) \frac{\Delta v_i}{V}. \tag{2.16}$$

2.3.2.3.2 Tumor Control Probability (TCP)

Several mathematical tumor control probability models[26-32] have been used to fit clinical and laboratory data. Many radiobiologists agree that tumors and normal tissues have a characteristic sigmoidal dose-response relationship (see Figure 2.11). In clinical cases it is difficult to specify the point of calculation on the sigmoidal curve, because every tumor on every patient varies as a result of several factors. Tumors strongly depend on factors, such as oxygen and blood supply, factors that may differ throughout the tumor itself and that also may change during radiotherapy. All of these factors further complicate the tumor control probability understanding for any given lesion.

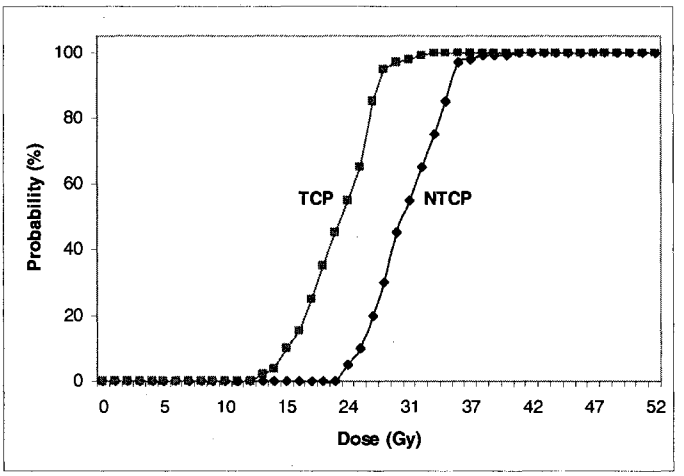

Figure 2.11: This graph shows the characteristic sigmoidal curves for normal tissue complication probability (NTCP) and tumor control probability (TCP).

The most common tumor control probability model is the Poisson model[26] which assumes the cellular lethality is based on Poisson statistics. This assumption means that the probability of a cellular lethality by a direct hit of radiation is extremely small, but because there are many particles in the beam, the mean hit will be a finite number. The equation giving the probability for uniform irradiation of the total organ (partial volume, $v = 1$) to dose D, $P(D, v = 1)$ is given as follows

$$P(D,1) = 2^{-e^{\left[e\cdot\gamma_n\left(1-\frac{D}{D_{50}}\right)\right]}}, \tag{2.17}$$

where D_{50} is the dose required to obtain 50% tumor response and γ_n is a dimensionless number equal to the maximum value of the normalized gradient of the dose-response curve.

Since the irradiation of the tumor is not homogenous, in order to calculate the response probability, the tumor dose-volume response should be modeled on the basic assumptions that the architecture of the tumor is able to be defined in terms of function subunits (FSU).[33,34] For tumors, it is assumed that all FSUs must be inactivated to eradicate it. Therefore, to calculate the response probability, the tumor should be divided

into volumes of constant dose. The calculation of the TCP for the inhomogeneous irradiation is done by taking the product of the response probabilities of the smaller volumes or tumorlets as expressed in the following equation:

$$\mathrm{TCP} = \Pi_i [P(D_i, v_i)], \tag{2.18}$$

where the $P(D_i, v_i)$ is the response of the i^{th} fractional volume v_i irradiated to a dose D_i. The Poisson model used with the fractional volume taken into account with the inhomogeneous irradiation is as follows:

$$P(D,v) = 2^{-e\left[e\cdot\gamma\left(1-\frac{D}{D_{50}}\right)+\ln v\right]}. \tag{2.19}$$

The γ in this study is taken to have a value of 3 as was done by Oliveira.[24] The fraction volume per dose bin is $v = V_i/V_{ref}$, where the dose bin volume is divided by the total volume. The D_{50} should increase with increasing volume of tumor with an approximate log-linear relationship. When assuming a simple form of the dose-response relationship, the Poisson model takes the form of

$$P(D,1) = e^{-N_0 e^{\left(\frac{-D}{D_0}\right)}}, \tag{2.20}$$

where D_0 is the "effective mean lethal dose" and N_0 describes the number of clonogens. Assuming that the clonogenic cell density is $10^7 cm^{-3}$, this will yield $N_0 = 10^7 V$[24,35], where V is the target volume (cubic centimeters). After substituting and rearranging the above terms for N_0 and $D = D_{50}$, the following expression for D_{50} is derived

$$D_{50} = D_0 \ln\left(\frac{10^7 V}{0.693}\right) \tag{2.21}$$

The D_0 value must be known in order to calculate the D_{50}. Taking D_0 to have a value of 3.7 Gy, which is considered to be representative of a "generic tumor," will yield

a TCP of approximately 0.5 for a dose of 60 Gy delivered to 10^7 clonogens using the 2 Gy/fraction radiation therapy scheme. [24,34]

Since the stereotactic radiosurgery is conducted in a single fraction, the original DVH data must be converted to a conventional 2 Gy/fraction scheme so as to fit into the TCP parameters. First, the single fraction doses ($D_{1\text{-fraction}}$) is converted to equivalent 2 Gy per fraction doses ($D_{2\text{ Gy/fraction}}$) using the following BED formalism expression

$$D_{2\text{Gy/fraction}} = D_{1\text{-fraction}} \frac{\left(\frac{\alpha}{\beta} + D_{1\text{-fraction}}\right)}{\left(\frac{\alpha}{\beta} + 2\right)}. \tag{2.22}$$

After the single fraction DVH has been converted to equivalent 2 Gy/fraction DVH, the dose-response probability equation (2.19) can be applied to each dose bin, also taking into account the partial volume for each. The TCP for the treatment plan is then calculated by taking the product of the dose-response probabilities (2.18). In this study, there will be no consideration to treatment time or the oxygen level of the tumor as was the case in other analyses.[24,35,36]

2.3.2.3.3 Normal Tissue Complication Probability (NTCP)

As with TCP models, numerous Normal Tissue Complication Probability (NTCP) models[30,31,37] have been exhibited to explain complications that may occur in normal tissue during irradiation of the tumor by using dose-reponse curves (see Figure 2.11).

The four parameter NTCP model proposed by Lyman[37] in 1985 has been most widely used in the radiation oncology field. For this specific model, the probability for

normal tissue complication to occur for a uniform irradiation of a normal tissue volume V with a dose D is given by the following expression[37]:

$$\mathrm{NTCP} = \frac{1}{\sqrt{2\pi}} \int_{-\infty}^{t(D,v)} e^{\frac{-t^2}{2}} dt' \tag{2.23}$$

$$v = \frac{V_{\mathrm{eff}}}{V_{\mathrm{ref}}} \tag{2.24}$$

$$t = \frac{(D - TD_{50}(v))}{(m \cdot TD_{50}(v))} \tag{2.25}$$

$$TD_{50}(1) = TD_{50}(v) \cdot v^{n} \tag{2.26}$$

The four parameters of the model are given by TD_{50}, m, n and V_{ref}, which have to be adjusted to clinical data for each tissue type by using a specified biological end point. $TD_{50}(1)$ is the tolerance dose for the whole organ volume where there is 50% probability of complications occurring, V_{ref} is the reference volume to which the fractional volume refers to and is obtained from the CT images or taken as a general volume from clinical data, parameter m is related to the slope of the dose-response curve, and parameter n describes the volume effect.

In clinical practice, the Lyman model has to be adjusted to replicate the non-homogeneous irradiation of the normal tissue. Therefore, the model is modified by introducing a histogram-reduction procedure, which transforms the dose volume histogram obtained for a specific outlined structure into a single step histogram

(signifying a uniform dose irradiation). There are two methods used to conduct a histogram-reduction that lead to similar NTCP-values. The first method, introduced by Lyman and Wolbarst[38] in 1987 consists of the two rightmost dose bins of the cumulative DVH replaced by an equivalent value. The NTCP value is then calculated with the same above equations and is repeated until a single-step histogram is achieved. The second method, introduced by Burman and Kutcher[39] in 1991, converts the original differential DVH for a non-homogenous irradiation of normal tissue structure into a single step DVH with an effective volume V_{eff} at the dose D_{max}. The single-step histogram then corresponds to a homogeneous irradiation of the fractional volume $v = V_{eff} / V_{ref}$ and the NTCP is then calculated including the other parameters previously mentioned.

In 1991 Emami et al. [40] published tolerance doses for various tissues and fractional volumes which were developed from clinical experience. The authors considered the values obtained to be high, therefore creating a level of uncertainty. Since then, the data has been used to fit into the Lyman model and calculate NTCP values. The values provided by Emami *et al.*[40] were based on a typical 2 Gy/ fraction radiation therapy scheme and only provide data for uniform irradiation of 1/3, 2/3 and 3/3 organ volume and for NTCP values of 5% and 50%. The endpoint for these tolerance doses was necrosis of the brain and brain stem. For this study, the fit parameters for the Lyman model were utilized from Burman *et al*[41] as was done also by Oliveira[24].

In this study, in order to calculate the NTCP values for the comparison of radiosurgery treatment plans using different modalities, the single fraction doses ($D_{1\text{-}fraction}$) had to first be converted to a typical 2 Gy/fraction dose ($D_{2\ Gy/fraction}$) using the BED formalism expression (2.22). The α/β value for normal tissues are 2.0 Gy for brain

and other normal tissue organs with the exception of the brain stem, α/β has a value of 2.5 Gy.[24]

The effective volume had to be calculated with the following expression:

$$V_{\text{eff}} = \sum V_{\text{i}} \left(\frac{D\text{i}}{D_{\max}} \right)^{\frac{1}{n}}, \tag{2.27}$$

where V_{i} is the sub-volume of the irradiated at the 2 Gy/ fraction dose, D_{i} and $D_{\max}$ is the maximum dose for the equivalent DVH. The summation of these sub-volumes yields the effective volume.

Once the parameters[24,41] were obtained and equations (2.24), (2.25) and (2.26) were calculated, the complication probability was calculated by taking the integration using the NTCP equation (2.23).

The following chapter will describe how the physical and biological parameters were calculated and used accordingly for the comparison of the different stereotactic radiosurgery treatment plans developed from each technique. The setup and materials used will also be explained.

2.4 REFERENCES

[1] BrainSCAN Software Guide Revision 1.0 - Version 5.2x" (BrainLAB, AG, Heimstetten, Germany, 2002).

[2] R. Mohan, C. Chui, and L. Lidofsky, "Energy and angular distributions of photons from medical linear accelerators," Med. Phys. **12**, 592-597 (1985).

[3] R. Mohan, C. Chui, and L. Lidofsky, "Differential pencil beam dose computation model for photons," Med. Phys. **13**, 64-73 (1986).

[4] "SimuPlan treatment planning system manual-version for Apple Macintosh power PC computers" (SimuPlan Sociedad Limitada, Valencia, Spain, 2000).

[5] B. G. Pike, E. B. Podgorsak, T. M. Peters, and C. Pla, "Dose distributions in dynamic stereotactic radiosurgery," Med. Phys. **14**, 780-789 (1987).

[6] M. R. Bussiere and J. A. Adams, "Treatment Planning for Conformal Proton Radiation Therapy," Tech. Canc. Res. Treat., **2**, 389-399, (2003).

[7] H. Paganetti, A. Niemierko, M. Ancukiewicz, L. E. Gerweck, M. Goitein, J. S. Loeffler, H. D. Suit, and D. Phil, "Relative biological effectiveness (RBE) values for proton beam therapy," Int. J. Radiat. Oncol., Biol., Phys. **53**, 407-421 (2002).

[8] L. Hong, M. Goitein, M. Bucciolini, R. Comiskey, B. Gottschalk, S. Rosenthal, C. Serago, and M. Urie, "A pencil beam algorithm for proton dose calculations," Phys. Med. Biol. **41**, 1305-1330 (1996).

[9] "Leksell Gamma Knife ® 4C System Description Guide," (Elekta, Stockholm, Sweden, 2004).

[10] A. Wu, G. Lindner, A. H. Maitz, A. M. Kalend, L. D. Lunsford, J. C. Flickinger, W. D. Bloomer, "Physics of gamma knife approach on convergent beams in stereotactic radiosurgery," Int. J. Radiat. Oncol., Biol., Phys. **18**, 941-949 (1990).

[11] A. Wu, "Physics and dosimetry of the gamma knife," Neurosurg. Clinics of N.A., **3**, 35-50 (1992).

[12] R. E. Drzymala, R. Mohan, L. Brewster, J. Chu, M. Goitein, W. Harms, and M. Urie, "Dose-volume histograms," Int. J. Radiat. Oncol., Biol., Phys. **21**, 71-78 (1991).

[13] B. G. Clark, L. Souhami, C. Pla, A. S. Al-Amro, J. P. Bahary, J. G. Villemure, J. L. Caron, A. Olivier, and E. B. Podgorsak, "The integral biologically effective dose to predict brain stem toxicity of hypofractionated stereotactic radiotherapy," Int. J. Radiat. Oncol., Biol., Phys. **40**, 667-675 (1998).

14 G. J. Kutcher, "Quantitative plan evaluation: TCP/NTCP models," Front. Radiat. Ther. Oncol. **29**, 67-80 (1996).

15 International Commission on Radiation Units and Measurement, Inc. Report 62, Prescribing, Recording and Reporting Photon Beam Therapy (Supplement to ICRU Report 50) (ICRU, Bethesda, MD, 1999).

16 A. V. Riet, C. A. Mak, M. A. Moerland, L. H. Elders, and W. V. D. Zee, "A conformation number to quantify the degree of conformality in brachytherapy and external beam irradiation: Application to the prostate," Int. J. Radiat. Oncol., Biol., Phys. **37**, 731-736 (1997).

17 D. Baltas, C. Kolotas, K. Geramani, R. F. Mould, G. Ioannidis, M. Kekchidi, and N. Zamboglou, "A conformal index (COIN) to evaluate implant quality and dose specification in brachytherapy," Int. J. Radiat. Oncol., Biol., Phys. **40**, 515-524 (1998).

18 N. J. Lomax and S. G. Scheib, "Quantifying the degree of conformity in radiosurgery treatment planning," Int. J. Radiat. Oncol., Biol., Phys. **55**, 1409-1419 (2003).

19 L. Feuvret, G. Noel, J. J. Mazeron, and P. Bey, "Conformity index: A review," Int. J. Radiat. Oncol., Biol., Phys. **64**, 333-342 (2006).

20 E. Shaw, R. Kline, M. Gillin, L. Souhami, A. Hirschfeld, R. Dinapoli, and L. Martin, "Radiation Therapy Oncology Group: Radiosurgery Quality Assurance Guidelines," Int. J. Radiat. Oncol., Biol., Phys. **27**, 1231-1239 (1993).

21 International Commission on Radiation Units and Measurement, Inc. Report 50, Prescribing, Recording and Reporting Photon Beam Therapy (ICRU, Bethesda, MD, 1993).

22 J. F. Fowler, "The linear quadratic formula and progress in fractionated radiotherapy-Review article," Br. J. Radiol. **62**, 679-694 (1989).

23 E.J. Hall and A.J. Giaccia, Radiobiology for the Radiologist (Lippincott Williams & Wilkins Publishers, Philadelphia, PA, 2006).

24 S. C. Oliveira, Comparison of three linac-based stereotactic radiosurgery techniques, M. Sc. Thesis, McGill University, Montreal, Quebec, (2003).

25 P. W. Hoban, L. C. Jones, and B. G. Clark, "Modeling late effects in hypofractionated stereotactic radiotherapy," Int. J. Radiat. Oncol., Biol., Phys. **43**, 199-210 (1998).

[26] T. R. Munro and C. W. Gilbert, "The relation between tumor lethal doses and the radiosensitivity of tumor cells," Br. J. Radiol. **34**, 246-251 (1961).

[27] T. E. Schultheiss, C. G. Orton, and R. A. Peck, "Models in radiotherapy: Volume effects," Med. Phys. **10**, 410-415 (1983).

[28] M. Goitein and T. E. Schultheiss, "Strategies for treating possible tumor extension: Some theoretical considerations," Int. J. Radiat. Oncol., Biol., Phys. **11**, 1519-1528 (1985).

[29] G. J. Kutcher and C. Burman. "Calculation of complication probability factors for non-uniform normal tissue irradiation: The effective volume method," Int. J. Radiat. Oncol., Biol., Phys. **16**, 1623-1630 (1989).

[30] G. J. Kutcher, Z. Fuks, H. Brenner, A. P. Brown, C. Burman, E. Cheng, L. Coia, K. Krippner, J. M. Manolis, R. Mohan, J. R. Simpson, M. Urie, B. Vikram, and R. Wallace, "Three-dimensional photon treatment planning for carcinoma of the nasopharynx," Int. J. Radiat. Oncol., Biol., Phys. **21**, 169-182 (1991).

[31] A. Niemierko and M. Goitein, "Modeling of normal tissue response to radiation: The critical volume model," Int. J. Radiat. Oncol., Biol., Phys. **25**, 135-145 (1993).

[32] P. Okunieff, D. Morgan, A. Niemierko and H. D. Suit, "Radiation dose-response of human tumors," Int. J. Radiat. Oncol., Biol., Phys. **32**, 1227-1237 (1995).

[33] W. Schlegel, T. Bortfeld, and A. L. Grosu, New Technologies in Radiation Oncology (Springer, Berlin, Heidelberg, NewYork, 2006).

[34] V. Smith, L. Verhey, and C. F. Serago, "Comparison of radiosurgery treatment modalities based on complication and control probabilities," Int. J. Radiat. Oncol., Biol., Phys. **40**, 507-513 (1998).

[35] S. Webb and A. E. Nahum, "A model for calculating tumour control probability in radiotherapy including the effects of inhomogeneous distributions of dose and clonogenic cell density," Phys. Med. Biol. **38**, 653-666 (1993).

[36] J. E. Mignano, M. J. Engler, J. S. Tsai, and D. E. Wazer, "Comparison of radiobiologic modeling for one- and two- isocenter dose distributions applied to ellipsoidal radiosurgery targets," Int. J. Radiat. Oncol., Biol., Phys. **49**, 833-837 (2001).

[37] J. T. Lyman, "Complication probability as assessed from dose-volume histograms," Radiat. Res. **104**, S13-S19 (1985).

[38] J. T. Lyman and A. B. Wolbarst, "Optimization of radiation therapy, III: A method of assessing complication probabilities from dose-volume histograms," Int. J. Radiat. Oncol., Biol., Phys. **13**, 103-109 (1987).

[39] G. J. Kutcher, C. Burman, L. Brewster, M. Goitein, and R. Mohan, "Histogram reduction method for calculating complication probabilities for three-dimensional treatment planning evaluations," Int. J. Radiat. Oncol., Biol., Phys. **21**, 137-146 (1991).

[40] B. Emami, J. Lyman, A. Brown, L. Coia, M. Goitein, J. E. Munzenrider, B. Shank, L. J. Solin, and M. Wesson, "Tolerance of normal tissue to therapeutic irradiation," Int. J. Radiat. Oncol., Biol., Phys. **21**, 109-122 (1991).

[41] C. Burman, G. J. Kutcher, B. Emami, and M. Goitein, "Fitting of normal tissue tolerance data to an analytical function," Int. J. Radiat. Oncol., Biol., Phys. **21**, 123-135 (1991).

CHAPTER 3

METHODS AND MATERIALS

3.1 PHANTOM TARGETS

3.1.1 Phantom Targets and Setup

The comparison study amongst the four stereotactic radiosurgery techniques was performed using six phantom test cases in which the lesions varied in size, shape and volumetric complexity. Table 3.1 provides the general shape and volume of the tumor and critical organ for each of the six phantom test cases. The lesions created for the comparisons were placed near critical structures. The tumors were less than a millimeter away from a critical organ and for some cases, surrounded a portion of the critical organ.

Case Number	Organ	Volume (cm^3)	General Shape
Test Case 1	Tumor	26.2	Irregular & surrounding critical organ
	Critical Organ	2.3	Ellipsoid
Test Case 2	Tumor	6.6	Oblate spherical
	Critical Organ	1.1	Ellipsoid
Test Case 3	Tumor	18.4	Ellipsoid with hemispherical ends (z-axis)
	Critical Organ	3.2	Triangular
Test Case 4	Tumor	16.5	Irregular & surrounding critical organ
	Critical Organ	1.8	Ellipsoid
Test Case 5	Tumor	24	Irregular with 4 extending points & surrounding critical organ
	Critical Organ	1.8	Ellipsoid
Test Case 6	Tumor 1	8	Spherical
	Tumor 2	6	Ellipsoid
	Critical Organ	9.1	Triangular

Table 3.1: General description of the tumors and critical organs examined in the treatment planning comparison using various radiosurgical techniques and machines.

The six test cases were developed to challenge the planner's ability: 1) to conform the prescription dose distribution to the tumor volume (PITV) and 2) maintain tumor dose homogeneity (MDPD) while minimizing the dose to the surrounding tissues.

Treatment planning was conducted on the test cases by using a modified Alderson Rando® anthropomorphic phantom (Radiology Support Devices Inc., Long Beach, CA, USA). Two slabs from the head phantom were replaced with a single, duplicate machined "water equivalent" solid piece with a centered square opening for the tumor case block inserts. The individual tumor cases were made of machinable wax. Each tumor test case was composed of two matching wax blocks that were inserted in the square opening in the head phantom. The structures in the blocks were machined by drilling with an electric tool to create the three-dimensional shapes (see Figure 3.1). The volumes of the structures were measured using water through a pipette with ±2% accuracy. The air-volumes were measured to have a known reference volume for each structure prior to outlining the lesions and critical organs in each treatment planning system from CT images. The reference volume was done because a treatment planning system that would allow all techniques to be planned on it did not exist, and some planning systems could not import DICOM-RT in this thesis project. Therefore, each structure had to be contoured in each treatment planning system and was modified accordingly to be within ±2% of the reference volume measured and each structure contoured was visually compared and corrected per CT slice on all four treatment planning systems.

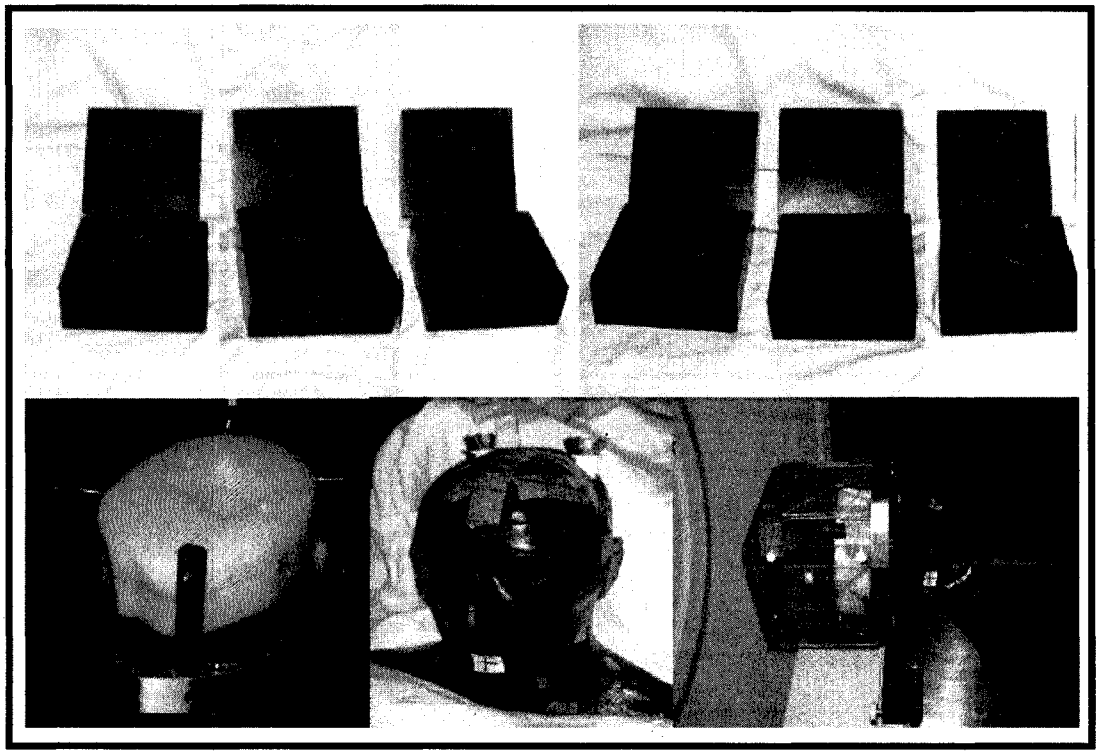

Figure 3.1 The phantom test cases block insert for Cases 1 through 6 in order from left to right(top row). The frame attached to the modified slab insert for the Rando head phantom. The square opening can be seen as the 4 pins fixed to the slab were never unattached during the scanning (bottom left). Alderson Rando® Phantom (bottom middle). The Rando® phantom completely assembled with insert case pair blocks and CT attachment on the stereotactic radiosurgery frame prior to acquiring images (bottom right).

3.1.2 Collection of Images for the Different Treatment Planning Systems

The collection of the diagnostic images was performed on a Picker PQ-5000 CT scanner (Philips Medical Systems, Cleveland, OH, USA) installed at the Montreal General Hospital. For each collection of image sets, six cases total, the Alderson Rando® phantom was assembled with the modified machined "water equivalent" solid piece to which the stereotactic radiosurgery frame was anchored with four screws. The tumor and critical organ pair blocks were inserted in the square opening (each case individually) and after the phantom head was reassembled, the CT-compatible localizer box was attached to the frame. Image slices were acquired from the top of the skull to the upper portion of the frame with a 2 mm slice thickness (increment) (see Figure 3.2).

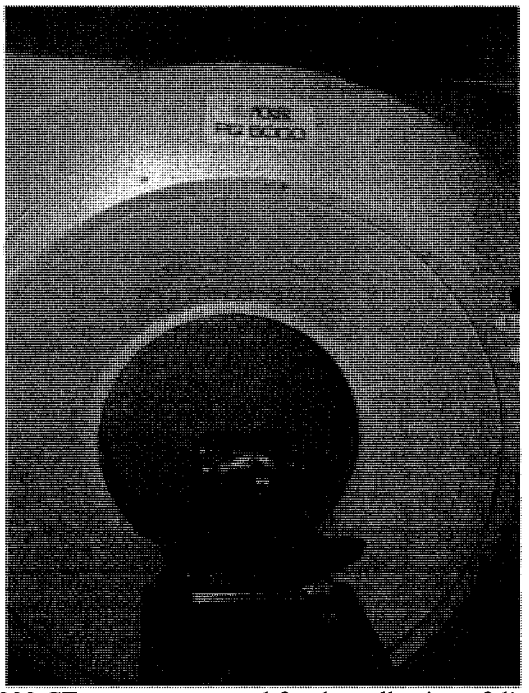

Figure 3.2: The Picker PQ-5000 CT scanner was used for the collection of diagnostic images for the six test case studies.

The CT image series for the six test cases were sent to the individual treatment planning systems, where the structures were contoured onto each appropriate image slice. The outlined volumes were within ±2% of the reference volume measured as discussed in Section 3.1.1. The images were localized relative to the stereotactic coordinate frame or, as explained in Section 2.2.3 for proton therapy, using the CMS XiO treatment planning system.

3.2 GENERATING OPTIMUM TREATMENT PLANS

3.2.1 Static Conformal Beam Technique (Linac)

The BrainSCAN version 5.2x treatment planning system (BrainLAB, AG, Heimstetten, Germany) was used for the static conformal beam radiosurgery technique based on the BrainLAB m3 micro-multileaf collimator, as explained in Section 2.2.1. The static beams used with this technique are noncoplanar to spread the dose over a large

volume throughout the normal brain tissue, and the beam entry points are in the upper hemisphere of the skull to avoid opposing beams and any other overlapping of the photon beams that may increase the dose to normal tissue.

The typical treatment planning procedure is as follows: during the planning for each specific case, the planner first placed an isocenter in the center-of-mass of the lesion. Additional beams added are focused onto the isocenter located within the lesion and are modified accordingly using the BEV display. As explained in Section 2.2.1, the collimator is optimized to minimize the dose to normal tissue, and the individual leafs are adjusted to account for the beam penumbra and minimization of dose to normal tissue as well. A typical margin of 0.4 mm is added to each beam and the target is fully covered by the 80% isodose surface. The plan is then normalized to the 100% isodose surface for the maximum dose to display the homogeneity inside the lesion.

Several plans were developed for each test case using different number of beams. Typically, six to twelve beams per lesion were used during the planning. Plans were evaluated using two-dimensional isodose displays to quickly inspect the coverage and conformity around the tumor and minimization of dose to the critical structures. DVHs were processed to inspect the doses delivered to the volumes covered per dose bin. Calculating the DVHs gave the planner an additional tool for deciding whether or not the plan could be further optimized to improve the PITV and MDPD physical parameters.

3.2.2 Static Cone-Based Beam Technique (Linac)

The static cone-based beam technique used the SimuPlan, version 8.1c treatment planning system. The typical treatment planning procedure proceeds as follows: For the

various phantom test cases, the planner selects different field collimator sizes to conform the dose distribution to the lesion. Typically, ten static noncoplanar beams are used per isocenter for this technique, as described in detail in Section 2.2.2 giving a spherical dose distribution inside the target when a single beam is used for radiosurgery. Depending on the size, shape and complexity of the tumor, the planner has to decide on the number of isocenters to be used to adequately cover the tumor. Generally, if the tumor is spherical-like in shape, the planner can use a single isocenter, providing the dose distribution adequately covers the lesion with the specified collimator size, and the result will be a higher level isodose surface prescription value. If a single isocenter is used, the prescription isodose surface is of the order of 80%.

The majority of the tumor phantom test cases involved in our study were larger lesions, irregular in shape and near a critical structure as discussed in Section 3.1.1. The goal of the planner was to conform the dose distribution to the lesion; however, to obtain this goal with minimal dose to healthy tissue, typical treatment plans had 20-30 isocenters per lesion. One case had 43 isocenters, and a spherical and ellipsoid shaped lesions had 3 or less isocenters. A high number of isocenters is not practical in the clinic due to the high demand of time on the patient and the treatment team. Nonetheless, the plans with high number of isocenters were performed to see how well the treatment planning system could adjust to the irregular shape of the lesions.

The planner had to manually place the isocenters within the lesion to cover fully the tumor volume and this was done by visually inspecting the isodose lines superimposed on the two-dimensional axial images. By changing the collimator sizes and carefully moving the isocenters on the three-dimensional coordinates, the planner

strived to achieve relatively low PITV values (see Chapter 4). Also, the use of DVHs was essential for determining the volume percentages covered by each dose bin and also aided the planner in adjusting the isocenters accordingly. Typically, dose for the larger and/or irregular shaped lesions in the study were prescribed to the 50% isodose surface, which was then renormalized to 100% to obtain the dose homogeneity inside the tumor.

3.2.3 Proton Therapy (Spread-Out Bragg Peak Technique)

For treatment planning in proton stereotactic radiosurgery using the spread-out Bragg peak (SOBP) technique, the CMS XiO treatment planning system was used.

The planner had to use a different approach when planning the treatment for the six different phantom cases using protons. The proton beam characteristics were described in Section 2.2.3; the exit dose was not a concern in the planning and the planner could use opposing beams. Moreover, treatment planning was performed using the gantry delivery system which had modulation increments of 6 mm, as opposed to the STAR delivery system that had a 1 mm increment modulation capability. The latter was unavailable for the study.

During treatment planning for the individual phantom cases, the planner, after localization was conducted as described in Section 2.2.3, placed an isocenter in the center-of-mass for the outlined lesion. Using three to four fields or portals per lesion, the planner selected each point of entry, while avoiding critical structures. The prescription isodose was approximately 90% for all test cases; therefore, the dose inside the lesion was homogeneous, giving a low MDPD (see Chapter 4). With each portal, the planner had to shape the field so as to contour the shape of the lesion which included the 50-90%

isodose surfaces. Once done, the beam modulation was calculated and entered to ensure that the SOBP of the 90% isodose contour covered the tumor for the beam. Also, the air-gap distance between the compensator (placed at the end of nozzle) and the patient was 2 cm. The compensator distance was also calculated and entered for each port by the planner. After each beam was completed, the planner optimized the plans by visually inspecting the two-dimensional axial images and by the use of the DVHs. Again, the planner encompassed the entire lesion by the prescription isodose which was then renormalized to 100% to the prescribed dose for the lesion.

3.2.4 Leksell Gamma Knife

The Leksell Gamma Knife® 4C's treatment planning system for stereotactic radiosurgery was the GammaPlan® 4C. The typical treatment planning procedure is as follows: For developing a radiosurgery treatment plan, the planner first measures the distance to the skull (head phantom) using the "bubble" skull attachment, as shown in Figure 2.4. There are 24 fixed points that the planner has to measure, annotate and enter into the treatment planning system. These distances are incorporated during the dose calculation by the planning system.

In our work, an exact replica of the test phantom was used for measurement of the points. The "bubble" attachment was placed on the stereotactic frame, which the planner then had to make minor adjustments for a better contour of the skull in the planning system. For each phantom test case, the planner executed the GammaPlan ® 4C Wizard^{TM} to obtain a more efficient method of placing the isocenters throughout the lesion using an 8 mm size collimator helmet. The 8 mm collimator helmet was used to

give a more conformal dose distribution in the lesion, than would be obtained with the larger size helmets. The GammaPlan ® 4C Wizard™ solution was not exact since the planner strictly selected the 8 mm collimator size helmet. In addition, the manual placement of isocenters with the 4 mm size collimator helmet by the planner was done to complete the planning.

Some treatments in the clinic with the Gamma Knife may have up to 18 isocenters, but typically less than 10 isocenters are used for treatment planning clinical and dose delivery. Similar to the static cone beam technique using SimuPlan, the planner was trying to test the ability of the planning system to achieve a low PITV. The planner was able to get reasonable solutions (see Chapter 4) for dose conformity, but the treatment plans for the larger and/or irregular sized lesions typically had 20-30 isocenters.

Using the two-dimensional axial images, the planner ensured that the lesion was encompassed by the highest isodose surface. Similar to the SimuPlan treatment planning system, once the planner had selected the highest isodose surface that covered the lesion, renormalized to 100% was performed to the prescription dose. Using the DVHs the planner was able to optimize the plans by viewing the volume covered by the dose distribution and evaluate whether or not the critical organ was being spared.

3.3 PLAN EVALUATION

For all six phantom test cases, the lesions, regardless of their shape or size, were given a prescription dose of 20 Gy; therefore, the RTOG protocol 90-05[1] was not followed for the dose prescription guidelines for diameters of lesion. The prescription dose was prescribed to the highest isodose surface that fully encompassed the lesion for

all proton and linac techniques. For Gamma Knife treatment planning a treatment plan was considered acceptable if more than 97% of the lesion was covered by the prescription isodose contour. Here, we followed the practice in effect in the clinic where the treatment planning was performed. The selection of an optimum treatment plan per technique for each test case study was performed by selecting a plan that best satisfied tumor coverage with minimal dose to the nearby critical structures and normal tissue. While a comparison of optimal plans created by several independent users would have been beneficial, it was not possible within the scope of this thesis. All plans were created by a single user.

The selected treatment plan for each technique for each test case study provided the DVH data which was used to calculate the physical and biological indices, as described in Section 2.3. Since each treatment planning system had its own DVH algorithm that may have created different results, this factor was not taken into consideration in this study. The resulting uncertainty associated with these differences was not assessed.

3.3.1 Conformity (PITV) and Homogeneity (MDPD) Indices

The physical indices, as described in Section 2.3.2.2, were used for the comparison study between the four techniques. As described earlier, when calculating the conformity index (PITV), the ratio of the prescribed isodose volume to the tumor volume was determined. The conformity index (PITV) was automatically provided only in the static conformal beam technique for each treatment plan using the BrainSCAN treatment planning system. For the remaining three techniques, PITV was calculated

manually using the cumulative DVH at the prescription dose of 20 Gy for the tumor and normal tissue volumes. The calculation was the volume of the prescription isodose surface which included the sum of normal tissue volume and tumor volume divided by the actual tumor volume. When calculating the homogeneity index (MDPD), the maximum dose in the treatment plan was divided by the prescription dose. The homogeneity index was calculated manually for each test case and for each technique.

3.3.2 Integral Biological Effective Dose (IBED)

The integral biological effective dose (IBED) was calculated for each optimum treatment plan for each technique and for all phantom test cases that included the tumor, critical organs including the brain stem for test case 6 and normal tissue. The volumes for these structures were obtained from the CT images after being contoured, and for the normal brain tissue, a reference volume of 1500 cm^3 was used for the IBED calculations.

The IBED calculations were performed using EXCEL spreadsheets (Microsoft Corporation, Seattle, WA, USA) with the differential DVHs acquired for the structures outlined in each treatment plan. Each dose bin from the DVH was calculated to obtain the incremental BED (ΔBED), as described in Section 2.3.2.3.1 using equation (2.15). After the incremental BEDs were calculated for each dose bin, the sum of all ΔBEDs gave the IBED for the specific structure being examined. The IBED calculation for the brain was only summed from specific dose levels and higher, since the Gamma Plan could only calculate dose within the dose matrix. Therefore, the $IBED_{brain}$ was calculated by summing from a specific dose bin and higher, such as following: Test case 1 (≥15 Gy); Test case 2 (≥10 Gy); Test case 3 (≥15 Gy); Test case 4 (≥15 Gy), Test case 5 (≥15

Gy); and Test case 6 (≥18 Gy). Table A.1 in Appendix A displays an EXCEL spreadsheet example on how the IBED was calculated for the tumor in Test case 2 using the static conformal beam technique.

3.3.3 Tumor Control Probability (TCP)

Tumor control probabilities (TCPs) were calculated using EXCEL spreadsheets, as explained in Section 2.3.2.3.2; for all six test case studies for each optimum treatment plan selected from each technique. The differential DVH data acquired from each plan was used for TCP calculations, but first the single fraction dose bins had to be converted into fractionated dose bins using a 2 Gy per fraction scheme. The conversion was performed using equation (2.22) with the α/β ratio for the tumor having a value of 10 Gy.

After the 2 Gy per fraction equivalent differential DVH was calculated for each dose bin, equation (2.19) was used to calculate the probability for each dose bin. The individual Poisson probabilities had to be multiplied; therefore, the product of the individual probabilites gave the TCP for each treatment plan. Table A.2 in Appendix A displays an example of a TCP calculation for the static conformal beam technique treatment plan for test case 2.

3.3.4 Normal Tissue Complication Probability (NTCP)

The normal tissue complication probability (NTCP) calculated for each critical organ, including the brain stem for test case 6, used the Lyman model, as described in Section 2.3.2.3.3. Calculation of NTCP for each optimum treatment plan from each

technique for each case was performed by using equation (2.23) incorporating the clinical data, as discussed in Section 2.3, along with the fitting parameters as shown in Table 3.2.

	Fit Parameters				
Organ	V_{ref}	n	m	TD_{50}	**End point**
Brain	Whole organ	0.25	0.15	60	Necrosis/ infarction
Brain stem	Whole organ	0.16	0.14	65	Necrosis/ infarction

Table 3.2: Above are the fit parameters used for the calculations as discussed in Section 2.3. (Courtesy of C. Burman, G. J. Kutcher, B. Emami, and M. Goitein, "Fitting of normal tissue tolerance data to an analytical function," Int. J. Radiat. Oncol., Biol., Phys. **21**, 123-135 (1991).

Similar to TCP calculations, the 2 Gy per fraction equivalent differential DVH needed to be calculated first from the single fraction DVH for each dose bin using equation (2.22) with the following α/β ratios: 2.0 Gy (critical organ and normal brain tissue) and 2.5 Gy (brain stem). Then, for each 2 Gy per fraction equivalent differential dose bin, a partial effective volume needed to be calculated, which then through the summation of all partial effective volumes provided V_{eff} as performed using equation (2.27). Using V_{eff} and V_{ref}, the planner could then acquire the fractional volume, v and obtain the $D_{\max}$ (maximum dose from the 2 Gy per fraction equivalent DVH) from the dose bins. Using the appropriate clinical parameters ($TD_{50}(1)$, m, and n) and calculated values, equations (2.24), (2.25) and (2.26) were then used to calculate the upper limit, parameter t for equation (2.23). NTCP values for each optimum treatment plan representing each technique were calculated by solving each integral using equation (2.23). The integral was calculated using the software program, MAPLE 10 (Maplesoft^{TM},Waterloo, ON). The limits taken for the integration were from $-\infty$ to the calculated t value. Table A.3 in the Appendix shows an example of the calculated NTCP value for normal brain tissue using the static conformal beam technique for test case 2.

3.4 REFERENCES

1 E. Shaw, R. Kline, M. Gillin, L. Souhami, A. Hirschfeld, R. Dinapoli, and L. Martin, "Radiation Therapy Oncology Group: Radiosurgery Quality Assurance Guidelines," Int. J. Radiat. Oncol., Biol., Phys. **27**, 1231-1239 (1993).

CHAPTER 4

RESULTS AND DISCUSSION

4.1 PHANTOM TARGETS TO BE EVALUATED BY FOUR RADIOSURGICAL TECHNIQUES

The optimum stereotactic radiosurgery treatment plans created with each of the treatment techniques are compared by using the physical and biological indices described and defined in Chapter 2 and Chapter 3. Treatment plans for each test case are analyzed taking into consideration the lesions' general shape, volume, and complexity. The conformity parameter, PITV, is used to select the optimum treatment plan for each technique. Also, the dose homogeneity parameter, MDPD, is used in the comparison among the different techniques for the treatment of given lesion.

The lesions, as described in Section 3.1.1, are more laborious and exceptional test case studies for the planner than one would typically encounter in the clinic. The lesions are complex, since they are located near a critical organ and sometimes surround the critical organ. The different test case studies are designed to be limiting cases for the various techniques in their capabilities for dose conformity and dose homogeneity. Since the same dose of 20 Gy is prescribed for all test cases regardless of tumor size, the dose administered may not be optimal and parameters, such as NTCP and TCP, may not be accurate in an absolute sense in regards to predicting actual outcomes. Therefore, the results calculated for NTCP and TCP should be viewed in a relative sense in the ranking of the techniques.

The actual NTCP and TCP values calculated in the different test case studies, are presented in Sections 4.2 and 4.3, and should not be viewed as absolute but rather as a

relative measurement between the treatment plans created. The following sections will present and discuss the results for the calculated physical and biological parameters from the four stereotactic radiosurgery techniques for each studied with six test phantoms.

4.2 RESULTS FROM COMPARITIVE STUDY—PHYSICAL AND BIOLOGICAL PARAMETERS

Tables 4.1 through 4.6 display the best plan created by the planner for each test case study for each technique. While an in-depth error analysis was not performed on these results, there could be some uncertainty due to differences in contouring, DVH algorithms and in dosimetry models for the different planning systems used. As mentioned earlier, the PITV parameter is used as a planning tool for deciding the optimum plan from each technique. Several parameters are presented, such as TCP, NTCP and IBED, for the tumor and brain, including IBED brain stem for test case 6.

Test Case 1 Lesion: 26.2 cm^3	Static cone-based	Gamma Knife	Static Conformal	Proton SOBP
PITV	2.14	2.30	1.35	1.55
MDPD	1.98	2.50	1.17	1.14
TCP(%)	16.64	28.50	5.26	2.72
$NTCP_{brain}$(%)	88.70	99.00	0.00	2.71
$IBED_{tumor}$ (Gy_{10})	95.52	124.47	72.83	70.20
$IBED_{brain}$ (Gy_2)	9.48	12.30	3.63	5.01
Beam(s)/Isocenter(s) combination	4 isocenters	29 isocenters	10 beams	4 fields

Table 4.1: Physical parameters (PITV and MDPD), biological parameters (TCP, NTCP, IBED for the tumor and brain) and the number of beams/isocenters for each optimum treatment plan acquired using the static cone-based, Gamma Knife, static conformal beam and proton SOBP techniques for test case 1 are presented.

Test Case 2 Lesion: 6.6 cm^3	Static cone-based	Gamma Knife	Static Conformal	Proton SOBP
PITV	1.70	2.15	1.20	1.39
MDPD	1.25	2.50	1.20	1.11
TCP(%)	47.76	52.28	16.75	9.44
$NTCP_{brain}$(%)	0.18	100.00	0.01	0.02
$IBED_{tumor}$ (Gy_{10})	81.84	189.58	73.35	69.50
$IBED_{brain}$ (Gy_2)	1.79	4.54	1.13	1.66
Beam(s)/Isocenter(s) combination	1 isocenter	1 isocenter	10 beams	3 fields

Table 4.2: Physical parameters (PITV and MDPD), biological parameters (TCP, NTCP, IBED for the tumor and brain) and the number of beams/isocenters for each optimum treatment plan acquired using the static cone-based, Gamma Knife, static conformal beam and proton SOBP techniques for test case 2 are presented.

Test Case 3 Lesion: 18.4 cm^3	Static cone-based	Gamma Knife	Static Conformal	Proton SOBP
PITV	1.70	2.20	1.27	1.47
MDPD	2.00	2.00	1.22	1.12
TCP(%)	64.26	29.49	13.63	3.54
$NTCP_{brain}$(%)	9.45	97.70	0.16	0.80
$IBED_{tumor}$ (Gy_{10})	115.08	108.58	75.95	69.74
$IBED_{brain}$ (Gy_2)	3.99	7.16	2.03	3.74
Beam(s)/Isocenter(s) combination	3 isocenters	26 isocenters	10 beams	3 fields

Table 4.3: Physical parameters (PITV and MDPD), biological parameters (TCP, NTCP, IBED for the tumor and brain) and the number of beams/isocenters for each optimum treatment plan acquired using the static cone-based, Gamma Knife, static conformal beam and proton SOBP techniques for test case 3 are presented.

Test Case 4 Lesion: 16.5 cm^3	Static cone-based	Gamma Knife	Static Conformal	Proton SOBP
PITV	2.01	2.28	1.36	1.53
MDPD	2.00	2.00	1.20	1.12
TCP(%)	15.47	35.84	10.80	4.27
$NTCP_{brain}$(%)	15.39	97.65	0.25	0.73
$IBED_{tumor}$ (Gy_{10})	93.87	109.34	74.07	70.08
$IBED_{brain}$ (Gy_2)	6.16	6.81	2.28	3.31
Beam(s)/Isocenter(s) combination	4 isocenters	26 isocenters	10 beams	3 fields

Table 4.4: Physical parameters (PITV and MDPD), biological parameters (TCP, NTCP, IBED for the tumor and brain) and the number of beams/isocenters for each optimum treatment plan acquired using the static cone-based, Gamma Knife, static conformal beam and proton SOBP techniques for test case 4 are presented.

Test Case 5 Lesion: 24 cm^3	Static cone-based	Gamma Knife	Static Conformal	Proton SOBP
PITV	2.30	2.30	1.63	1.66
MDPD	1.72	1.89	1.20	1.13
TCP(%)	20.60	13.82	7.57	2.73
$NTCP_{brain}$(%)	70.69	98.11	3.98	3.71
$IBED_{tumor}$ (Gy_{10})	91.57	97.63	74.06	70.05
$IBED_{brain}$ (Gy_2)	9.19	9.92	5.11	5.50
Beam(s)/Isocenter(s) combination	7 isocenters	30 isocenters	10 beams	3 fields

Table 4.5: Physical parameters (PITV and MDPD), biological parameters (TCP, NTCP, IBED for the tumor and brain) and the number of beams/isocenters for each optimum treatment plan acquired using the static cone-based, Gamma Knife, static conformal beam and proton SOBP techniques for test case 5 are presented.

Test Case 6 Lesion 1: 8 cm^3 Lesion 2: 6 cm^3		Static cone-based	Gamma Knife	Static Conformal	Proton SOBP
PITV		2.49	2.21	1.45	1.40
MDPD		1.98	1.95	1.21	1.11
TCP_{tumor1}(%)		26.93	51.07	20.18	8.05
TCP_{tumor2}(%)		43.97	47.46	16.85	7.83
$NTCP_{brain}$ (%)		17.50	95.60	0.23	0.38
$NTCP_{brain\ stem}$(%)		0.82	0.84	0.22	0.00
$IBED_{tumor1}$ (Gy_{10})		77.90	110.22	75.02	69.67
$IBED_{tumor2}$ (Gy_{10})		96.66	110.40	72.41	68.89
$IBED_{brain}$ (Gy_2)		5.04	5.04	1.45	1.93
$IBED_{brain\ stem}$ ($Gy_{2.5}$)		27.35	40.35	15.94	3.87
Beam(s)/Isocenter(s) combination	Lesion 1	1 isocenters	24 isocenters	10 beams	3 fields
	Lesion 2	3 isocenters	23 isocenters	10 beams	3 fields

Table 4.6: Physical parameters (PITV and MDPD), biological parameters (TCPs, NTCPs, IBED for the tumors, brain stem and brain) and the number of beams/isocenters for each optimum treatment plan acquired using the static cone-based, Gamma Knife, static conformal beam and proton SOBP techniques for test case 6 are presented.

According to Tables 4.1 through 4.6, the technique creating treatment plans with the lowest PITV value is the static conformal beam technique, followed closely by the proton SOBP technique (with the exception of the complex test case 6 where the PITV value for the proton SOBP technique is lower than that for the static conformal technique), followed by the static cone-based technique and finally by the Gamma Knife technique, with the exception of the test case 5 and test case 6. In test case 5, the two techniques produced the same PITV value and in test case 6, the PITV value for the Gamma Knife technique is slightly lower than that for the static cone-based technique.

The proton SOBP technique produced the lowest MDPD value, followed by the static conformal beam technique for all test cases. The next two higher MDPD parameter values are produced by the static cone-based technique, followed by the Gamma Knife technique with the exception of test case 3 and test case 4 (both techniques produced the

same MDPD value) and in test case 6 where the Gamma Knife technique had a lower MDPD value than the static cone-based technique.

The Gamma Knife technique achieved the highest TCP parameter value, followed by the static cone-based technique for all test cases with the exception of test case 3 and test case 5, where the static cone-based technique achieved the highest TCP value. Following these two techniques, the next two techniques, static conformal beam technique and proton SOBP technique, produced lower TCP values for all test cases, in which the proton SOBP technique had the lowest TCP values for all test cases.

The static conformal beam technique produced the lowest $NTCP_{brain}$ value for all test cases, followed by the proton SOBP technique with the exception of test case 5 in which the proton SOBP technique created the lowest $NTCP_{brain}$ value (see Table 4.5). The static cone-based technique and the Gamma Knife technique produced higher $NTCP_{brain}$ values than the previously discussed two techniques, in which the Gamma Knife technique produced the highest $NTCP_{brain}$ values when compared to all four techniques. For the complex study, test case 6, the proton SOBP technique achieved the lowest $NTCP_{brain\ stem}$ value, followed by the static conformal beam technique, the static cone-based, and finally, by the Gamma Knife technique which had the highest $NTCP_{brain\ stem}$ value.

From the Tables 4.1 through 4.6, the Gamma Knife technique produced the highest $IBED_{tumor}$ value, followed by the static cone-based technique with the exception of test case 3 (the static cone-based technique produced a higher $IBED_{tumor}$ value than the Gamma Knife technique). The static conformal beam technique produced the third

lowest $IBED_{tumor}$ value. Overall, the proton SOBP technique produced the lowest $IBED_{tumor}$ value compared to all techniques.

The static conformal beam technique produced the lowest $IBED_{brain}$ value for all test cases, followed by the proton SOBP technique. After the proton SOBP technique, the next two higher $IBED_{brain}$ values are produced by the static cone-based technique and then the Gamma Knife technique. The Gamma Knife technique had the highest $IBED_{brain}$ value (with the exception of test case 6 where both test cases had equivalent $IBED_{brain}$ values).

From the physical and biological parameter calculations, and in general, the static conformal beam technique and the proton SOBP technique produced the lowest physical and biological parameters in all test cases.

4.3 CORRELATION BETWEEN PHYSICAL AND BIOLOGICAL PARAMETERS

Several physical and biological parameters are evaluated for all test case studies to emphasize the correlation between parameters. The parameter pairs analyzed are the following: PITV and NTCP/$IBED_{brain}$ (including $IBED_{brain\ stem}$ for test case 6) and MDPD and TCP/$IBED_{tumor}$. The parameters are paired as such because the dose conformity or PITV is expected to have a greater effect on the NTCP/$IBED_{brain}$, when more normal brain tissue is irradiated. Similar, dose homogeneity, MDPD, is expected to have a greater effect on the tumor than PITV; therefore, dose homogeneity is paired with TCP/$IBED_{tumor}$. To clarify certain biological parameters, the volumes of normal tissue (including brain stem for test case 6) and tumor(s) accumulating specific doses during treatment are discussed in this section.

The Figures 4.1(a) through 4.1(f) present $NTCP_{brain}$ and PITV relation for all the test case studies. As a generalization from the $NTCP_{brain}$ and PITV parameter pairs, the static conformal beam technique and the proton SOBP technique, consistently, had low $NTCP_{brain}$ values in all test case studies. Compared with the static conformal beam and proton SOBP techniques, overall, the static cone-based technique had low $NTCP_{brain}$ values. The Gamma Knife technique had the highest $NTCP_{brain}$ values for all the test cases.

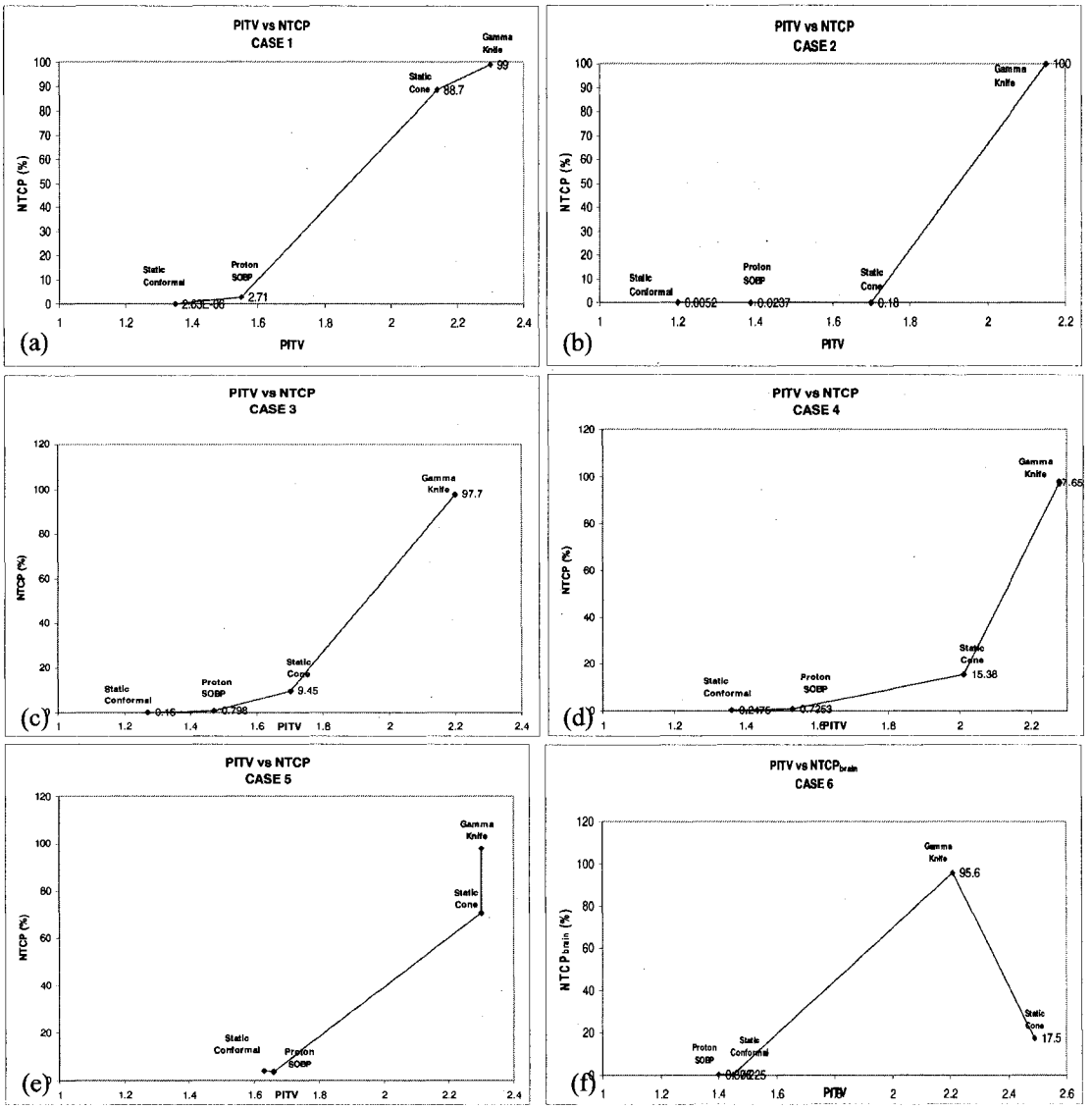

Figures 4.1 (a) and (f): Graphs present the $NTCP_{brain}$ and PITV relation for all techniques for test case 1 through test case 6.

It is observed that the more conformal the stereotactic technique is capable of performing, the lower the PITV value is achieved, such as observed with the static conformal beam and the proton SOBP techniques. With a higher PITV value, a larger portion of normal brain tissue is irradiated at the prescription dose, and higher, depending on the isodose prescription surface used. A high dose received by normal brain tissue may lead to complications and the figures showing the $NTCP_{brain}$ and PITV relation amplify this issue.

The low $NTCP_{brain}$ value can be explained with the low volume of normal brain tissue irradiated inside the prescription isodose surface and concurs with the low PITV value obtained for each test case. From Tables 4.7 and 4.8, the proton SOBP technique and the static conformal beam technique had small volumes of normal tissue inside the prescription isodose surface that received 22 Gy and higher (except test case 2 which had none) and no normal brain tissue received 25 Gy and higher in all test cases. Consistently, the static conformal beam technique had low PITV values with the exception of test case 5, which had a PITV value of 1.63. Again, this is noted where the volume of normal brain tissue receiving the prescription dose is slightly higher than the tumor volume. From Tables 4.7 and 4.8, the volume of normal brain tissue receiving the prescription dose, 20 Gy, the proton SOBP technique covered less normal tissue volume than half the tumor volume with the exception of test cases 1, 4 and 5, which is noted with a PITV values between 1.5 and 1.6.

Analyzing the remaining two techniques, the static cone-based and the Gamma Knife techniques, a contrast is observed with the $NTCP_{brain}$ values. The static cone-based

Test Case 1 Lesion: 26.2 cm^3	Static cone-based	Gamma Knife	Static Conformal	Proton SOBP
20 Gy Brain Volume (cm^3)	30.77	34.60	9.30	14.44
22 Gy Brain Volume (cm^3)	19.41	28.90	2.55	1.85
25 Gy Brain Volume (cm^3)	12.92	21.80	0.00	0.00
Test Case 2 Lesion: 6.6 cm^3	**Static cone-based**	**Gamma Knife**	**Static Conformal**	**Proton SOBP**
20 Gy Brain Volume (cm^3)	4.72	7.80	1.35	2.51
22 Gy Brain Volume (cm^3)	2.99	6.90	0.00	0.00
25 Gy Brain Volume (cm^3)	0.00	5.90	0.00	0.00
Test Case 3 Lesion: 18.4 cm^3	**Static cone-based**	**Gamma Knife**	**Static Conformal**	**Proton SOBP**
20 Gy Brain Volume (cm^3)	12.78	22.40	4.80	8.67
22 Gy Brain Volume (cm^3)	7.72	18.80	0.90	0.24
25 Gy Brain Volume (cm^3)	2.13	12.80	0.00	0.00

Table 4.7: For each optimum treatment plan for test case 1 through test case 3 acquired using the static cone-based, Gamma Knife, static conformal beam and proton SOBP techniques, the volumes of normal tissue with respect to dose are displayed to show dose homogeneity within the normal brain tissue.

Test Case 4 Lesion: 16.5 cm^3	Static cone-based	Gamma Knife	Static Conformal	Proton SOBP
20 Gy Brain Volume (cm^3)	16.97	21.20	5.85	8.79
22 Gy Brain Volume (cm^3)	8.86	17.30	1.35	0.54
25 Gy Brain Volume (cm^3)	2.01	13.80	0.00	0.00
Test Case 5 Lesion: 24 cm^3	**Static cone-based**	**Gamma Knife**	**Static Conformal**	**Proton SOBP**
20 Gy Brain Volume (cm^3)	31.79	32.40	15.15	16.18
22 Gy Brain Volume (cm^3)	22.00	24.80	5.85	2.53
25 Gy Brain Volume (cm^3)	7.48	16.60	0.00	0.00
Test Case 6 Lesion 1: 8 cm^3 Lesion 2: 6 cm^3	**Static cone-based**	**Gamma Knife**	**Static Conformal**	**Proton SOBP**
20 Gy Brain Volume (cm^3)	22.64	17.50	5.25	6.55
22 Gy Brain Volume (cm^3)	13.96	14.90	1.20	0.13
25 Gy Brain Volume (cm^3)	1.20	10.90	0.00	0.00

Table 4.8: For each optimum treatment plan for test case 4 through test case 6 acquired using the static cone-based, Gamma Knife, static conformal beam and proton SOBP techniques, the volumes of normal tissue with respect to dose are displayed to show dose homogeneity within the normal brain tissue.

technique did provide a relatively low PITV value, but is higher than the static conformal and proton SOBP techniques. From Figures 4.1(a) and 4.1(e) and to a lesser degree, Figures 4.1 (c), 4.1(d) and 4.1(f), the $NTCP_{brain}$ values calculated for the static cone-based technique are higher, as the volumes of normal tissue receiving 20 Gy (prescription dose) and higher are consistently greater than seen with the static conformal beam and proton SOBP techniques. For example, test case 1, the $NTCP_{brain}$ value is 88.7% for the static cone-based technique and from Table 4.7, the amount of normal tissue receiving 20 Gy and higher is 30.77 cm^3 (more normal brain volume than the tumor volume) producing a higher PITV value than the static conformal beam and proton SOBP techniques. The volumes of normal tissue receiving 22 Gy and 25 Gy and higher are also greater, with the exception of test case 2 (normal tissue receiving 25 Gy and higher is similar) when compared to the static conformal and proton SOBP techniques in all test cases. When the $NTCP_{brain}$ value is high for the static cone-based technique, not only did it correspond to a high volume of normal tissue receiving 20 Gy and higher, but it also included larger volumes of normal tissue receiving 22 Gy and 25 Gy and higher (see Tables 4.7 and Table 4.8). In all test cases, the Gamma Knife technique produced high $NTCP_{brain}$ values and the high $NTCP_{brain}$ values are consistent with the greater volume of normal brain tissue receiving the prescription dose and higher, such as 22 Gy and 25 Gy and up as seen in Tables 4.7 and Table 4.8. This is observed with higher PITV values calculated with the Gamma Knife technique, since the normal brain tissue volume receiving the prescription dose always exceeded the tumor volume in all test cases.

According to Figures 4.2(a) through 4.2(g), the MDPD value is consistently low in all test cases for the proton SOBP and the static conformal beam techniques. The low

MDPD values calculated are low because a single isocenter is used per lesion by these two techniques and the dose distribution is more homogeneous. Therefore, higher prescription isodose surfaces are used to prescribe the dose, such as approximately 90% for the proton SOBP technique and approximately 80% for the static conformal beam technique.

The static cone-based and the Gamma Knife techniques had higher MDPD parameter values when compared to the static conformal beam and the proton SOBP techniques. The higher MDPD values are due to the multiple isocenters being superimposed to conform the dose distribution to the lesion. The use multiple isocenters created "hot" spots or higher doses throughout the lesion. The two techniques typically had their prescription isodose surfaces of approximately 50% for all test cases with the exception of test case 2 (static cone-based technique had prescription isodose surface of 80%). Therefore, the static cone-based and Gamma Knife techniques did not have homogeneous dose distributions within the tumors.

The TCP values are low for the static conformal beam and proton SOBP techniques and can be explained by the TCP equation, $\mathrm{TCP} = \Pi_i [P(D_i, v_i)]$(2.18), which is the product of the probabilities per dose bin, $P(D,v) = 2^{-e\left[e\cdot\gamma\left(1-\frac{D_i}{D_{50}}\right)+\ln v\right]}$(2.19). As explained in Chapter 2, TCP is dependent on dose and volume, and the parameter D_{50}, where $D_{50} = D_0 \ln(\frac{10^7 V}{0.693})$ (2.21), will increase accordingly with the size of the tumor to obtain a higher TCP value. In all test cases treated by the static conformal beam and the proton SOBP techniques, the volumes of tumor receiving higher than 25 Gy are nonexistent.

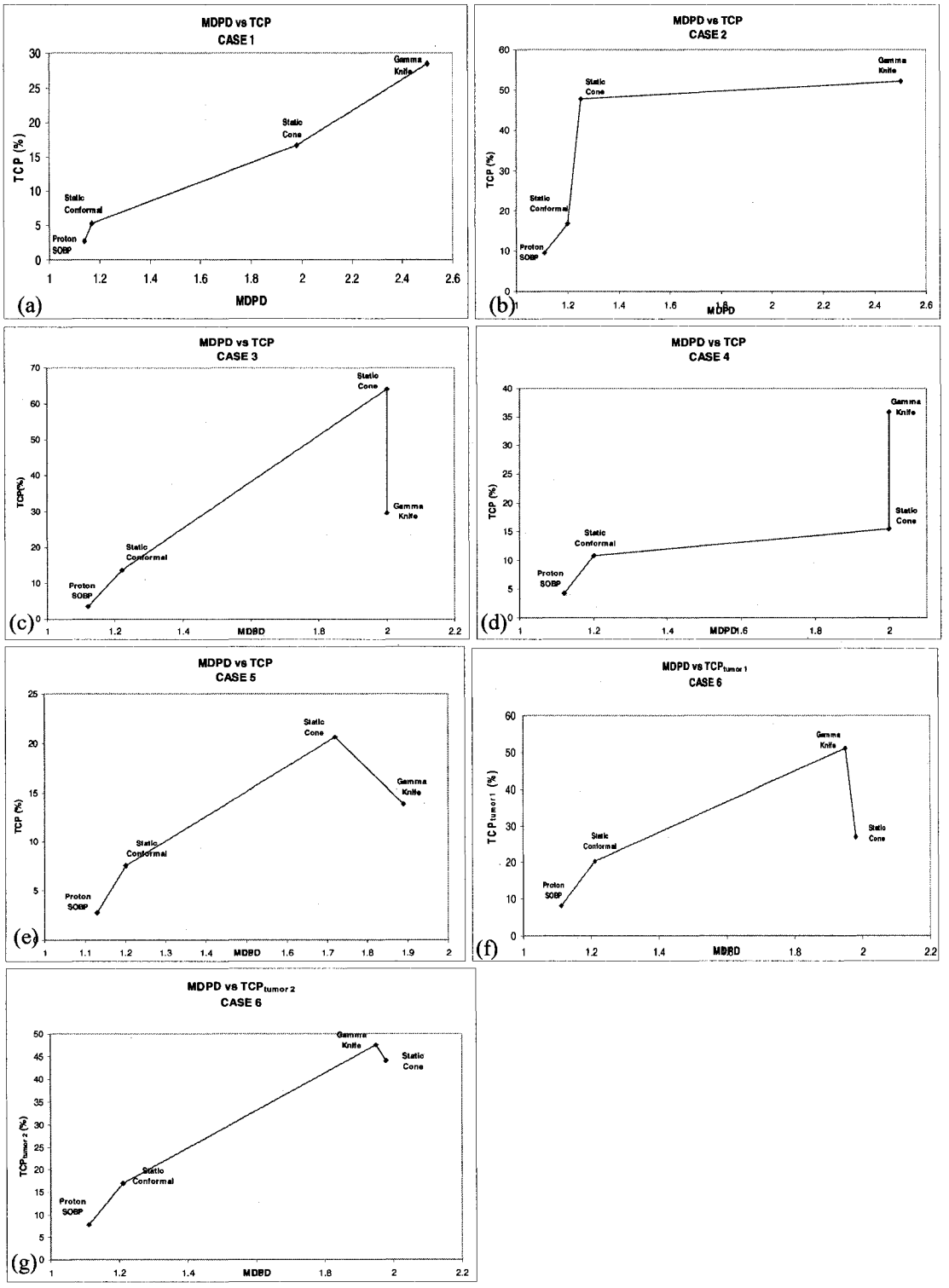

Figures 4.2 (a) and (g): Graphs present the TCP and MDPD relation for all techniques for test case 1 through test case 6.

The probability from a single dose bin, equation (2.19) will increase if the tumor volume receiving D_i decreases. On the other hand, the probability will decrease if the tumor volume receiving D_i increases for that dose bin. D_{50} has an impact on how the probability per dose bin reacts with the dose, D_i, received for that dose bin, as does the tumor volume receiving that dose. For example, in test case 6 study (tumor 1), the Gamma Knife technique has a TCP value of 51% and has a D_{50} of 68.73 Gy. The dose distribution for test case 6 is inhomogeneous and high doses are created with multiple isocenters superimposed. Table 4.9 presents how the TCP value will decrease as the volume of tumor receives an increasing homogenous dose of 20 Gy by reducing "hot" spots. In test case 6 study (tumor 1), if the tumor volumes received high doses, the TCP value increased. The drastic change in TCP values, as shown in Table 4.9, describe that the point of TCP calculation may be on a steeper part of the sigmoidal curve. This example was common how the Gamma Knife and the static cone-based techniques produced high TCP values relative when compared to the consistently low TCP values calculated by the static conformal beam and the proton SOBP techniques with homogeneous dose distributions.

Isodose distribution (%) within tumor	TCP (%)
50-100	51.0
50-90	37.0
50-80	12.0
50-70	2.0
50-60	0.2
50	0.1

Table 4.9: The table presents how the TCP decreases and the tumor receives a more homogeneous dose distribution. High TCP values are obtained with increasingly high doses with larger tumor volumes receiving the high doses.

The static cone-based and the Gamma Knife techniques, created "hot" spots within the prescribed isodose surface on the lesion. Regarding the equations above

dealing with TCP, it is evident that these higher doses received with their respective tumor volumes increased the TCP values relative to the static conformal and proton SOBP techniques.

According to Figures 4.3(a) through 4.3(f), the $IBED_{brain}$ values increased monotonically with respect to PITV values with one exception, test case 6. For test case 6, the Gamma Knife technique and static cone-based technique have the same $IBED_{brain}$ value. The static conformal beam technique, having the lowest PITV values for all test cases, gave the lowest $IBED_{brain}$ value. Also, since the IBED equation,

$$IBED = \sum_i n \cdot d_i \left(1 + \frac{d_i}{\frac{\alpha}{\beta}} \right) \frac{\Delta v_i}{V}$$ (2.16), has a fractional volume parameter component, and

this component will increase the $IBED_{brain}$ value if more normal tissue per dose bin is irradiated. This agrees with normal tissue dose-volumes in Tables 4.7 and 4.8 by having the volumes of normal brain tissues receiving prescription doses and higher. The highest $IBED_{brain}$ value is produced by the Gamma Knife technique with the exception test case 6, where the static cone-based technique produced a similar value as the Gamma Knife technique. The $IBED_{brain}$ values are higher for these two techniques because of the multiple isocenters used which created "hot" spots within the prescription isodose surface. Since the dose conformity (PITV) is higher, more normal brain tissue in these test cases for these two techniques are exposed to higher doses than the static conformal and proton SOBP techniques. Tables 4.7 and 4.8 present the volume of normal brain tissue receiving higher doses than the prescription dose of 20 Gy and higher.

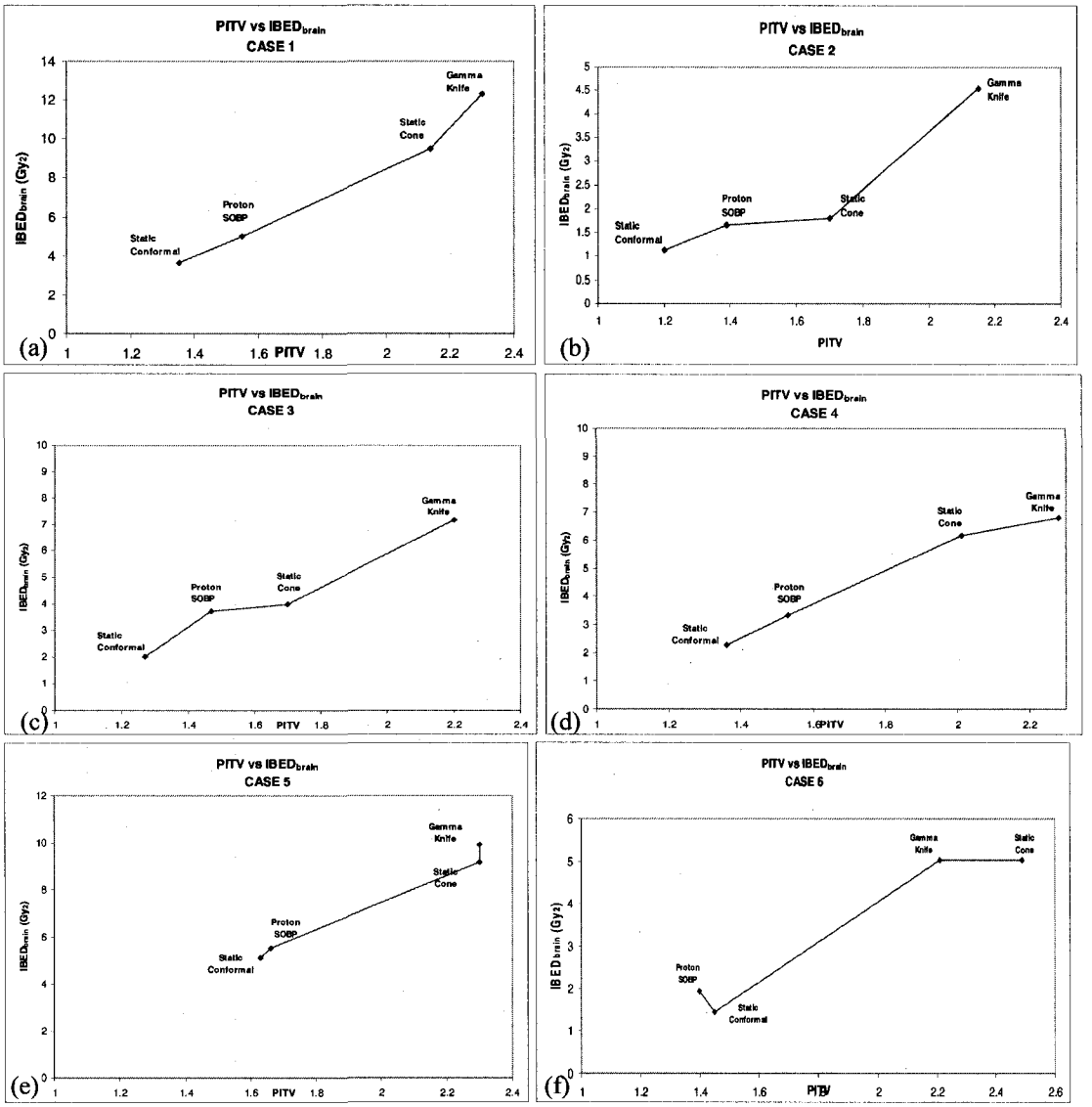

Figures 4.3 (a) and (f): Graphs present the $IBED_{brain}$ and PITV relation for all techniques for test case 1 through test case 6.

In general, the $IBED_{tumor}$ value, as observed in Figures 4.4(a) through 4.4(g), increased monotonically with respect to MDPD values with test case 3 as an exception. In test case 3, the static cone-based technique treated the tumor with a higher dose than prescribed due to the inhomogeneous dose distribution created with the multiple isocenters superimposed on the lesion. The proton SOBP technique produced the lowest

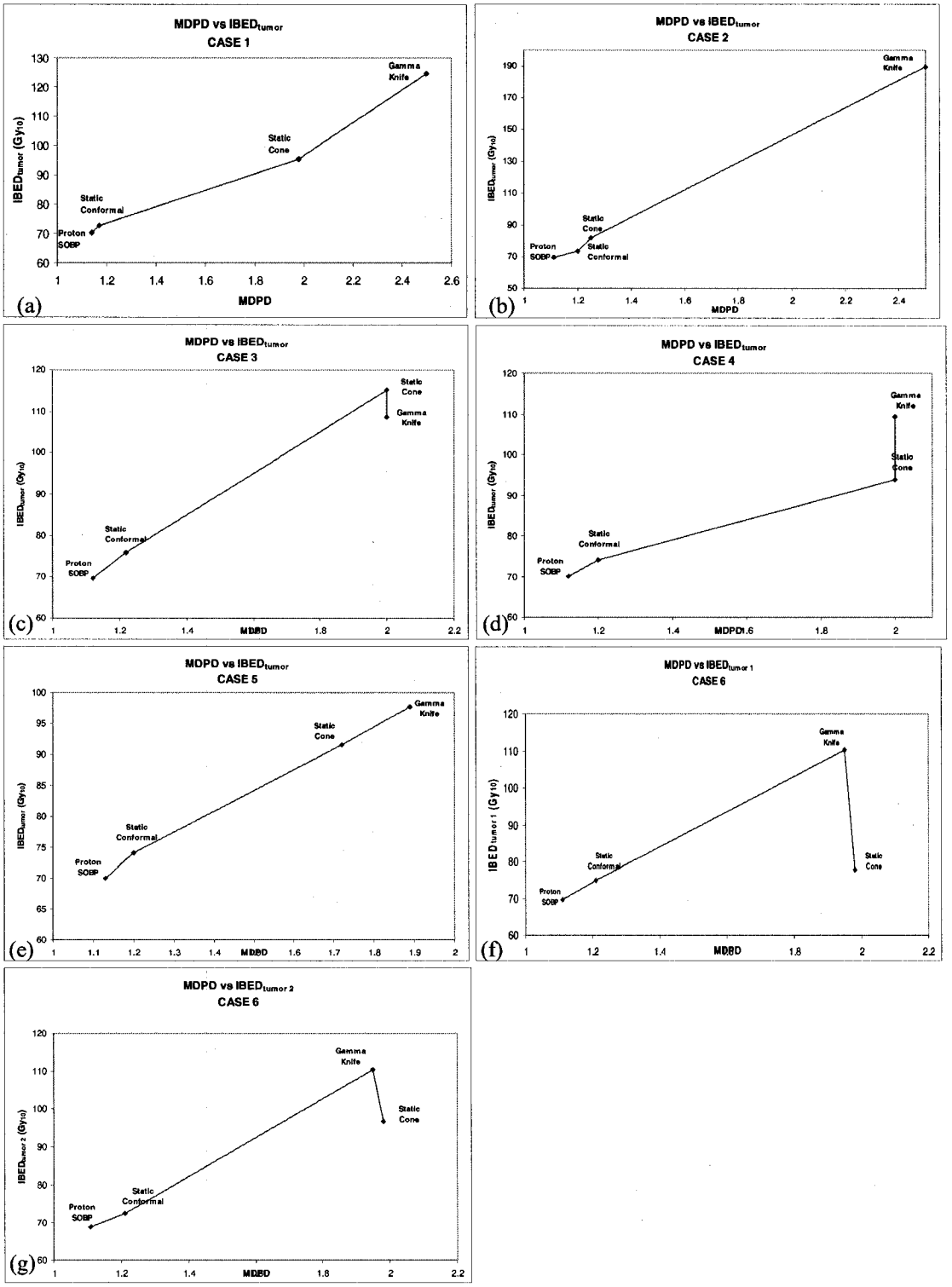

Figures 4.4 (a) and (g): Graphs present the IBED$_{tumor}$ and MDPD relation for all techniques for test case 1 through test case 6.

IBED$_{tumor}$ value for all test cases due to its homogeneous dose distribution. The static conformal beam technique had a slightly higher IBED$_{tumor}$ value than the proton SOBP

technique. These two techniques have low $IBED_{tumor}$ values because their dose distributions are homogeneous. Again, the IBED equation, $IBED = \sum_i n \cdot d_i \left(1 + \frac{d_i}{\frac{\alpha}{\beta}}\right) \frac{\Delta v_i}{V}$ (2.16), has a fractional volume parameter component, and this component will increase the $IBED_{tumor}$ value if more tumor tissue is irradiated at higher doses per dose bin. From Table 4.10 and 4.11, it is noted that the static conformal beam and the proton SOBP techniques do not deliver doses higher than 25 Gy to the lesion. On the other hand, the static cone-based and the Gamma Knife techniques deliver higher doses to the lesions. As explained previously, these techniques use multiple isocenters which create "hot" spots due to the multiple isocenters being superimposed to conform the dose distribution. Therefore, these two techniques had higher $IBED_{tumor}$ values because larger tumor volumes are irradiated at higher doses as observed in Tables 4.10 and 4.11.

Test Case 1 Lesion: 26.2 cm^3	**Static cone-based**	**Gamma Knife**	**Static Conformal**	**Proton SOBP**
20 Gy Tumor Volume (cm^3)	25.65	25.20	26.12	26.20
22 Gy Tumor Volume (cm^3)	22.75	23.60	20.92	17.99
25 Gy Tumor Volume (cm^3)	19.23	20.20	0.00	0.00
30 Gy Tumor Volume (cm^3)	3.93	11.10	0.00	0.00
35 Gy Tumor Volume (cm^3)	0.66	6.00	0.00	0.00
Test Case 2 Lesion: 6.6 cm^3	**Static cone-based**	**Gamma Knife**	**Static Conformal**	**Proton SOBP**
20 Gy Tumor Volume (cm^3)	6.74	6.40	6.69	6.31
22 Gy Tumor Volume (cm^3)	6.70	6.10	5.13	3.22
25 Gy Tumor Volume (cm^3)	0.48	5.50	0.00	0.00
Test Case 3 Lesion: 18.4 cm^3	**Static cone-based**	**Gamma Knife**	**Static Conformal**	**Proton SOBP**
20 Gy Tumor Volume (cm^3)	18.21	17.50	17.92	18.13
22 Gy Tumor Volume (cm^3)	17.95	16.10	16.08	10.07
25 Gy Tumor Volume (cm^3)	14.22	13.20	0.00	0.00
30 Gy Tumor Volume (cm^3)	6.79	6.40	0.00	0.00
35 Gy Tumor Volume (cm^3)	2.65	1.10	0.00	0.00

Table 4.10: For each optimum treatment plan for test case 1 through test case 3 acquired using the static cone-based, Gamma Knife, static conformal beam and proton SOBP techniques, the volumes of tumor with respect to dose are displayed to show dose homogeneity within the tumor tissue.

Test Case 4 Lesion: 16.5 cm^3	Static cone-based	Gamma Knife	Static Conformal	Proton SOBP
20 Gy Tumor Volume (cm^3)	15.91	15.70	16.26	16.05
22 Gy Tumor Volume (cm^3)	13.29	14.70	14.01	11.15
25 Gy Tumor Volume (cm^3)	8.40	12.20	0.00	0.00
30 Gy Tumor Volume (cm^3)	2.92	6.30	0.00	0.00
35 Gy Tumor Volume (cm^3)	0.60	0.83	0.00	0.00
Test Case 5 Lesion: 24 cm^3	**Static cone-based**	**Gamma Knife**	**Static Conformal**	**Proton SOBP**
20 Gy Tumor Volume (cm^3)	23.57	23.00	23.96	23.92
22 Gy Tumor Volume (cm^3)	22.16	20.60	20.19	16.90
25 Gy Tumor Volume (cm^3)	12.95	14.10	0.00	0.00
30 Gy Tumor Volume (cm^3)	2.08	5.60	0.00	0.00
35 Gy Tumor Volume (cm^3)	0.00	0.94	0.00	0.00
Test Case 6 Tumor1: 8 cm^3 Tumor2: 6 cm^3	**Static cone-based**	**Gamma Knife**	**Static Conformal**	**Proton SOBP**
20 Gy Tumor1 Volume (cm^3)	9.04	7.90	7.99	8.15
22 Gy Tumor1 Volume (cm^3)	8.82	7.50	6.95	4.56
25 Gy Tumor1 Volume (cm^3)	0.50	6.10	0.00	0.00
20 Gy Tumor2 Volume (cm^3)	5.96	6.00	5.93	5.98
22 Gy Tumor2 Volume (cm^3)	5.52	5.60	4.57	2.99
25 Gy Tumor2 Volume (cm^3)	3.20	4.60	0.00	0.00
30 Gy Tumor2 Volume (cm^3)	0.96	3.00	0.00	0.00
35 Gy Tumor2 Volume (cm^3)	0.28	0.60	0.00	0.00

Table 4.11: For each optimum treatment plan for test case 4 through test case 6 acquired using the static cone-based, Gamma Knife, static conformal beam and proton SOBP techniques, the volumes of tumor with respect to dose are displayed to show dose homogeneity within the tumor tissue.

According to Figure 4.5 (a) and (b), the parameter pairings of PITV with $NTCP_{brain\ stem}$ and PITV with $IBED_{brain\ stem}$ increase monotonically for the static conformal beam and the proton SOBP techniques, but did not do the same for the static cone-based and the Gamma Knife techniques since the values decreased. The Gamma Knife technique had a lower PITV value than the static cone-based technique, but the $NTCP_{brain\ stem}$ and the $IBED_{brain\ stem}$ values are higher for the Gamma Knife technique. The $NTCP_{brain\ stem}$ value is slightly higher for the Gamma Knife technique than the static cone- based technique. But because the static cone-based technique had slightly higher

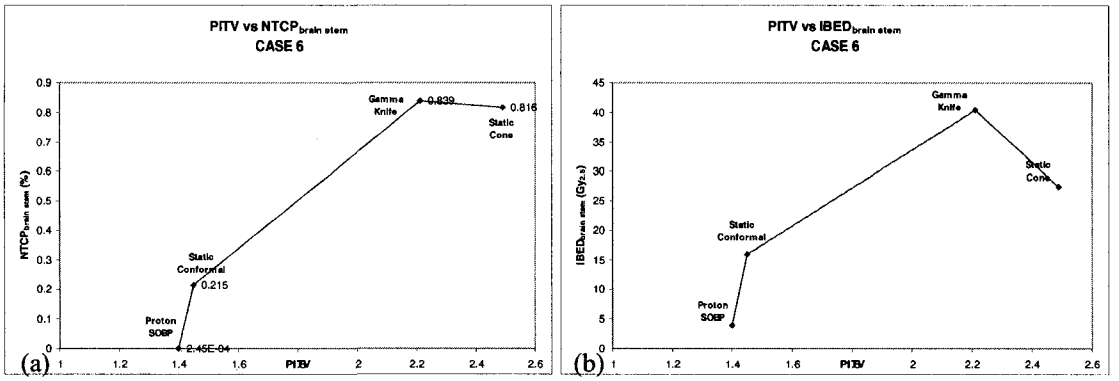

Figures 4.5 (a) and (b): Graphs present the $NTCP_{brain\ stem}$ /$IBED_{brain\ stem}$ and PITV, respectively for all techniques for test case 6.

volume of brain stem tissue receiving 10 Gy and higher, see Table 4.12; therefore, both techniques had comparable $NTCP_{brain\ stem}$ values. In regards to the $IBED_{brain\ stem}$ values, the proton SOBP and static conformal beam techniques had the lowest values due to their homogeneous dose distributions and decreased brain stem volumes receiving dose of 5 Gy to 15 Gy and higher as shown in Table 4.12. The Gamma Knife technique had the

Test Case 6 Brain stem: 9.1 cm^3	Static cone-based	Gamma Knife	Static Conformal	Proton SOBP
5 Gy Brain stem Volume (cm^3)	4.76	7.70	2.85	0.74
10 Gy Brain stem Volume (cm^3)	1.82	2.80	0.73	0.17
15 Gy Brain stem Volume (cm^3)	0.30	0.20	0.11	0.00

Table 4.12: For each optimum treatment plan for test case 6 acquired using the static cone-based, Gamma Knife, static conformal beam and proton SOBP techniques, the volumes of brain stem with respect to dose are displayed to show dose homogeneity within the brain stem tissue.

highest $IBED_{brain\ stem}$ value amongst all four techniques due to its inhomogeneous dose distribution with larger volumes receiving the lower doses. Also, the static cone-based technique had a smaller $IBED_{brain\ stem}$ value than the Gamma Knife technique. But like it, the static cone-based technique had an inhomogeneous dose distribution as well giving it the third highest $IBED_{brain\ stem}$ value.

4.4 ANALYSIS

Overall, the static conformal beam technique and the proton SOBP technique provided the lowest PITV and MDPD values for all treatment plans. The dose distributions could be shaped with ease to the lesion's shape than with other two techniques having spherical dose distributions per isocenter at high isodose surfaces. In some test cases where the lesions are drastically irregular in shape (test cases 1, 4 and 5), consistently, both techniques provided low PITV values, unlike the static cone-based technique and the Gamma Knife technique that produced higher PITV values for the same test cases. Though the static cone-based and the Gamma Knife techniques could improve their conformity by increasing the number of isocenters with respective collimator sizes, this is not always achievable due to other factors, such as the complexity of the lesion and the sparing of surrounding normal brain tissues. Creating low PITV values with the static cone-based and the Gamma Knife techniques did not always occur because the dose distribution became a function of the multiple spherical dose distributions. As for the static conformal beam and proton SOBP techniques, the micro-multileaf collimator and the brass aperture, respectively, provided a simpler planning method for a beam field that could be modified instantly.

The high prescription isodose surfaces for the static conformal beam technique (~80%) and the proton SOBP technique (~90%) provided the most homogenous dose distributions in the test case studies amongst the described techniques for stereotactic radiosurgery. Regardless of the tumor shape encountered, both techniques obtained the lowest MDPD values for all test cases including test case 6. For test case 6, the fields were placed on the two lesions in near proximity of the brain stem, and high prescription

isodose surfaces were achieved with both techniques. On the other hand, the static cone-based technique and the Gamma Knife technique could not achieve a high prescription isodose surface in the majority of the test case studies since most cases involved irregularly shaped lesions. Typical prescription isodose surface for the static cone-based and the Gamma Knife techniques is approximately 50%. Due to the numerous isocenters used per lesion, the static cone-based and the Gamma Knife techniques created "hot" spots within the prescription isodose surface leading to an inhomogeneous dose distribution.

The correlation between PITV and NTCP is observed with all test cases. With the drastic irregularly shaped lesions in most test cases, numerous isocenters were required to bring the static cone-based and Gamma Knife techniques within dose conformity requirements. As a result, inhomogeneous dose distributions were produced that its effect made the $NTCP_{brain}$ value higher for these two techniques. Since the prescription isodose surface covered some normal tissue, higher doses are created within these areas as seen with the two-dimensional dose displays. Test case 1 amplified this effect for both techniques since the lesion had long protruding segments that made it difficult to shape the dose distribution with the lesion. Therefore, high doses or "hot spots" are produced by the interaction of multiple isocenters and with high PITV values, this led to higher $NTCP_{brain}$ values for the static cone-based and the Gamma Knife techniques.

For all test cases, the $IBED_{brain}$ values did increase with an inhomogeneous dose distribution (increasing PITV) and with the increase in volume of tumor receiving the prescription dose and higher. The $IBED_{brain}$ relative values are highest for the Gamma Knife technique in all test cases, especially for the irregularly shaped lesions. Again, the

$IBED_{brain}$ value increased since the normal tissue inside the prescription isodose surface received higher doses created by the superposition of isocenters.

Inhomogeneous dose distributions created by the multiple isocenters required for the static cone-based and Gamma Knife techniques to spare normal tissue by conforming to the irregularly shaped lesions, higher TCP and MDPD relative values are observed in most test cases when compared to the static conformal beam and the proton SOBP techniques. The exception is when a single isocenter is used for the static cone-based technique for test case 2 (spherical oblate lesion) and the prescription isodose surface is approximately 80%.

The $IBED_{tumor}$ values presented a strong link with the dose to tumor volume relation. For all test cases, the $IBED_{tumor}$ values did increase with an inhomogeneous dose distribution (increasing MDPD) and with the increase in tumor volume receiving higher doses. In particular, test case 5 clearly shows how the $IBED_{tumor}$ value increased with the tumor volume receiving higher doses than 20 Gy. In this test case, the static cone-based technique had 2.08 cm^3 of tumor tissue receiving 30 Gy, and the Gamma Knife technique had 5.60 cm^3 tumor tissue receiving 30 Gy. The other two techniques had none higher than 22 Gy given to the tumor. Since the static cone-based and the Gamma Knife techniques led to inhomogeneous dose distributions, the $IBED_{tumor}$ value is higher for these techniques with a few exceptions for the static cone-based technique, such as in test case 2 and in test case 6 for tumor 1(both lesions "spherical").

In conclusion, trends are observed, each having some exceptions, but in general, the following combination of parameters displayed monotonically increasing trends: NTCP and $IBED_{brain}$ with PITV and TCP and $IBED_{tumor}$ with MDPD. With the

irregularly shaped lesions presented in the six test cases, the static conformal beam and the proton SOBP techniques are capable of conforming the dose distribution to the lesion, obtaining low PITVs and low MDPDs; therefore, high prescription surfaces are used regardless of the lesion shape. With the other two techniques, static cone-based and the Gamma Knife techniques, this is more challenging since the dose distributions are typically more inhomogeneous. Because the dose distribution is inhomogeneous, higher NTCP, TCP, $IBED_{tumor}$ and $IBED_{brain}$ values are observed in all test cases with the static cone-based and the Gamma Knife techniques.

CHAPTER 5

CONCLUSIONS

5.1 SUMMARY OF WORK

The thesis involved four techniques used for stereotactic radiosurgery: the static conformal beam, static cone-based, proton SOBP, and the Gamma Knife techniques. Phantom target lesions are created in the center of the modified anthropomorphic Rando® head and the targets ranged in shape and volume, but most are irregularly shaped lesions. From each test case study, optimum treatment plans are selected from each technique and compared by using physical and biological indices. The data extracted, using differential DVHs, for each outlined structure is compared amongst the selected treatment plans. The physical and biological parameters used are the following: the ratio of the prescription isodose volume to tumor volume (PITV), the ratio of maximum dose to prescription dose (MDPD), integral biological effective dose (IBED), tumor control probability (TCP), and normal tissue complication probability (NTCP).

The static conformal beam and the proton SOBP techniques had the lowest PITV and MDPD values for all test cases satisfying the physical index requirements when compared with the static cone-based and the Gamma Knife techniques. Using the static cone-based and Gamma Knife techniques, and lesions became more irregularly shaped and/ or complex, the PITV value increased, as is evident in most test cases. Also, the dose distribution became inhomogeneous with the use of multiple isocenters having the dose distributions overlap, producing higher MDPDs.

By trying to shape the dose distribution on the lesion when using the static cone-based and the Gamma Knife techniques, multiple isocenters were required for irregularly shaped lesions, but at the same time, this led to an increase in dose inhomogeneity. By examining the correlation between NTCP with PITV and $IBED_{brain}$ with PITV, the static cone-based and the Gamma Knife techniques had higher values relative to the static conformal beam and the proton SOBP techniques in the test case studies. As the PITV value increased, so did the NTCP and $IBED_{brain}$ values, in most situations, but the values should be taken relative to each other. The Gamma Knife technique and, at times, the static cone-based technique, produced high NTCP values due to the irregularly shaped lesions and the high doses created by overlapping dose distributions from the multiple isocenters which are within the prescription isodose surface.

Analyzing the results for all techniques, as the MDPD value increased, the TCP and $IBED_{tumor}$ values increased as well, but the $IBED_{tumor}$ value had a stronger correlation with MDPD than with TCP. Consistently, the static conformal beam and the proton SOBP techniques had low MDPD values, concurring with their homogeneous dose distributions within the lesion. The static cone-based and the Gamma Knife techniques produced higher TCP and $IBED_{tumor}$ values relative to the other two techniques. Also, the ideal prescription dose may have not been administered to each test case which is dependent on the lesion diameter; therefore, relative values should be noted amongst the techniques. The higher TCP and $IBED_{tumor}$ values observed by the Gamma Knife technique, and at times, the static cone-based technique, are because the use of multiple isocenters and the "hot" spots created within the prescription isodose surface. The

higher doses received by the tumor led to higher TCP and $IBED_{tumor}$ values with these two techniques.

Finally, when planning treatment cases, it is imperative to spare the normal brain tissue surrounding the tumor tissue since the amount of dose received may lead to normal tissue complications. In clinical practice, the RTOG protocol 90-05 provides tools for the planner in regards to dose conformity and homogeneity. The radiation oncology team will accomplish these requirements, but it will depend on several factors: 1) equipment; 2) complexity of the treatment case; 3) experience of the treatment planner; and 4) time available for patient treatment. From the study, the more complex or irregular the lesion is and depending on the available equipment is able to conform the dose distribution while maintaining the dose homogeneity, the physical parameter, PITV, does agree with the biological parameter, NTCP.

5.2 FUTURE WORK

As for future work, this project could be expanded in numerous methods. The first method would be the comparison amongst more conformal techniques such as the intensity-modulated stereotactic radiosurgery, proton SOBP (using STAR planning vice gantry planning) and proton intensity-modulated therapy technique. Comparing conformal techniques could be beneficial to experiment with tolerances of dose falloff near critical structures. Placing dose constraints on nearby critical structures will have an impact in the treatment planning techniques; therefore, making the planning more challenging and realistic with ability to prescribe higher doses.

Using past and/or present real patient case studies of specific brain tumors consisting of 30 to 50 cases for each tumor type should be incorporated in the study. The ability to evaluate the limits concerning actual size, volume and location of the lesion would be interesting to test the available conformal techniques. Follow-up on patients may be added to inspect the success rates of the techniques.

APPENDIX A

Dose Interval %	Dose Interval (cGy)	Tumor Differential DVH (cm^3)	ΔBED (Biological Effective Dose) (Tumor)
0	0	0	0
1	20	0	0
2	40	0	0
3	60	0	0
4	80	0	0
5	100	0	0
6	120	0	0
7	140	0	0
8	160	0	0
9	180	0	0
10	200	0	0
…	…	…	…
105	2100	0.20971	2.03763
106	2120	0.1809	1.785888
107	2140	0.22177	2.2241876
108	2160	0.26264	2.6756352
109	2180	0.37319	3.8613468
110	2200	0.41406	4.35072
111	2220	0.40267	4.2961884
112	2240	0.48977	5.3053056
113	2260	0.57151	6.2845628
114	2280	0.61841	6.9025632
115	2300	0.64722	7.33194
116	2320	0.59496	6.8397312
117	2340	0.61238	7.1434584
118	2360	0.51322	6.0740736
119	2380	0.26264	3.1534048
120	2400	0.00603	0.07344
121	2420	0	0
		$IBED_{tumor}$	**73.3507372**

Dose Interval %	Dose Interval (cGy)	Brain Differential DVH (cm^3)	ΔBED (Biological Effective Dose) (Brain)
0	0	284.7	0
1	20	374.1	0.054868
2	40	221.25	0.0708
3	60	142.8	0.074256
4	80	59.55	0.044464
5	100	32.85	0.03285
6	120	27	0.03456
7	140	25.95	0.041174
8	160	25.95	0.049824
9	180	21.6	0.049248
10	200	18.6	0.0496
…	…	…	…
105	2100	0	0
106	2120	0	0
107	2140	0.15	0.025038
108	2160	0.15	0.025488
109	2180	0	0
110	2200	0	0
111	2220	0	0
112	2240	0.15	0.027328
113	2260	0	0
114	2280	0	0
115	2300	0	0
116	2320	0.15	0.029232
117	2340	0	0
118	2360	0	0
119	2380	0	0
120	2400	0	0
		$IBED_{brain}$	**1.126626**

Table A.1—An example of an EXCEL spreadsheet presenting the calculation for the $IBED_{tumor}$ and $IBED_{brain}$ for test case 2, using the static conformal beam technique.

Tumor Differential DVH (cm^3)	D_1 Single Fraction (Gy)	D_2 2 Gy Fractions (Gy)	*P(Do, vo)*	
0	0	0	1	
0	0.2	0.17	1	
0	0.4	0.346666667	1	
0	0.6	0.53	1	
0	0.8	0.72	1	
…	…	…	…	
0.00603	19.6	48.34666667	0.993417821	
0	19.8	49.17	1	
0.01742	20	50	0.984473639	
0.02345	20.2	50.83666667	0.981125697	$D_{50} = D_0 \ln(\frac{10^7 V}{0.693})$
0.05829	20.4	51.68	0.958092929	$D_{50} = 68.03084956$
0.08777	20.6	52.53	0.943444873	
0.12797	20.8	53.38666667	0.926262138	Tumor Volume = 6.7 cm^3
0.20971	21	54.25	0.892986509	
0.1809	21.2	55.12	0.915792437	$P(D,v) = 2^{-e\left[e\cdot\gamma\left(1-\frac{D}{D_{50}}\right)+\ln v\right]}$
0.22177	21.4	55.99666667	0.907481618	$\gamma = 3.0$
0.26264	21.6	56.88	0.90174669	
0.37319	21.8	57.77	0.876267929	
0.41406	22	58.66666667	0.876679335	
0.40267	22.2	59.57	0.891492642	
0.48977	22.4	60.48	0.882262751	
0.57151	22.6	61.39666667	0.877251957	
0.61841	22.8	62.32	0.880856359	
0.64722	23	63.25	0.888016604	
0.59496	23.2	64.18666667	0.907029539	
0.61238	23.4	65.13	0.914206546	
0.51322	23.6	66.08	0.935117491	
0.26264	23.8	67.03666667	0.969853457	
0.00603	24	68	0.999374052	
0	24.2	68.97	1	
		TCP	**0.167530218**	

Table A.2—An example of an EXCEL spreadsheet presenting the calculation for the TCP for test case 2 using the static conformal beam technique.

Tumor Differential DVH (cm^3)	D_1 Single Fraction (Gy)	D_2 2 Gy Fractions (Gy)	Sub-Volume Effective (cm^3)	D_{max} (Gy)
				146.16
284.7	0	0	0	
374.1	0.2	0.11	1.20017E-10	**Effective**
221.25	0.4	0.24	1.60847E-09	**Volume:**
142.8	0.6	0.39	7.2389E-09	1.29715225
59.55	0.8	0.56	1.28328E-08	
32.85	1	0.75	2.27754E-08	$v = V_{eff}/V_{ref}$
27	1.2	0.96	5.02498E-08	0.000864768
25.95	1.4	1.19	1.14028E-07	
25.95	1.6	1.44	2.44497E-07	**TD50(v)**
21.6	1.8	1.71	4.04691E-07	349.8858076
18.6	2	2	6.52107E-07	
18	2.2	2.31	1.12307E-06	***t***
16.95	2.4	2.64	1.80414E-06	-3.881758051
14.7	2.6	2.99	2.57447E-06	
13.95	2.8	3.36	3.89598E-06	***n***
15	3	3.75	6.49983E-06	**0.25**
0.15	20.8	118.56	0.064942632	
0	21	120.75	0	***m***
0	21.2	122.96	0	**0.15**
0.15	21.4	125.19	0.080733853	
0.15	21.6	127.44	0.086696222	**TD50(1)**
0	21.8	129.71	0	**60**
0	22	132	0	
0	22.2	134.31	0	
0.15	22.4	136.64	0.114574649	
0	22.6	138.99	0	
0	22.8	141.36	0	
0	23	143.75	0	
0.15	23.2	146.16	0.15	
0	23.4	148.59	0	
0	23.6	151.04	0	
0	23.8	153.51	0	**NTCP**
0	24	156	0	5.19E-05

Table A.3—An example of an EXCEL spreadsheet presenting the calculation for the NTCP for test case 2 using the static conformal beam technique.

BIBLIOGRAPHY

(N.B. The numbers in the square parentheses refer to the pages in which the references are cited)

1 D. Baltas, C. Kolotas, K. Geramani, R. F. Mould, G. Ioannidis, M. Kekchidi, and N. Zamboglou, "A conformal index (COIN) to evaluate implant quality and dose specification in brachytherapy," Int. J. Radiat. Oncol., Biol., Phys. **40**, 515-524 (1998).

[40]

2 B. G. Baumert, A. J. Lomax, V. Miltchev, and J. B. Davis, "A comparison of dose distributions of proton and photon beams in stereotactic conformal radiotherapy of brain lesions," Int. J. Radiat. Oncol., Biol., Phys. **49**, 1439-1449 (2001).

[17]

3 B. G. Baumert, I. A. Norton, and J. B. Davis, "Intensity-modulated stereotactic radiotherapy vs. stereotactic conformal radiotherapy for the treatment of meningioma located predominantly in the skull base," Int. J. Radiat. Oncol., Biol., Phys. **57**, 580-592 (2003).

[17]

4 B. G. Baumert, I. A. Norton, A. J. Lomax, and J. B. Davis, "Dose conformation of intensity-modulated stereotactic photon beams, proton beams, and intensity-modulated proton beams for intracranial lesions," Int. J. Radiat. Oncol., Biol., Phys. **60**, 1314-1324 (2004).

[17]

5 O. O. Betti and V. E. Derechinsky, "Hyperselective Encephalic Irradiation with Linear Accelerator," Acta Neurochir. Suppl. (Wien) **33**, 385-390 (1984).

[3]

6 BrainSCAN Software Guide Revision 1.0 - Version 5.2x" (BrainLAB, AG, Heimstetten, Germany, 2002).

[11,24,26]

7 R. A. Brown, "Stereotactic headframe for use with the CT body scanners," Invest Radiol. **14**, 300-304 (1979).

[6]

8 C. Burman, G. J. Kutcher, B. Emami, and M. Goitein, "Fitting of normal tissue tolerance data to an analytical function," Int. J. Radiat. Oncol., Biol., Phys. **21**, 123-135 (1991).

[17,50,51]

9 M. R. Bussiere and J. A. Adams, "Treatment Planning for Conformal Proton Radiation Therapy," Technol. Cancer Res. Treat., **2**, 389-399, 2003).

[13,14,30,33]

10 R. M. Cardinale, S. H. Benedict, Q. Wu, R. D. Zwicker, H. E. Gaballa, and R. Mohan, "Comparison of three stereotactic radiotherapy techniques; arcs vs. noncoplanar fixed fields vs. intensity modulation," Int. J. Radiat. Oncol., Biol., Phys. **42**, 431-436 (1998).

[17]

11 B. G. Clark, L. Souhami, C. Pla, A. S. Al-Amro, J. P. Bahary, J. G. Villemure, J. L. Caron, A. Olivier, and E. B. Podgorsak, "The integral biologically effective dose to predict brain stem toxicity of hypofractionated stereotactic radiotherapy," Int. J. Radiat. Oncol., Biol., Phys. **40**, 667-675 (1998).

[39,45]

12 B. G. Clark, J. L. Robar, and A. M. Nichol, "Analysis of treatment parameters for conformal shaped field stereotactic irradiation: Comparison with non-coplanar arcs," Phys. Med. Biol. 3089-3103 (2001).

[17]

13 F. Colombo, A. Benedetti, F. Pozza, A. Zanardo, R. C. Avanzo, G. Chierego, and C. Machetti, "Stereotactic radiosurgery utilizing a linear accelerator," Appl. Neurophysiol. **48**, 133-145 (1985).

[3]

14 F. Colombo, A. Benedetti, F. Pozza, R. C. Avanzo, C. Machetti, G. Chierego, and A. Zanardo, "External Stereotactic Irradiation by Linear accelerator," Neurosur. **16**, 154-159 (1985).

[3]

15 W. T. Couldwell, and M. Apuzzo, "Initial experience related to the use of the Cosman-Roberts-Wells stereotactic instrument," J. Neurosurg. **72**, 145-148 (1990).

[6]

16 R. E. Drzymala, R. Mohan, L. Brewster, J. Chu, M. Goitein, W. Harms, and M. Urie, "Dose-volume histograms," Int. J. Radiat. Oncol., Biol., Phys. **21**, 71-78 (1991).

[16,39]

17 B. Emami, J. Lyman, A. Brown, L. Coia, M. Goitein, J. E. Munzenrider, B. Shank, L. J. Solin, and M. Wesson, "Tolerance of normal tissue to therapeutic irradiation," Int. J. Radiat. Oncol., Biol., Phys. **21**, 109-122 (1991).

[17,50]

18 L. Feuvret, G. Noel, J. J. Mazeron, and P. Bey, "Conformity index: A review," Int. J. Radiat. Oncol., Biol., Phys. **64**, 333-342 (2006).

[40]

19 J. F. Fowler, "The linear quadratic formula and progress in fractionated radiotherapy-Review article," Br. J. Radiol. **62**, 679-694 (1989).

[42,44]

20 M. Goitein, and T. E. Schultheiss, "Strategies for treating possible tumor extension: Some theoretical considerations," Int. J. Radiat. Oncol., Biol., Phys. **11**, 1519-1528 (1985).

[45]

21 A. Grzadziel, A. L. Grosu, and P. Kneschaurek, "Three-dimensional conformal versus intensity-modulated radiotherapy dose planning in stereotactic radiotherapy: Application of standard quality parameters for plan evaluation," Int. J. Radiat. Oncol., Biol., Phys. **66**, S87-S94 (2006).

[17]

22 E. J. Hall and A.J. Giaccia, Radiobiology for the Radiologist (Lippincott Williams & Wilkins Publishers, Philadelphia, PA, 2006).

[42,44]

23 R. J. Hamilton, F. T. Kuchnir, P. Sweeney, S. J. Rubin, M. Dujovny, C. A. Pelizzari, and G. T. Y. Chen, " Comparison of static conformal field with multiple noncoplanar arc techniques for stereotactic radiosurgery or stereotactic radiotherapy," Int. J. Radiat. Oncol., Biol., Phys. **33**, 1221-1228 (1995).

[17]

24 G. Harsh, J. S. Loeffler, A. Thornton, A. Smith, M. Bussiere, and P. H.Chapman, "Stereotactic Proton Radiosurgery," Neurosurg. Clinics of N.A. **10**, 243-256 (1999).

[13]

25 P. W. Hoban, L. C. Jones, and B. G. Clark, "Modeling late effects in hypofractionated stereotactic radiotherapy," Int. J. Radiat. Oncol., Biol., Phys. **43**, 199-210 (1998).

[45]

26 L. Hong, M. Goitein, M. Bucciolini, R. Comiskey, B. Gottschalk, S. Rosenthal, C. Serago, and M. Urie, "A pencil beam algorithm for proton dose calculations," Phys. Med. Biol. **41**, 1305-1330 (1996).

[30]

27 International Atomic Energy Agency (IAEA), Radiation Oncology Physics: A Handbook for Teachers and Students. E. B. Podgorsak, (International Atomic Energy Agency, Vienna, Austria, 2005).

[4]

28 International Commission on Radiation Units and Measurement, Inc. Report 50, Prescribing, Recording and Reporting Photon Beam Therapy (ICRU, Bethesda, MD, 1993).

[41]

29 International Commission on Radiation Units and Measurement, Inc. Report 62, Prescribing, Recording and Reporting Photon Beam Therapy (Supplement to ICRU Report 50) (ICRU, Bethesda, MD, 1999).

[40]

30 J.Y. Jin, F. F. Yin, S. Ryu, M. Ajlouni and J. H. Kim, "Dosimetric study using different leaf-width MLCs for treatment planning of dynamic conformal arcs and intensity-modulated radiosurgery," Med. Phys. **32**, 405-411 (2004).

[17]

31 V. S. Khoo, M. Oldham, E. J. Adams, J. L. Bedford, S. Webb, and M. Brada, "Comparison of intensity-modulated tomotherapy with stereotactically guided conformal radiotherapy for brain tumors," Int. J. Radiat. Oncol., Biol., Phys. **45**, 415-425 (1999).

[17]

32 H. M. Kooy, L. A. Medzi, J. S. Loeffler, E. Alexander, C. W. Cheng, E. G. Mannarino, E. J. Holupka, and R. L. Siddon, "Treatment planning for stereotactic radiosurgery of intracranial lesions," Int. J. Radiat. Oncol., Biol., Phys. **21**, 44-45 (1991).

[9]

33 G. J. Kutcher and C. Burman. "Calculation of complication probability factors for non-uniform normal tissue irradiation: The effective volume method," Int. J. Radiat. Oncol., Biol., Phys. **16**, 1623-1630 (1989).

[45]

34 G. J. Kutcher, C. Burman, L. Brewster, M. Goitein, and R. Mohan, "Histogram reduction method for calculating complication probabilities for three-dimensional treatment planning evaluations," Int. J. Radiat. Oncol., Biol., Phys. **21**, 137-146 (1991).

[50]

35 G. J. Kutcher, Z. Fuks, H. Brenner, A. P. Brown, C. Burman, E. Cheng, L. Coia, K. Krippner, J. M. Manolis, R. Mohan, J. R. Simpson, M. Urie, B. Vikram, and R. Wallace, "Three-dimensional photon treatment planning for carcinoma of the nasopharynx," Int. J. Radiat. Oncol., Biol., Phys. **21**, 169-182 (1991).

[45,48]

36 G. J. Kutcher, "Quantitative plan evaluation: TCP/NTCP models," Front. Radiat. Ther. Oncol. **29**, 67-80 (1996).

[39]

37 B. Larsson, L. Leksell, B. Rexed, P. Sourander, W. Mair, B. Andersson, "The high-energy proton beam as a neurosurgical tool," Nature **182**, 1222-1223 (1958).

[2]

38 B. Larsson, K. Liden, and B. Sorby, "Irradiation of small structures through intact skull," Acta Radiol. Ther. Phys. Biol. **13**, 513-534 (1974).

[3]

39 L. Leksell, "The stereotaxis method and radiosurgery of the brain," Acta Chir. Scand. **102**, 316-319 (1951).

[1]

40 L. Leksell, and B. Jernberg, "Stereotaxis and tomography. A technical note," Acta Neurochir. **52**, 1-7 (1980).

[6]

41 L. Leksell, D. Leksell and Y. Schwebel, "Stereotaxis and nuclear magnetic resonance," J. Neurol. Neurosurg Psychiatry **48**, 14-18 (1985).

[6]

42 "Leksell Gamma Knife ® 4C System Description Guide," (Elekta, Stockholm, Sweden, 2004).

[14,15,34]

43 R. Lin, E. B. Hug, R. A. Schaefer, D. W. Miller, J. M. Slater, and J. D. Slater, "Conformal proton radiation therapy of the posterior fossa: A study comparing protons with three-dimensional planned photons in limiting dose to auditory structures," Int. J. Radiat. Oncol., Biol., Phys. **48**, 1219-1226 (2000).

[17]

44 N. J. Lomax and S. G. Scheib, "Quantifying the degree of conformity in radiosurgery treatment planning," Int. J. Radiat. Oncol., Biol., Phys. **55**, 1409-1419 (2003).

[40]

45 W. Lutz, K. R. Winston, and N. Maleki, "A system for stereotactic radiosurgery with a linear accelerator," Int. J. Radiat. Oncol., Biol., Phys. **14**, 373-381 (1988).

[3]

46 J. T. Lyman, "Complication probability as assessed from dose-volume histograms," Radiat. Res. **104**, S13-S19 (1985).

[17,48,49]

47 J. T. Lyman and A. B. Wolbarst, "Optimization of radiation therapy, III: A method of assessing complication probabilities from dose-volume histograms," Int. J. Radiat. Oncol., Biol., Phys. **13**, 103-109 (1987).

[17,50]

48 L. Ma, P. Xia, L. J. Verhey, and A. L. Boyer, "A dosimetric comparison of fan-beam intensity modulated radiotherapy with Gamma Knife stereotactic radiosurgery for treating intermediate intracranial lesions," Int. J. Radiat. Oncol., Biol., Phys. **45**, 1325-1330 (1999).

[17]

49 T. R. Mackie and J. R. Palta, Teletherapy: Present and Future (Advanced Medical Publishings, Madison, WI, 1996).

[1,8]

50 J. E. Mignano, M. J. Engler, J. S. Tsai, and D. E. Wazer, "Comparison of radiobiologic modeling for one- and two- isocenter dose distributions applied to ellipsoidal radiosurgery targets," Int. J. Radiat. Oncol., Biol., Phys. **49**, 833-837 (2001).

[17,48]

51 R. Mohan, C. Chui, and L. Lidofsky, "Energy and angular distributions of photons from medical linear accelerators," Med. Phys. **12**, 592-597 (1985).

[26]

52 R. Mohan, C. Chui, and L. Lidofsky, "Differential pencil beam dose computation model for photons," Med. Phys. **13**, 64-73 (1986).

[26]

53 T. R. Munro and C. W. Gilbert, "The relation between tumor lethal doses and the radiosensitivity of tumor cells," Br. J. Radiol. **34**, 246-251 (1961).

[45,46]

54 A. Niemierko and M. Goitein, "Modeling of normal tissue response to radiation: The critical volume model," Int. J. Radiat. Oncol., Biol., Phys. **25**, 135-145 (1993).

[45,48]

55 P. Okunieff, D. Morgan, A. Niemierko and H. D. Suit, "Radiation dose-response of human tumors," Int. J. Radiat. Oncol., Biol., Phys. **32**, 1227-1237 (1995).

[45]

56 S. C. Oliveira, Comparison of three linac-based stereotactic radiosurgery techniques. M. Sc. Thesis, McGill University, Montreal, Quebec (2003).

[17,44,47,48,50,51]

57 A. Olivier, T. M. Peters, and G. Bertrand, "Stereotaxic systems and apparatus for use with MRI, CT and DSA," Appl. Neurophysiol. **48**, 94-96 (1986).

[8]

58 H. Paganetti, A. Niemierko, M. Ancukiewicz, L. E. Gerweck, M. Goitein, J. S. Loeffler, H. D. Suit, and D. Phil, "Relative biological effectiveness (RBE) values for proton beam therapy," Int. J. Radiat. Oncol., Biol., Phys. **53**, 407-421 (2002).

[30]

59 T. M. Peters, J. A. Clark, A. Olivier, E. P. Marchand, G. Mawko, M. Diemeregard, L. W. Muresan, and R. Ethier, "Integrated stereotaxic imaging with CT, MRI, and DSA," Radiol. **161**, 821-826 (1986).

[8]

60 B. G. Pike, E. B. Podgorsak, T. M. Peters, and C. Pla, "Dose distributions in dynamic stereotactic radiosurgery," Med. Phys. **14**, 780-789 (1987).

[9,29]

61 E. B. Podgorsak, A. Olivier, M. Pla, P. Y. Lefebvre, and J. Hazle, "Dynamic stereotactic radiosurgery," Int. J. Radiat. Oncol., Biol., Phys. **14**, 115-125 (1988).

[3,13]

62 A. V. Riet, C. A. Mak, M. A. Moerland, L. H. Elders, and W. V. D. Zee, "A conformation number to quantify the degree of conformality in brachytherapy and external beam irradiation: Application to the prostate," Int. J. Radiat. Oncol., Biol., Phys. **37**, 731-736 (1997).

[40]

63 W. Schlegel, T. Bortfeld, and A. L. Grosu, New Technologies in Radiation Oncology (Springer, Berlin, Heidelberg, NewYork, 2006).

[5,46]

64 T. E. Schultheiss, C. G. Orton, and R. A. Peck, "Models in radiotherapy: Volume effects," Med. Phys. **10**, 410-415 (1983).

[45]

65 C. F. Serago, A. F. Thornton, M. M. Urie, P. Chapman, L. Verhey, S. J. Rosenthal, K. P. Gall, and A. Niemierko, "Comparison of proton and x-ray conformal dose distributions for radiosurgery applications," Med. Phys. **22**, 2111-2116 (1995).

[17]

66 E. Shaw, R. Kline, M. Gillin, L. Souhami, A. Hirschfeld, R. Dinapoli, and L. Martin, "Radiation Therapy Oncology Group: Radiosurgery Quality Assurance Guidelines," Int. J. Radiat. Oncol., Biol., Phys. **27**, 1231-1239 (1993).

[40,41,64]

67 A. S. Shiu, H. M. Kooy, J. R. Ewton, S. S. Tung, J. Wong, K. Antes, and M. H. Maor, "Comparison of miniature multileaf collimation (mmlc) with circular collimation for stereotactic treatment," Int. J. Radiat. Oncol., Biol., Phys. **37**, 679-688 (1998).

[17]

68 "SimuPlan treatment planning system manual-version for Apple Macintosh power PC computers" (SimuPlan Sociedad Limitada, Valencia, Spain, 2000).

[13,27]

69 V. Smith, L. Verhey, and C. F. Serago, "Comparison of radiosurgery treatment modalities based on complication and control probabilities," Int. J. Radiat. Oncol., Biol., Phys. **40**, 507-513 (1998).

[17,46,48]

70 T. D. Soldberg, K. L. Boedeker, R. Fogg, M. T. Selch, and A. A. F. DeSalles , "Dynamic arc radiosurgery field shaping: A comparison with static field conformal and noncoplanar circular arcs," Int. J. Radiat. Oncol., Biol., Phys. **49**, 1481-1491 (2001).

[17]

71 C.A. Tobias, J. H. Lawrence, J. L. Born, R. K. McCombs, J. E. Roberts, H. O. Anger, B. V. A. Low-Beer, and C. B. Huggins, "Pituitary Irradiation with High-Energy Proton Beams A Preliminary Report," Cancer Research **18**, 121-134 (1958).

[2]

72 J. Van Dyk, (editor), The Modern Technology of Radiation Oncology (Medical Physics Publishing, Madison, WI, 1999).

[1]

73 L. J. Verhey, V. Smith, and C. F. Serago, "Comparison of radiosurgery treatment modalities based on physical dose distributions," Int. J. Radiat. Oncol., Biol., Phys. **40**, 497-505 (1998).

[17]

74 S. Webb and A. E. Nahum, "A model for calculating tumour control probability in radiotherapy including the effects of inhomogeneous distributions of dose and clonogenic cell density," Phys. Med. Biol. **38**, 653-666 (1993).

[17,47,48]

75 D. C. Weber, J. Bogner, J. Verwey, D. Georg, K. Dieckmann, L. Escude, M. Caro, R. Potter, g. Goitein, A. J. Lomax and R. Miralbell, "Proton beam radiotherapy versus fractionated stereotactic radiotherapy for uveal melanomas: A comparative study," Int. J. Radiat. Oncol., Biol., Phys. **63**, 373-384 (2005).

[17]

76 R.R. Wilson, "Radiological Use of Fast Protons," Radiology **47**, 487-491 (1946).

[2]

77 K. R. Winston and W. Lutz, "Linear Accelerator as a Neurosurgical Tool for Stereotactic Radiosurgery," Neurosur. **22**, 454-463 (1988).

[3]

78 S. Y. Woo, W. H. Grant, D. Bellezza, R. Grossman, P. Gildenberg, L. S. Carpenter, M. Carol, and E. B. Butler, "A comparison of intensity modulated conformal therapy with a conventional external beam stereotactic radiosurgery system for the treatment of single and multiple intracranial lesions," Int. J. Radiat. Oncol., Biol., Phys. **35**, 593-597 (1996).

[17]

79 A. Wu, G. Lindner, A. H. Maitz, A. M. Kalend, L. D. Lunsford, J. C. Flickinger, W. D. Bloomer, "Physics of gamma knife approach on convergent beams in stereotactic radiosurgery," Int. J. Radiat. Oncol., Biol., Phys. **18**, 941-949 (1990).

[36]

80 A. Wu, "Physics and dosimetry of the gamma knife," Neurosurg. Clinics of N.A., **3**, 35-50 (1992).

[36]

81 C. Yu, G. Luxton, G. Jozsef, M. L. J. Apuzzo, and Z. Petrovich, "Dosimetric comparison of three photon radiosurgery techniques for an elongated ellipsoid target," Int. J. Radiat. Oncol., Biol., Phys. **45**, 817-826 (1999).

[17]